3D Food Printing

from structure to perception

Sicong Zhu

Propositions

1. Printability of aqueous food pastes can be derived from rheological properties.

   (this thesis)

2. Accurate 3D food printing requires balancing of fusion and solidification behaviour.

   (this thesis)

3. Personalized nutrition should not be based on individual dietary requirements only.

4. The benefits of Sci-hub to overcome barriers in disseminating science outweigh violation

   of legal constraints.

5. One cannot be disappointed without expectation.

6. To facilitate submission of 'original' propositions, a database of propositions is necessary.

Propositions belonging to the thesis entitled

3D food printing: From structure to perception

Sicong Zhu

Wageningen, 22 June 2022

3D Food Printing:

From structure to perception

Sicong Zhu

3D Food Printing:

From structure to perception

Sicong Zhu

Thesis

submitted in fulfilment of the requirements for the degree of doctor

at Wageningen University

by the authority of the Rector Magnificus,

Prof. Dr A.P.J. Mol,

in the presence of the

Thesis Committee appointed by the Academic Board

to be defended in public

on Wednesday 22 June 2022

at 1:30 p.m. in Omnia.

Contents

Chapter 1

Introduction and thesis outline

1.1.3D printing

3D printing is a technology that employs computer-aided designs to build objects on a platform through layer-by-layer deposition. In the past decades, 3D printing has been increasingly applied in a wide array of applications related to construction, art, education and medical services. 3D printing provides distinct advantages such as fast prototyping, the ability to make complex object shapes, and efficient production of customized items (Portanguen et al., 2019).

The number of scientific studies investigating the principles and applications of 3D food printing is rapidly increasing. A total of 761 publications have been published about 3D food printing (Fig 1.1) during the past ten years from 2011 to 2021. The studies indicate that 3D food printing offers the opportunity to create foods with complex geometries, new textures and/or personalized nutritional profiles. Furthermore, 3D food printing has been suggested to contribute to a more sustainable production of food products as it allows for on-demand manufacturing leading to reduction of food waste in the chain (Portanguen et al., 2019; Sun et al., 2015). Very recently also a number of start-up companies popped up such as Revo Foods and Redefine Meat™ that successfully apply 3D printing for manufacturing of foods.
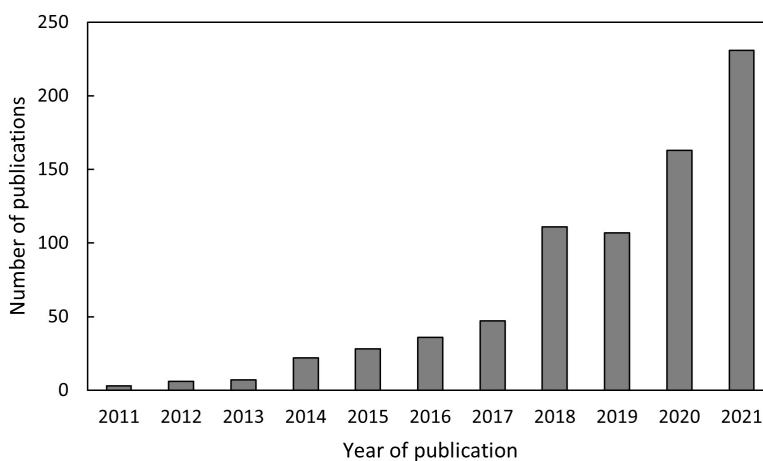
Figure 1.1. Number of publications per year about 3D food printing in academic journals during 2011-2021 from database Scopus. Search keywords contained either "3D printing", "3D food printing", "additive manufacturing" or "three-dimensional printing", and contain "food" in the abstract.

1.2. Types of 3D printers

Additive manufacturing (AM), commonly known as 3D printing, has been initially developed in the 1980s (Perrot & Amziane, 2017) for materials such as metals and plastic rather than food. According to ISO/ASTM52900-15, there are seven categories of AM processes including material extrusion, vat photopolymerization, material jetting, binder jetting, powder bed fusion, direct energy deposition and sheet lamination (Burstein, 2014). Among the various AM technologies, four of them (extrusion, material jetting, binder jetting, and powder bed fusion) are nowadays investigated for food materials. Depending on the consistency of the printed food material, different 3D food printing technologies are employed: inkjet printing (material jetting) for liquids, extrusion-based printing (material extrusion) for semi-solids, and powder bed printing (binder jetting and powder bed fusion) for powders. A schematic overview of the three categories of 3D food printing technologies is shown in Figure 1.2.

Figure 1.2. Three types of 3D food printing technologies: 1) extrusion-based printing, 2) inkjet printing and 3) powder bed printing.

1.2.1. Extrusion based 3D printing

Extrusion-based 3D printing is currently the most widely studied 3D food printing method. The method employs a syringe from which a food material is extruded to build up a food product layer-by-layer on a platform according to a computer-aided design.
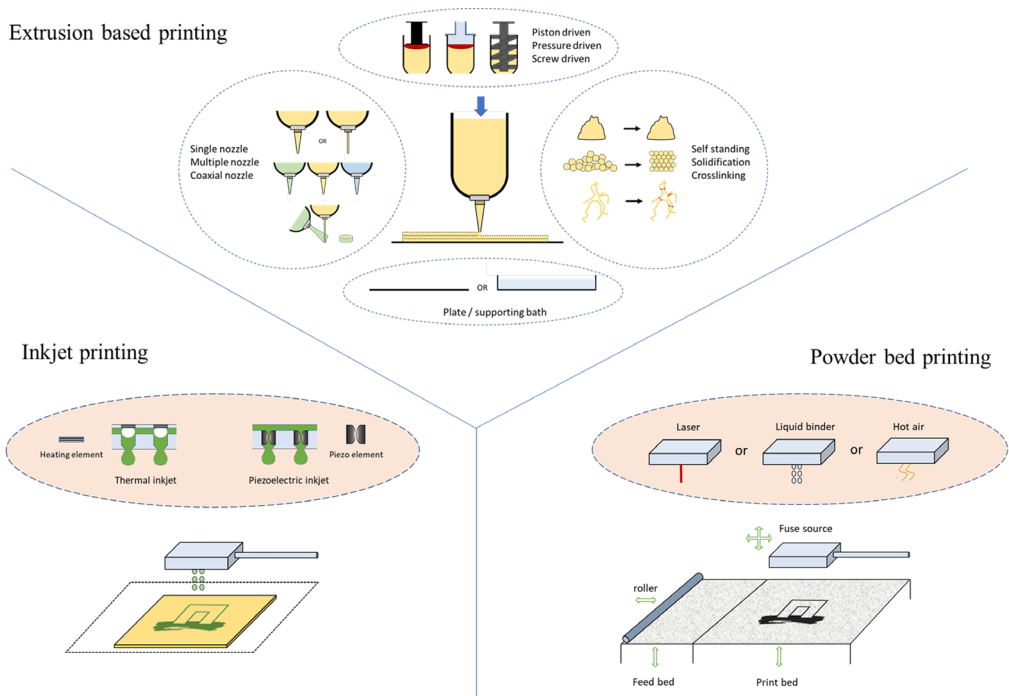
Food materials can be printed either at room or elevated temperatures. Room temperature printing is suitable for semi-solid pastes that are self-standing. For solid materials such as cheeses and chocolates, an elevated temperature is used to melt the materials to reduce extrusion forces. Once the melted material is deposited onto a platform, it should quickly solidify to hold its shape. Another way to solidify extruded materials is through chemical crosslinking. For example, calcium chloride solutions may be applied to quickly solidify food materials with alginate (Mallakpour et al., 2021).

Current commercial food printers offer the possibility to print with single or multiple materials. Correspondingly, a printer has either one syringe (single nozzle) or several syringes (multi-nozzle) to allow food material deposition. In recent years, also coaxial nozzles have been developed to allow two food materials to be co-extruded during 3D food printing (Ko et al., 2021; Uribe-Wandurraga et al., 2020).

1.2.2. Inkjet printing

During inkjet printing low viscous formulations are dispensed through printheads using thermal or piezoelectric-driven devices. In a thermal-driven printhead, an electrical pulse generates heat inducing formation of a vapour bubble, which pushes out a droplet from the nozzle. In a piezoelectric-driven printhead, an electrical pulse leads to deformation of a piezoelectric material generating a pressure pulse in the fluid, which results in ejection of a droplet of ink from the nozzle (Morita et al., 2016).

FoodJet B.V. is a Dutch company that builds industrial-scale 2D/3D inkjet food printers using arrays of pneumatic membrane nozzle-jets that can jet droplets of a low viscous food ink (e.g., molten chocolates, jams, sauces) onto a food placed on a conveyer belt (De Grood & De Grood, 2013; Godoi et al., 2016). Multiple overlapping layers can be applied by going through multiple "printing-cooling-printing" cycles and results in a 3D printed structure rather than a 2D printed pattern. Currently, inkjet printing has not been applied yet to create

complex 3D shapes, but it is commercially applied to print 2D decorations, decorations of limited height (sometimes referred to as 2D+ printing) or to precisely fill cavities of food products.

1.2.3.   Powder bed printing

A less commonly used printing technology is powder bed printing. Powder bed printing creates three-dimensional structures by applying a fusion source to bind neighbouring powder particles. Fusion of particles is induced using lasers, hot air or liquid binders. Initially, powder bed printing was developed for non-food materials such as stainless steel, cement and sand (Ingaglio et al., 2019; Mirzababaei & Pasebani, 2019; Sivarupan et al., 2021). Up to now, not many food materials were studied for their application in powder bed printing. Selective laser sintering and hot air sintering have been studied for crystal sugars (Jonkers et al., 2020), while binder jet printing was only investigated for food materials like cellulose (Holland, Foster, et al., 2018; Holland, Tuck, et al., 2018).

Powder bed printing has some distinct advantages compared to extrusion-based printing, such as high-speed production, the ability to create products with high solid content, structuring with flexible material compositions, and readily printing colour onto parts (Gibson et al., 2021). Thanks to the presence of supporting powder around the printed object, powder bed printing also offers more freedom to design more complex 3D shapes. Therefore, further exploration of possible food materials suitable for powder bed printing has the potential to create novel food products.

1.3. 3D Food Printing: structure, texture and sensory

Several recent studies have demonstrated that 3D printing can be used to alter food structures on a macroscopic length scale (> 1 mm), which is realized by changing printing pattern or infill density of a pre-designed objects. Changes in the macroscale structure of food products may ultimately lead to changes in food texture. Various 3D printed foods ranging from solid foods such as chocolates (Mantihal et al., 2019), cookies (Noort et al., 2017) and crispy snacks (Derossi et al., 2020; Z. Liu et al., 2020) to semi-solid foods such as gels (Vancauwenberghe et al., 2018) and food pastes (Liu, Bhandari, et al., 2018) were studied to explore the influence of the macroscopic structure on instrumental texture properties. A higher infill density in printed foods was often associated with harder texture, and infill

patterns influenced the fracture behaviour and hardness of 3D printed snacks (Derossi et al., 2020; Liu, Bhandari, et al., 2018; Liu et al., 2020; Mantihal et al., 2019). Only few studies demonstrated that 3D printing may lead to structural changes of foods at microscopic length scale (<1 mm). For instance, a reduction in fat droplet size was observed when processed cheese was 3D printed, which was suggested to be the result of the applied shear forces and heat treatment during the 3D printing process (Le Tohic et al., 2018). On the other hand, even though several studies quantified instrumental texture properties of 3D printed foods, so far, no study described the impact of structural modifications by 3D food printing on texture perception.

3D printing can also impact consumer and sensory perception of foods and its effect depends on the formulation and printing designs. A few recent studies explored sweetness perception (Khemacheevakul et al., 2021; Kistler et al., 2021), saltiness perception (Fahmy et al., 2021), texture preference (Mantihal et al., 2019) and mastication behaviour (Punpongsanon et al., 2020) of 3D printed foods. As an example, Kistler et al (2021) used 3D printing to prepare confectionery products with an inhomogeneous spatial distribution of sucrose. While the overall sugar content was similar, panellists perceived candies with a large sucrose concentration gradient between the inner core and outer shell sweeter than candies with a homogeneous sucrose distribution.

1.4. Challenges for 3D food printing

Printing food materials is not a trivial process, and the full potential of 3D printing should go beyond simply creating appealing food shapes. Currently, three challenges for 3D food printing exist: 1) how do rheological material properties influence printability, 2) how can 3D printing create food structures that cannot be created by traditional food processing methods, and 3) how can 3D food printing be used to alter sensory perception of foods to achieve healthier products while maintaining appealing sensory properties.

1.4.1. Rheological properties of materials affecting 3D printing

3D printing requires food materials with specific rheological and mechanical properties. Food materials need to be smoothly printed, but after printing materials should maintain their shape after deposition and post-processing. A better understanding of the rheological

properties plays a crucial role in optimizing 3D printing processing conditions. Therefore, many studies attempted to quantitatively link rheological properties of food materials to printability and their stability after printing.

Rheological properties of foods are largely determined by their microscale (10^{-6} - 10^{-3} m) and mesoscale (10^{-7} - 10^{-6} m) structure (Ho et al., 2013). During the past years, many studies focused on recipe development and printing process optimization for foods such as food hydrocolloid gels (Chow et al., 2021; Paolillo et al., 2021; Phuhongsung et al., 2020; Tunick, 2011; Vancauwenberghe et al., 2017; Wang et al., 2018; Yang et al., 2018), doughs (Caulier et al., 2020; Derossi et al., 2020; Severini, Azzollini, et al., 2018; Zhang et al., 2018), food pastes (He, Zhang, & Guo, 2020; Lille et al., 2018; Liu et al., 2018; Liu, Zhang, et al., 2018; Oyinloye & Yoon, 2020; Severini, Derossi, et al., 2018), chocolates (Hao et al., 2010; Mantihal et al., 2017, 2019) and processed cheeses (Le Tohic et al., 2018; Ross et al., 2021). All these studies provide valuable information and contribute to the further development of 3D food printing. However, when it comes to real applications, it still takes trial-and-error optimization of the formulation to obtain a food material that is well printable (i.e., by extrusion) and solidifies or gels quickly after deposition. It is currently not possible to predict whether a material is printable due to a lack of knowledge on the relationship between rheological properties of food materials and printing conditions. Rational guidelines to develop recipes considering rheological properties suitable for 3D printing are thus needed.

1.4.2. Create unique structures using 3D printing

Contrary to numerous studies that focus on changing food structures at the macroscopic length scale using extrusion-based 3D printing technologies, only few studies investigated changing food structures at the microscopic length scale that may take place during the printing process. In fact, 3D printing can create unique structures that are not commonly made by traditional manufacturing methods. An example of this could be a food structure with aligned fibrils that mimics the structure of animal muscle. During the past few years, several start-up companies proposed to create 3D printed plant-based meat analogues, and some of them launched first (prototype) products. Recently, aligned fibrous structures were 3D printed (Kim et al., 2021; Ko et al., 2021) with a proper printing pattern design. However, the diameter of those 3D printed aligned fibrous structures was around 1 mm, which is larger

than that of real muscle fibres (20-100 µm). Creating unique fibrous structures at both macroscale and microscale using 3D printing technology is, therefore, a challenge. To create unique structures, alternative printing formulations, adapted printing procedures and different printing technologies need to be assessed.

1.4.3. Modifying sensory perception using 3D printed foods

An often-reported advantage of 3D food printing is its ability to create novel food structures, which may lead to a change in perceived texture. During traditional product development foods are often modified through recipe reformulation, e.g., to lower the caloric content of a food. However, reformulation of foods negatively affects the texture sometimes and, as a result, the acceptance of foods by consumers. An alternative approach is to modify food structure towards improved textural properties without modification of the recipe. Modifications of food texture by changing the macroscopic food structure are appealing because it is well established that texture properties of foods can be used to modify eating behaviours and palatability of foods, which can improve control over food and energy intake (Bolhuis & Forde, 2020; McCrickerd et al., 2017; Punpongsanon et al., 2020; Stribiţcaia et al., 2020). As previously mentioned, many studies showed the impact of structural modifications on instrumental texture properties of 3D printed foods. Despite showing promising results, these studies did not explore how structural modifications of 3D printed foods can be applied to modify texture and mouthfeel perception.

An inhomogeneous distribution of tastants (e.g., sugar, salt, flavour, etc.) in foods is known to enhance the sensory perception of these tastants (le Berrre et al., 2013; Mosca et al., 2013; Noort et al., 2012). Many studies focus on tastant variation in single-bite foods, while other studies focus more on tastant contrast between different bites. For multiple bites it is for example found that saltiness of the first bite affects the consumer expectation for the saltiness of the subsequent bites (Dijksterhuis et al., 2014). For sugar-containing foods, the last bite appeared decisive for consumer's overall sweetness judgement (Mosca et al., 2014). These studies clearly showed that overall sensory perception of foods can be manipulated by creating a food with a tailored bite-to-bite variance. The manual production of food with taste contrasts only allows simple tastant distribution patterns and can be time-consuming and inaccurate. With 3D printing, one can realize a more complex design in component/tastant

distribution both for single-bite food (as mentioned in section 1.3) and foods with a tailored bite-to-bite variation. So far, only few studies explored the effect of tastant concentration differences between bites, and none of them applied 3D printing technology for sample preparation. If we can better understand how to alter sensory perception by manipulating food structure and tastant distribution using 3D printing technology, 3D printing is a suitable means to facilitate the design of healthier foods.

1.5. Aim and outline of the thesis

The aim of the thesis is to (1) understand the relation between material properties and printing conditions to arrive at a desired printed food, and (2) to describe how 3D food printing can be effectively used to modulate food structure and thus texture and taste perception of foods. Three different printing technologies, i.e., extrusion-based printing (**Chapter 2, 4** and **6**), powder bed printing (**Chapter 3**) and inkjet printing (**Chapter 5**), are used in the different chapters.

Extrusion-based and powder bed printing are used to investigate the relation between formulation and 3D printing setting to create foods of desired structure and design in **Chapter 2 and 3**. **Chapter 2** describes the relation between printability and rheological properties of formulations for extrusion-based printing by using tomato paste as the model system. Rheological properties such as flow stress, storage modulus and viscosity are analysed and related to printing stability and extrudability. **Chapter 3** reports about an investigation on powder bed printing technology to create printed high protein structures with different textures as influenced by composition and binder content. Ingredient mixtures of calcium caseinate (CaCas), starch and medium-chain triglyceride (MCT) with different binder content are prepared by powder bed printing and characterized on instrumental textural properties.

Chapter 4, 5, and **6** report how 3D printing can be used to modify food structures at the micro- and macroscale, and how the modified structures alter sensory perception. **Chapter 4** describes the influence of extrusion flow conditions on microstructure of fibrous structures formed during extrusion-based printing. Mixtures of sodium caseinate (NaCas) and sodium alginate are printed in a fluid gel supporting bath, and the impacts of extrusion speed and nozzle geometry on the final structure and instrumental texture are assessed both at the micro- and macroscale. **Chapter 5** describes the use of inkjet printing technology to create an

inhomogeneous distribution of food compounds at the macroscale. The influence of bite-to-bite variation in chocolate content of chocolate-coated rice waffles on consumers' sensory perception and liking is assessed. A macroscale inhomogeneous food compound distribution is studied in **Chapter 6**, where protein bars with different macroscale structure are made using extrusion-based printing technology. The influence of the macroscopic structure of 3D printed protein bars with chocolate fillings is not only assessed on instrumental texture properties but more importantly on texture perception.

Chapter 7 provides a general discussion of the main findings of this thesis and the prospect for future applications and remaining challenges for 3D food printing.
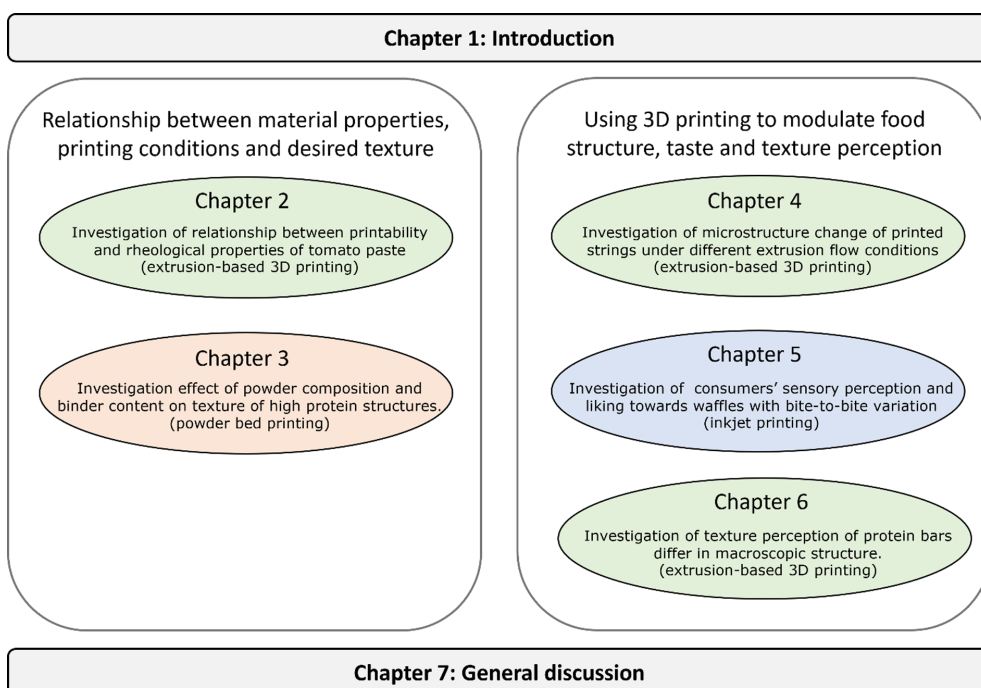

Figure 1.3. Schematic outline of the content in this thesis.

Chapter 2

Extrusion-based 3D printing of food pastes:
Correlating rheological properties with
printing behaviour

Abstract

Development of 3D food printing applications requires in-depth knowledge on printing behaviour of food materials. In extrusion-based 3D printing, having the right rheological properties is vital to achieve successful printing. The objective of this research is to investigate potential correlations between printability of formulations and simple rheological properties. We used tomato paste as a model system to investigate the correlation between printing stability, dispensability and rheological properties. The results showed a linear correlation between ingredient's flow stress, viscosity and corresponding printing stability. The dispensing pressure necessary to extrude tomato paste increased linearly with increasing flow stress. From additional experiments with more aqueous-based food formulations it was found that their printability aligned well with the gained correlation of tomato paste; however, for fat-based products different printing behaviour was observed. This work provides a general guideline for selecting aqueous food formulations with desired printability based on their rheological properties, e.g., flow stress.

2.1. Introduction

Three-dimensional (3D) printing, also known as additive manufacturing, is a technique which prints computer-aided designed objects on a platform through layer-by-layer deposition. The first working 3D printer was developed in the 1980's and used photopolymer and plastic as printing material (Horvath, 2014). The first generation of 3D printers printed materials like metals, ceramics and polymers and were not meant for printing foods (Godoi et al., 2016). The first 3D food printer was developed around 10 years ago employing a syringe-based extruder to deposit food pastes on a platform (Vesco et al., 2009). The syringe-based extrusion printer typically uses food pastes of high viscosity (Liu et al., 2017).

Whether a food paste is suitable for application via 3D printing depends on the rheological properties of that material. Recently, two important criteria for assessing the suitability of a material were proposed. Those are its ease of deposition and the ability to hold its structure post deposition (Godoi et al., 2016). A material that meets these criteria can be easily extruded and can provide sufficient stability to the printed object. The object should not collapse during printing and possible post treatment (e.g., baking). In order to smoothly extrude a food paste from a defined printing nozzle, a certain mechanical force is required. The magnitude of this force depends on the rheological properties, as well as on the geometry of the nozzle (Schutyser et al., 2017).

Many studies explored formulation flexibility for 3D food printing. Wang et al. (2018) investigated printing of fish surimi gel, where it was observed that surimi gels made with 1.5g NaCl/100g surimi mixture are most appropriate for 3D printing when considering geometrical accuracy and object dimensions. Yang et al. (2018) printed lemon juice gels with added potato starch and concluded that lemon juice gel with 15 g/100 g potato starch was most suitable for 3D printing of cylinders and some other defined objects. Only a few studies describe the relation between rheological properties (e.g., viscosity) of formulations and the printing behaviour. Schutyser et al. (2017) investigated 3D printed objects from sodium caseinate dispersions with reversible gelation behaviour, and they applied a modified Poiseuille equation for power law fluids to describe the dispensing behaviour. Zhang et al. (2018) successfully 3D printed doughs with prebiotics. They found dynamic rheology measurements could be correlated to the printability of the dough in a qualitative but not a quantitative manner. Recently, Liu, et al. (2018) related rheological

properties and printing quality of mashed potato formulations supplemented with potato starch. They visually observed that a formulation with 2% added starch exhibited the best extrudability and shape retention of printed objects. Lille et al. (2018) studied printability of starch, protein and fibre-rich materials. An optimum printing formula was developed with a semi-skimmed milk powder-based paste. They indicated that the yield stress of the paste possibly could be related to visual shape stability of 3D printed structures. Concluding, in previous studies rheological properties were related to printability of food formulations. However, in all these studies the relationship was only investigated qualitatively, i.e., extrusion performance (in terms of clogging, discontinuous printing) and visual quality of a repeatedly printed object for different formulations.

The aim of the present work is to relate rheological properties of food pastes to printing stability and extrusion force in a quantitative manner. Understanding such relation allows us to predict printing behaviour of food ingredients and thus better design successful printing formulations and processes. To this end, we used tomato puree as a model system. By concentrating tomato paste via centrifugation, we prepared tomato pastes with different rheological properties. Their printability was assessed in terms of extrusion behaviour (*via* analysis of extrusion force) and shape stability (*via* measurement of maximum printed object height). Here, the effect of nozzle size is considered as well. In addition to tomato puree, we studied rheological properties and printability of several other readily available food formulations in a similar manner as tomato paste. This was done to explore the generic nature of correlations found for tomato paste.

2.2. Materials and methods

2.2.1. Materials

Jumbo tomato puree was purchased from a local supermarket (Jumbo, the Netherlands). Nutella® spread (Ferrero B.V., Italy), Speculoos paste Original (Lotus, the Netherlands), Zaanse Mayonnaise (Van Wijngaarden B.V., the Netherlands), Argeta® chicken meat spread (Droga Kolinska, Slovenia), Zonnatura vegeterian spread natrual flavour (Royal Wessanen NV, the Netherlands) were purchased from local supermarket (Albert Heijn, the Netherlands).

2.2.2. Characterization of tomato paste

Particle size distribution

The particle size distribution was measured in triplicate using laser diffraction analysis (Mastersizer3000, Malvern Instruments), applying the Fraunhofer optical model. The volume-based diameter (d_{43}) was defined as:

$$d_{43} = \sum_i n_i d_i^4 / \sum_i n_i d_i^3 \tag{2.1}$$

where n_i is the percentage of particles with a diameter d_i (μm).

Light microscopy of commercial tomato puree

One gram of tomato puree was diluted with one gram of distilled water and examined directly after vortex shaking. Shape and structure of cell wall material were studied using light microscopy (Zeiss AxioScope, Germany).

2.2.3. Preparation of tomato pastes for 3D printing

Tomato puree was centrifuged at 20°C from 1,000 to 10,000 g force for 20 minutes. Centrifugation was performed using Sorvall Lynx 4000 (Thermo Scientific, USA) with F14-14 × 50 cy Fixed-Angle Rotor (Thermo Scientific, USA). After centrifugation, the pellet was collected and used for 3D printing and further rheology analysis. Soluble sugar content of supernatant was measured using a reflectometer (Atago, USA).

Dry matter content and density of tomato pellet paste

Three grams of tomato pellets were dried overnight in a hot air oven (Heraeus, Germany) at 105°C to determine the dry matter content. Pellet density was measured by weighing the obtained tomato pellet in a 0.715 mL container. Dry matter content and pellet density were all measured in triplicate.

Relative volume fraction

The original tomato puree has a defined solids volume fraction (φ_{puree}). After centrifugation the solids volume fraction in the tomato pellet φ_{pellet} can be calculated as:

$$\varphi_{pellet} = \frac{V_{puree} \times \varphi_{puree}}{V_{pellet}} \tag{2.2}$$

The relative volume fraction φ' of the solids in the centrifuged tomato pellet was defined as

$$\varphi' = \frac{\varphi_{pellet}}{\varphi_{puree}} = \frac{V_{puree}}{V_{pellet}} \qquad (2.3)$$

2.2.4. Rheology measurements

Stress amplitude sweep

Stress sweep analysis during oscillatory measurements were carried out with a logarithmically increasing shear stress from 1 to 1000 Pa at a fixed frequency of 1 Hz. Maximum storage and loss moduli in the linear regime were evaluated and compared to printability. The stress at which the G' and G'' crossed was taken as the flow point (Mezger, 2011). Each sample was measured in duplicate.

Creep test

In order to determine the shear stress used for the creep test, a series of creep tests were performed in advance to guarantee the applied shear stress was within the linear viscoelastic region. The shear stress was applied instantly, and 91 data pointes were taken over 300 s. Zero shear viscosity was calculated based on Burger's model (Mezger, 2011). Each sample was measured in duplicate.

2.2.5. Stability and dispensability characterization of 3D Printed materials

The ByFlow 3D printer (byFlow B.V., the Netherlands) was used to perform printing experiments. Printing was carried out at ambient temperature. A printing design of a hollow square column with a bottom dimension of 30 × 30 mm and wall thickness of 2.4 mm was created using Slic3r software. Grey tips (1.2 mm diameter) and green tips (0.8 mm diameter) (Nordson smooth flow tapered tips, Nordson Corporation, US) were used as extrusion nozzles. Printing experiments with the green nozzle required a printing speed of 25 mm/s, while three object perimeters were printed (Fig 2.1A). The experiments with the grey nozzle required a printing speed of 18 mm/s, while two object perimeters were printed (Fig 2.1B). The object designs for the two different printing speeds were to assure the same printing time for each layer for the two different nozzles. The printed layer height was set to 0.6 mm.
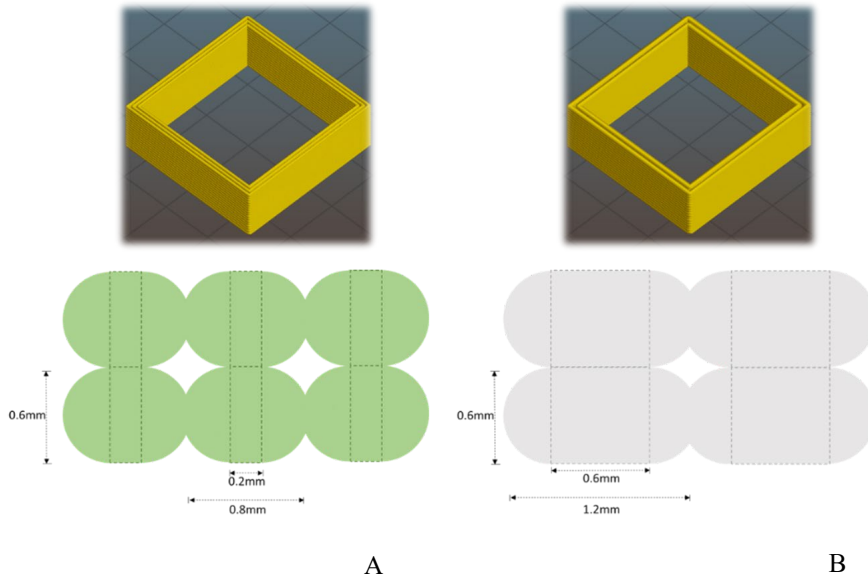
Figure 2.1. Schematic graph of layers printed using (A) green (0.8 mm) nozzle and (B) grey (1.2 mm) nozzle. Hollow squared column was illustrated using Slic3r software above the drawings.

Stability measurement

Printing was continued until the height at which the entire structure collapsed. Video recordings were taken using an IDS uEye camera (IDS imaging Development Systems GmbH, Germany) to monitor the whole printing process. Total printing time before collapsing was based on video recording, and the corresponding sample weight before collapsing was calculated. The stability limit was defined as the stress at the collapsing moment, which is equal to the total sample mass multiplied with the gravitational acceleration (9.81 m·s^{-2}) divided by the bottom surface area of the printed hollow cube (2.65 cm^2). Stability measurements of each material were carried out in duplicate.

Dispensability measurement

Dispensability was defined as the force needed to extrude food ingredient out of the nozzle. Ingredients were loaded into printing syringes used for 3D printing process. An in-house developed syringe holder was constructed to fixate the syringe during compression test. The compression test was performed using a texture analyser (Instron 5564, USA). The force was measured when extruding the material at continuous displacement of the piston. The piston speed was set at 0.03 mm/s for grey nozzle and 0.05 mm/s for green nozzle to mimic the 3D

printing process. A maximum compression distance of 10 mm was set, and an average compression force was calculated from the force measurements. All compression tests were done in duplicate.

2.3. Results and discussion

2.3.1. Characterization of tomato puree and centrifuged tomato pellet

Density, dry matter content, relative volume fraction, and the brix value of the corresponding supernatant of both tomato puree and centrifuged tomato pellets were measured in this study. The measured pellet density (1.1 g/mL) and the brix value of supernatant (28.4°) were observed constant for tomato puree and centrifuged tomato pastes and independent of the applied centrifugation force. The dry matter content of the centrifuged pellet increased slightly from 26.3 to 27.9 wt%, while the relative volume fraction (φ') of the tomato pellet almost doubled from 1 to 1.9 with increasing centrifugation force (Appendix A.2.1). The density of the pellet remained more or less constant, as the supernatants comprised high concentrations of sugar, which is reflected by the constant Brix value. The increased relative volume fraction (φ') corresponds to an increased solids volume fraction (φ_{pellet}) of tomato pellet, indicating a more packed system of the obtained tomato paste compared to the original tomato puree.

Tomato puree is a dispersed system composed of broken cells and tomato skin. In Figure 2.2 microscopic pictures of the original tomato puree and its particle size distribution are shown. As can be observed from Figure 2.2A, tomato puree consists mostly of broken cells. A larger particle of tomato skin can also be observed in Figure 2.2A. The volume-averaged particle size is 325 μm, which is similar to that measured in another study (Bayod et al., 2007).

From rheological analysis it was found that flow stress, G'_{max}, G''_{max}, and zero shear viscosity all increased with increasing centrifugation force (Appendix A.2.2). According to Bayod et al. (2007), pure tomato paste can be described as a highly concentrated and packed system of deformable particles. The viscosity of tomato paste is largely determined by the concentration and deformability of the particles such as tomato cells. Our observations are in agreement with these earlier observations. The higher the centrifugation force is, the larger

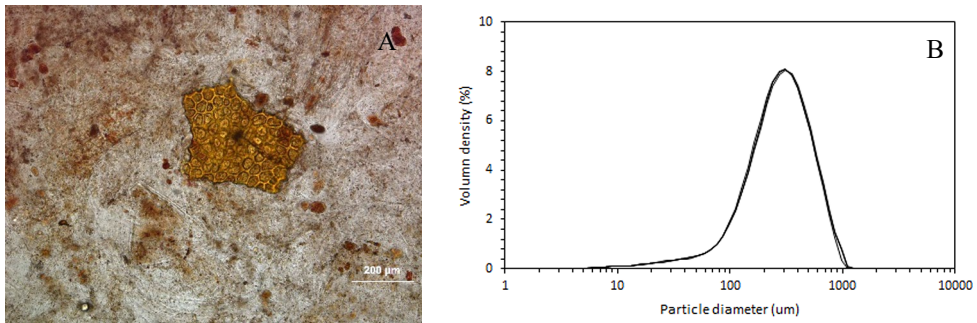the relative volume fraction of the tomato pellet is, and the larger the flow stress and viscosity are.

Figure 2.2. (A) Microscopic image and (B) Particle size distribution of commercial tomato puree.

2.3.2. Relationship between rheological properties of tomato paste and printing behaviour

The collapse of the printed tomato paste object was observed to differ depending on the pre-treatment, as shown in Figure 2.3. For non-concentrated tomato puree, collapsing occurred around 340 s. During printing the object started already buckling at 318 s and collapsed shortly after. At the moment of collapse, the walls of two sides of the column bended inwards and the other two bended outwards. For concentrated tomato paste (obtained by centrifugation at 8000 g-force) the object started buckling around 1440 s. Subsequently, after an additional 160 s of printing, the object collapsed to one side. Irrespective of these differences in buckling and collapse behaviours, we chose the height at the moment of collapse to be the most straight forward way of assessing the printing stability of a formulation.

The measured objected height at the moment of collapse was translated into a stress acting at the bottom plate by dividing the total sample weight at the collapse height by the bottom surface area of the printed hollow cube. It should be emphasized that the calculated stress at collapse is exerted by the total weight of the object onto the bottom plate, and this stress decreases proportionally at different heights in the object to zero at the top of the structure.
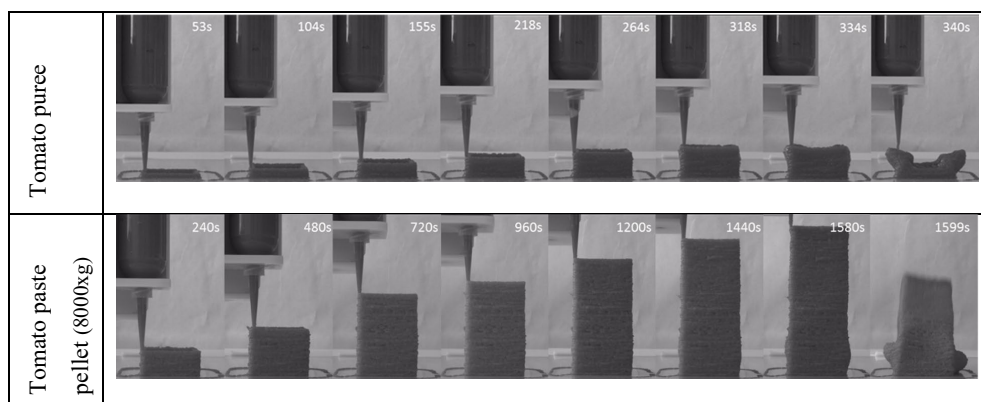
21

Figure 2.3. 3D printing of hollow square column using tomato puree and centrifuged paste printed with the 1.2 mm nozzle.

The stress at collapse was plotted versus the flow stress, zero shear viscosity, and storage modulus obtained from independent rheological experiments, as shown in Figure 2.4. The magnitude of the stress at collapse was larger for the larger grey nozzle (1.2 mm) compared to the smaller, green nozzle (0.8 mm). Furthermore, the calculated stress was found to behave proportional to flow stress, storage modulus and zero shear viscosity for the two used printing nozzle size (Fig 2.4). Despite rheological measurements are carried out at continuous deformation conditions, it appears well related to the stress at buckling under static loading conditions. Flow stress indicates the stress at which the structure of a viscoelastic material transits from a more solids to a liquid state. This may be connected to the point of collapse where the material close to the bottom of the plate experiences a high stress and thus starts deforming. Interestingly, the flow stress has a similar order of magnitude compared to the stress at the moment of collapse. Both storage and loss moduli were evaluated and compared to printability, where only the storage modulus was found to be systematically varying with stability of the printed structure. This may be explained as the storage modulus reflects the elastic properties of the material, i.e., rigidity, while the loss modulus reflects the viscous properties of the material. The zero shear viscosities have been determined during creep tests, where a material is exposed to a constant stress and the deformation is monitored as function of time. Subsequently, the Burgers model is used to determine the zero-shear rate viscosity, i.e., the viscosity at rest. This viscosity indicates the resistance towards deformation under long term loading and therefore could be expected correlated to stability.
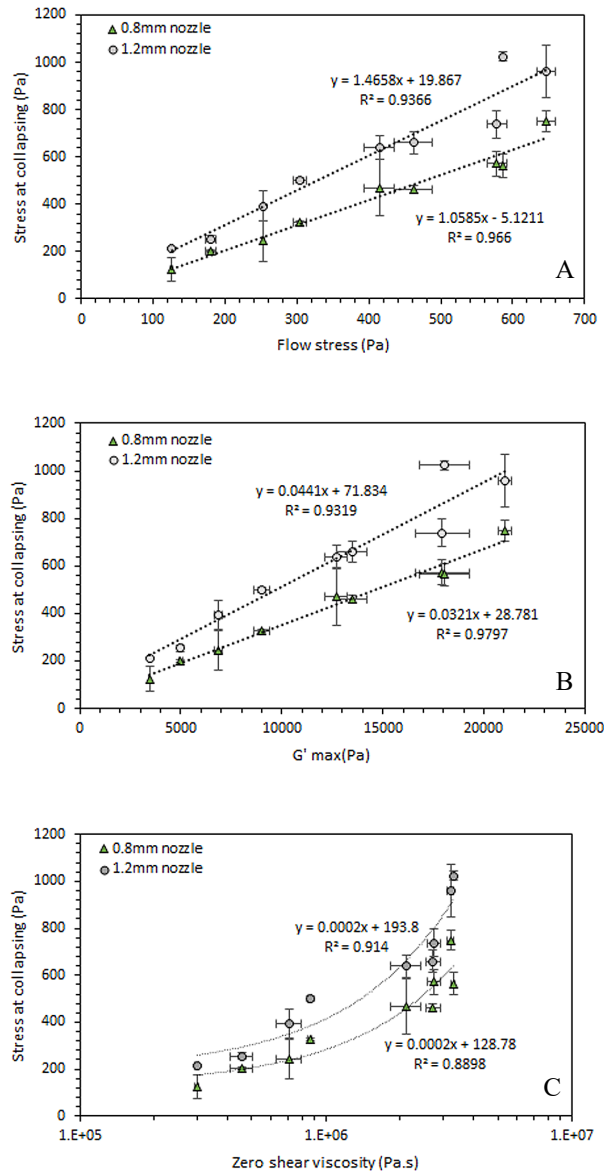
Figure 2.4. Correlating rheological properties with printing stability. Grey dots represent printed object with 1.2 mm nozzle. Green triangles represent printed object with 0.8 mm nozzle. (A) plot of stress at collapse versus flow stress. (B) plot of stress at collapse versus G'$_{max}$. (C) plot of stress at collapse versus zero shear viscosity.

In Figure 2.4 it can also be observed that the relation between rheological parameters and calculated stress are varying with nozzle diameter, which cannot be attributed to material

properties. Specifically, the height of collapse for objects and thus calculated stress at collapse is higher for objects printed with the larger (1.2 mm) nozzle. There are several reasons that may explain this observation. A first reason could be the increased rigidity of the structure printed with the 1.2 mm nozzle, having fewer individual threads printed. With a lower number of contact points, one could expect the structure to be more rigid and thus resistant to collapse. A second reason could be that the risk of clogging for the 0.8 mm nozzle is higher for the 1.2 mm nozzle. Small heterogeneities in printed paste properties may reduce stability of the total object and thus lead to reduced critical object height. Thirdly, increasing the complexity of the printing pattern by the higher number of threads for the 0.8 mm nozzle enhances the risk of column instabilities due to the printing process itself, e.g., more vibrations due to start-stop events.

A linear correlation was also observed between measured extrusion force and measured flow stress, as shown in Figure 2.5. The measured extrusion pressure was observed always higher than the measured flow stress and can be assumed to be related to the material properties that can vary during flow (e.g., shear thinning) and nozzle geometry. The effect of nozzle geometry is reflected by the measured extrusion forces for the two nozzle types, i.e., the extrusion force is higher for the smaller nozzle diameter. The moduli (G'_{max} and G''_{max}) and the zero-shear rate viscosity were found not linearly correlated to extrusion force, which may be explained by the fact that these parameters reflect the rheological properties of a non-deforming state of the material in contrast to flow stress.
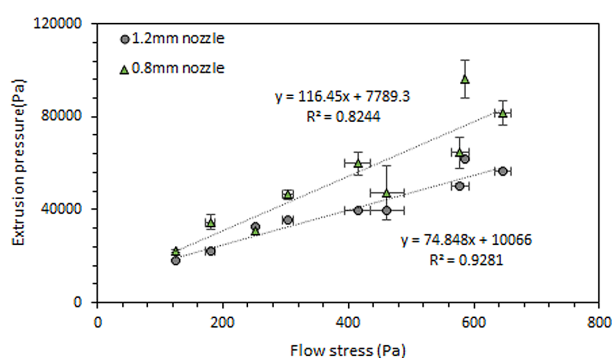

Figure 2.5. Correlating rheological properties with extrusion pressure of tomato paste. Grey dots represent extruding tomato paste with 1.2 mm nozzle. Green triangles represent extruding tomato paste with 0.8 mm nozzle.

2.3.3. Correlating rheological properties of other products with printing behaviour

Linear relationships between the printing stability and independently measured rheological properties were shown for the "tomato paste" model system. To increase the general applicability of our results, we evaluated if these relationships also hold for other printable formulations. Therefore, similar experiments were performed with five readily available printable food pastes: Nutella, Speculoos, vegepate, kippate and mayonnaise. These products represent a variety of pastes that we considered suitable for 3D printing, amongst others aqueous-based (vegepate, kippate and mayonnaise) and fat-based (Nutella and Speculoos). Density and measured rheological parameters of these products are summarised in Appendix A.2.3.

Experiments were again carried out with the 0.8 mm and 1.2 mm nozzles. Because similar results were obtained for both nozzle types, we only show here the results for the 1.2 mm nozzle relating stability and rheological parameters (Fig 2.6). Interestingly the flow stress in relation to the stress at collapse for the five food pastes aligns reasonably well with that of the tomato paste system (Fig 2.6A). Interestingly, vegepate deviated from the regression line with a better printing stability. This could be due to the moisture loss of the printed vegepate during the whole printing process, which lasted around 30 min.

G'_{max} did not have a clear linear correlation with printing stability when other commercial products were involved (Fig 2.6B). Zero shear viscosity shows only a weak linear correlation with printing stability (Fig 2.6C).
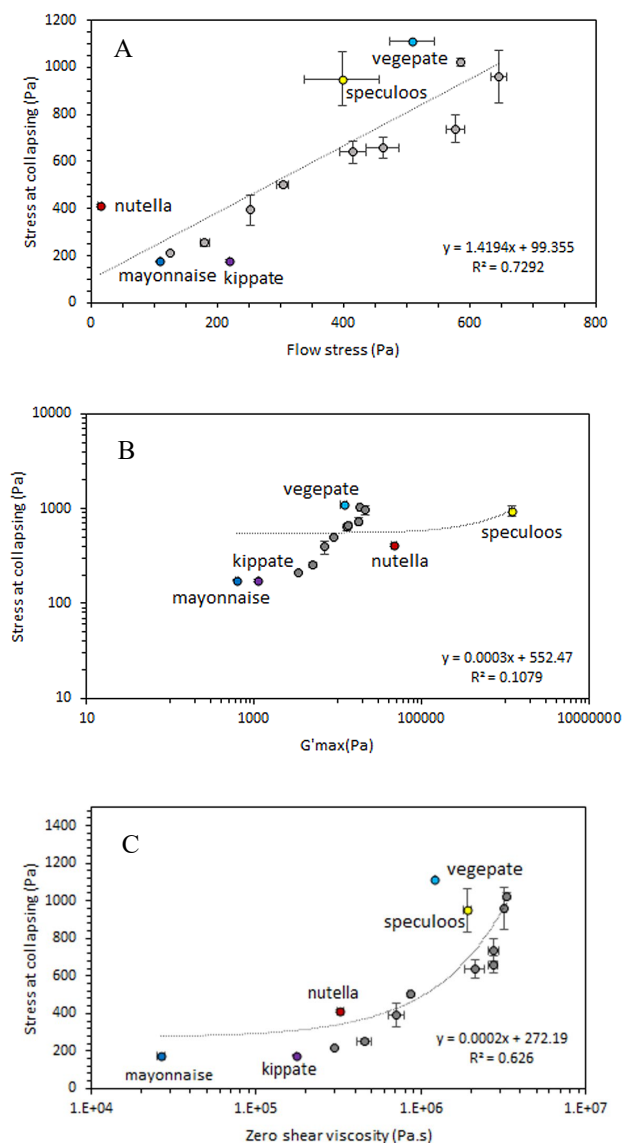
Figure 2.6. Correlating rheological properties with printing stability for all 5 commercial products together with tomato paste using 1.2 mm nozzle. Fitted linear regression is based on tomato paste and all commercial samples. (A) plot of stress at collapse versus flow stress. (B) plot of stress at collapse versus G'$_{max}$. (C) plot of stress at collapse versus zero shear viscosity.

Figure 2.7 shows the correlation plots of extrusion pressure and flow stress based on the experiments using the 1.2 mm nozzle. The results of vegepate, kippate and mayonnaise were in agreement with the data for tomato paste. However, Nutella and Speculoos required much higher extrusion pressure than expected.
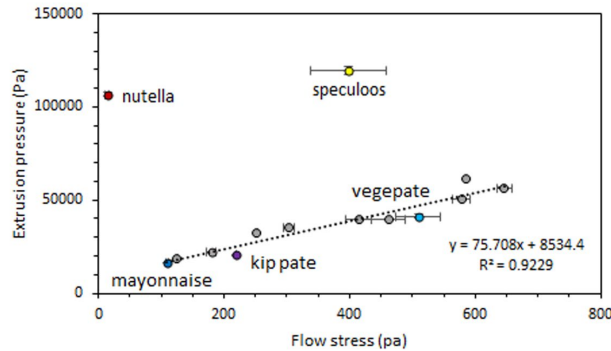

Figure 2.7. Correlating rheological properties with extrusion pressure of tomato paste and commercial samples extruded with 1.2 mm nozzle. Fitted linear regression is based on tomato paste, vegepate, kippate and mayonnaise. Grey dots represent tomato paste.

A possible explanation for this is that these fat-based paste materials strain harden during the extrusion process. This phenomenon is well known for fat systems when subjected to stress beyond their yield point. Initial yielding is probably related to the relative moving between fat flocs, while more energy is needed to induce slip of fat crystal planes to move across one another (Gonzalez-gutierrez & Scanlon, 2018). The different rheological behaviour for Nutella and Speculoos can be observed from stress sweep graphs when compared to those of water-based ingredients such as tomato puree and vegepate (Fig 2.8). Tomato puree and vegepate (Fig 2.8A) had a distinct cross over of G' and G'' at around 120 Pa and 500 Pa respectively. Afterwards G'' decreased faster than G' and broken structures of the two pastes were observed. G' and G'' of Nutella crossed over at around 15 Pa (Fig 2.8B). Both G' and G'' decreased when increasing shear stress to 20 Pa, and afterwards a slight increase was observed when we further increased shear stress to 200 Pa. During this whole yielding process, G' and G'' of Nutella remained similar.

G' and G'' of Speculoos decreased sharply and crossed over at shear stress of 400 Pa, and similar to what observed in Nutella, G'' and G' stayed closely together until 900 Pa. Results showed that Nutella and Speculoos behaved differently that commercial water-based

products when subjected to shear flow, and the shear stress needed to increase incrementally for additional structure change to occur after yielding.
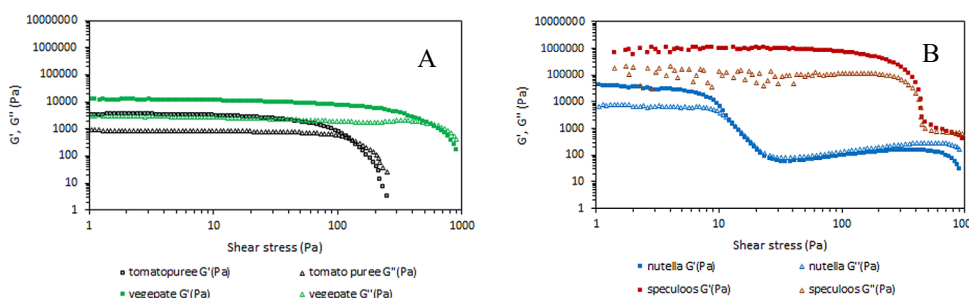

Fig 2.8. Stress sweep of commercial food products (A) tomato puree and vegepate, (B) Nutella and Speculoos.

We are fully aware that during the extrusion process, material encountered not only simple shear flow which happened along the syringe wall, but also elongational flow which took place near the symmetry axis of the syringe (Irgens, 2014). Nevertheless, we believe that our present work helps to provide a simple guideline when designing a 3D printing object based on measured shear rheology properties.

2.3.4. Application of present work

Conventional way of 3D printing design goes through a trial-and-error approach, as shown in Figure 2.9A. When designing a recipe, material is directly printed to check whether it is extrudable by the printer. Only when it is proven extrudable, further printing will be done to assess the stability. For such "trial-and-error" approach, one usually needs to go through many loops in order to obtain a proper recipe. Even though such conventional approach is easy to carry out, yet its disadvantages such as time-consuming, material wasting, and chance of damaging printing motor drive us to develop a better guideline using a more "rational approach" for material selection and printing design.

Based on our study, we concluded that for aqueous-based granular type of paste, printing stability and extrusion force is linearly correlated with material rheological property, namely the flow stress. Therefore, we proposed a "rational approach" for material selection (Fig 2.9B-D). For instance, one aims to print an object with a desired printing stability (Fig 2.9B)

without knowing what ingredient to use. Based on our obtained linear correlation between flow point and printing stability, one can easily predict the approximate flow point, and further get a rough estimation of how much extrusion force is needed. If the predicted extrusion force does not exceed the limit of the motor limit, one can then seek for the material having the predicted flow point by doing literature research or simple rheology measurement. In another case, for a material with a known flow point (Fig 2.9C), one can easily estimate the needed extrusion force and printing stability. When the estimated printability and extrudability meet both the desired printing height and printer limit, printing process can be started. Otherwise, a new recipe or different printing design will be suggested. Similar decision-making route also holds for the situation when one knows the printing limit of a certain printer (Fig 2.9D). By knowing the force limit of a printer, one can estimate required maximum flow point of printing material and maximum printing height of the printed object. If the desired printing stability exceeds the predicted maximum printing stability, it is then suggested to search for another printing design or use other type of material so as to avoid any printer damage.

We believe our guideline of "rational approach" not only can help people for a faster sorting of proper printing material that meets the printing design, but also reduce the potential risk of motor damage. Future work is suggested to strengthen the obtained linear models by taking other parameters such as printing speed, nozzle diameter, and geometric shapes into account.
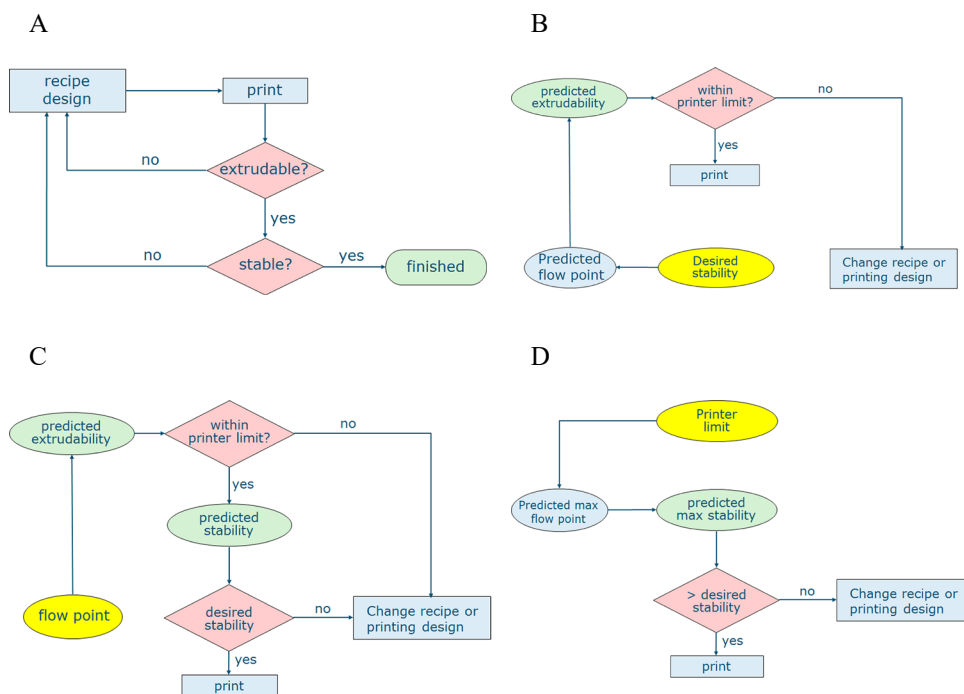
Figure 2.9. Schematic decision-making flow chart of 3D food printing design and material selection for aqueous-based paste (A: conventional "trail-and-error approach"; B-D: new guideline of "rational approach").

2.4. Conclusion

This study demonstrated the correlation between rheological properties and printing behaviour during extrusion-based 3D printing process at room temperature. Linear relationships were found between flow point and printing stability for both model system (tomato pastes) and other commercial samples. Dispensability of the studied water-based paste also showed linear relationships between flow point, while fat-based products had different dispensing behaviour. Further research such as extensional rheology analysis is needed to understand the different dispensing behaviour between water-based system and fat-based system. The authors suggest that the overall printing behaviour of water-based tomato paste systems can be well predicted with corresponding rheological properties, e.g., flow stress obtained by oscillatory stress sweep.

2.5. Appendix

Table A.2.1. Pellet density, dry matter content and relative solid volume fraction of centrifuged tomato paste.

Centrifugation force (xG)	0	1000	2000	3000	4000	5000	6000	8000	10000
Pellet Density ρ (g/mL)	1.1 ±0.1	1.1 ±0.0	1.1 ±0.0	1.1 ±0.0	1.1 ±0.0	1.1 ±0.0	1.1 ±0.0	1.1 ±0.0	1.2 ±0.0
Dry matter content (wt%)	26.3 ±0.0	26.0 ±0.1	26.2 ±0.1	26.6 ±0.0	27.0 ±0.1	27.0 ±0.1	27.2 ±0.0	28.3 ±0.1	27.9 ±0.0
Relative volume fraction φ'	1	1.1 ±0.0	1.3 ±0.0	1.5 ±0.1	1.5 ±0.0	1.5 ±0.0	1.6 ±0.0	1.7 ±0.0	1.9 ±0.0
Brix of supernatant (°)		28.4 ±0.2	28.4 ±0.2	28.4 ±0.2	28.4 ±0.1	28.4 ±0.2	28.4 ±0.2	28.4 ±0.1	28.4 ±0.1

Table A.2.2. Rheological parameters of centrifuged tomato paste.

Centrifugation force (xG)	0	1000	2000	3000	4000	5000	6000	8000	10000
Flow stress (Pa)	125.6 ±.1.1	180 ±7.4	252.7 ±1.98	304 ±9.05	414.64 ±20.58	461.95 ±26.66	577.85 ±14.07	585.5 ±0.85	646.6 ±12.59
G'_{max} (Pa)	3443.2 ±31.5	4980 ±97.2	6847.8 ±215.5	9004.3 ±412.7	12697 ±551.5	13460 ±770.75	17943 ±1315.2	18402 ±1219	21044.5 ±342.9
G''_{max} (Pa)	942.4 ±47.94	2021.2 ±201.17	1708.9 ±1.41	2028.4 ±205.84	2829.6 ±40.23	3267 ±160.8	4110.4 ±130.7	3997.9 ±374.1	4533.1 ±1.6
Zero shear viscosity (Pa.s)	299730 ±6024	455915 ±46011	713030 ±81204	859930 ±20025	2134950 ±297197	2733750 ±192686	2757100 ±182716	3300200 ±52608	3215300 ±101540

Table A.2.3. Density and measured rheological parameters of commercial food products.

	Mayonnaise	Kippate	Nutella	Speculoos	Vegepate
Density ρ (g/mL)	0.9 ±0.0	1.0 ±0.0	1.3 ±0.0	1.2 ±0.0	1.2 ±0.0
Flow stress (Pa)	109.6 ±1.8	219.8 ±0.1	14.4 ±2.7	398. 0 ±59.4	509.4 ±35.2
G'_{max} (Pa)	620.62 ±26.6	1125.6 ±24.6	46590.5 ±3690.4	1193200 ±70852.1	11746 ±1158.2
G''_{max} (Pa)	146.1 ±6.5	300.5 ±2.5	9025.2 ±1214.2	237500 ±22712.3	2961 ±254.7
Zero shear viscosity (Pa.s)	26391 ±1439.7	173970 ±0.0	323195 ±14927.0	1212950 ±6717.5	299730 ±6024.6

Chapter 3

Creating protein-rich snack foods

using binder jet 3D printing

Abstract

Rising consumer demand for healthy snacks drives a rapid market growth of protein-rich foods. While numerous studies explored extrusion-based 3D printing to prepare customized high protein foods, only a few studies explored the potential of binder jet 3D printing to structure food materials. In this study, we investigated the feasibility of binder jet 3D printing to create protein-rich structures using calcium caseinate (CaCas) powder. We successfully printed foods using powder mixtures of CaCas, starch, and medium-chain triglyceride (MCT) powder. Addition of native starch to CaCas enhanced effectively the printability of powder mixture. Foods with different instrumental texture properties were obtained by changing ingredient and binder composition. Food textures ranging from crumbly to springy were obtained by changing deposited binder amount and CaCas content in the powder mixtures. This study highlights the potential opportunities for industrial applications to create protein-rich products using binder jet 3D printing technology.

3.1. Introduction

According to regulations of the Food and Drug Administration (FDA), protein-rich foods need to contain at least 20% of the Reference Daily Intake (RDI) of protein, which is about 10 grams per serving (FDA, n.d.). In recent years, protein-rich snack foods are experiencing a quick market growth. A focus on healthy living and meal-time fragmentation are driving reasons for its growth in popularity (Fi Global, 2020). In other words, consumers are looking for a convenient way to boost health. A clear trend shows that an increasing number of consumers eat protein-rich snacks for their high nutritional value. However, most protein-rich foods, such as protein bars, usually have a fixed shape, which is not always attractive to customers. To meet the market growth of healthy protein-rich foods and to provide consumers with a unique eating experience, there is room to diversify these products by, for instance, creating palatable textures and appealing shapes or spatially distributing ingredients in the product. Conventionally, manufacturing technologies such as panning, sheeting, filling allow mass production of foods with coatings, layers, and fillings. However, food structures produced using conventional manufacturing technologies cannot easily realize complex shapes. A promising approach to prepare such customized foods is 3D printing, which is an emerging technology to create three-dimensional structures layer-by-layer according to predesigned digital models. Since 3D printing offers an opportunity for food customization, it is therefore of great interest to investigate its feasibility in creating protein-rich foods.

Different 3D food printing technologies, namely extrusion-based printing, inkjet printing, and powder bed printing have been developed for creating stable three-dimensional products (Godoi et al., 2016). Binder jet 3D printing relies on powder bed printing technology, in which a liquid binder is precisely deposited to agglomerate neighbouring powder particles to build a 3D-printed structure. During binder jetting, particles may be agglomerated by different mechanisms such as sintering, chemical reaction, and formation of liquid bridges (Pietsch, 2003). Compared with other 3D printing technologies, binder jet 3D printing has some distinct advantages such as high-speed production, the ability to create products with high solid content, structuring with flexible material compositions, and readily printing colour onto parts (Gibson et al., 2021). Binder jet printing has been studied for non-food materials such as stainless steel (Mirzababaei & Pasebani, 2019), cement (Ingaglio et al., 2019), and sand (Sivarupan et al., 2021). Parameters such as particle size and shape, binder

type and amount, printing parameters, and post-processing factors have been evaluated for their impact on green/sintered density, shrinkage rate, mechanical strength and shape retention of green/sintered parts. Unfortunately, binder jet printing of food materials is not trivial, especially when it comes to food powders that swell upon hydration. The swelling of powder particles impairs the printing process as a wet layer emerges above the surface, which causes misalignment and disruption of structures when a subsequent layer of powder is applied (Holland et al., 2019). To date, only a few studies investigated the possibility of using food materials (e.g., cellulose, xanthan gum) for binder jet 3D printing (Holland, Foster, et al., 2018; Holland, Tuck, et al., 2018), and only one patent stated a protein bar recipe made of whey protein and egg white albumin using binder jet 3D printing (Diaz et al., 2017). A possible reason for the lack of studies that use binder jet 3D printing for making of protein-rich structures is likely due to the swelling behaviour of protein powder particles upon absorption of water.

Many different protein sources such as sodium caseinate (Schutyser et al., 2017), milk protein (Lille et al., 2018; Liu et al., 2018), and various plant proteins (Oyinloye & Yoon, 2020; Phuhongsung et al., 2020) have been studied for extrusion-based food printing. A protein that is often used in protein-rich foods such as protein bars and protein shakes is calcium caseinate, one of the most common types of caseinates in the market (Augustin & Margetts, 2003). Calcium caseinate also shows interesting properties to make attractive foods with fibrous structures (Manski et al., 2007). Zhu et al. (2021) successfully printed protein bars containing calcium caseinate and whey proteins by extrusion-based printing. However, no studies reported the feasibility of binder jet printing of protein rich foods consisting of calcium caseinate. Several studies showed that casein and caseinate powders swell upon hydration (Gaiani et al., 2007; Ji et al., 2016; Kelly & Fox, 2016). As mentioned earlier, the swelling of protein powder particles upon hydration can result in failure of the binder jet 3D printing process. Therefore, it is important to find a solution to mitigate the negative impact of swelling on the process of binder jet 3D printing.

This study aims to investigate binder jet 3D printing to create printed structures of calcium caseinate (CaCas) with varying textures. Initial printing trials with CaCas powder showed significant swelling upon deposition of the binder onto the powder bed, which hampered subsequent application of powder layers. Native wheat starch was added to the protein

powder to mitigate the negative impact of swelling of caseinate powder upon hydration during the printing process. Powder mixtures with different caseinate and starch ratio were evaluated for their hydration and swelling behaviour using microscopy. Subsequently, food structures were printed using CaCas-starch powder mixtures with different binder content and extensively analysed on textural properties. As medium-chain triglycerides (MCT) are widely used in many protein-rich foods like protein bars, the influence of MCT powder addition to the used powder mixtures on the texture of printed samples was also evaluated.

3.2. Materials and methods

3.2.1. Materials

Agglomerated spray dried calcium caseinate (CaCas) was kindly provided by FrieslandCampina (Wageningen, The Netherlands). Native wheat starch and Tween 20 were purchased from Sigma-Aldrich (Darmstadt, Germany). MCT powder was provided by FrieslandCampina Kievit BV (Amersfoort, The Netherlands) and contained 69.1% medium chain triglyceride.

The binder used in this study was a 1 mM Tween 20 solution. After dissolving 1.23 g of Tween 20 into 1 L milli-Q water, the solution was filtered using an Amicon® stirred cell filtration setup, using a filter with a pore size of 0.2 μm.

3.2.2. Methods

Particle size distribution and particle morphology
Particle size distribution and circularity of CaCas, starch, and MCT powders were characterized by morphology analysis using the Malvern Morphologi 4 (Malvern Instrument Ltd, United Kingdom). At least 2000 particles were analysed for each powder. Circularity is calculated as the ratio of a particle perimeter to the perimeter of an equivalent area circle.

Flowability test
Flowability of CaCas, starch and MCT powders was evaluated by a fixed tunnel method (Beakawi Al-Hashemi & Baghabra Al-Amoudi, 2018). The powder is poured from a fixed funnel at a height of 10 cm onto a paper. The pouring of the powders is stopped when the heap reaches a predetermined diameter of 8 cm, and the subsequent height of the powder

heap is measured. The angle of repose is calculated as the arctan of the maximum height to average radius ratio. The angle of repose of each powder mixture was measured in duplicate.

Visualization of CaCas powder particle swelling

The swelling of CaCas particles was visualized and analysed with an optical microscope (Zeiss Axioscope). A droplet of prepared binder was added to few CaCas powder particles and transient hydration behaviour of the particles was monitored. The total hydration process was recorded for 120s to check the size change of CaCas particles.

Measurement of specific powder volume

CaCas and starch powders were manually mixed to obtain powder mixtures with different CaCas content (100, 86, 80, 67, 50, 0 wt%). Exactly 10 g of powder was loaded into a 50 mL graduated cylinder. Subsequently, the graduated cylinder was manually tapped for 5 minutes at a height of 5 cm using a tap frequency of around 110 times per minute to densify the powder. The tapping was applied to obtain a random dense powder packing. This packing is assumed comparable to the situation inside the powder bed printer, where a roller is applied to densify the powder. The volume of the tapped powder mixtures was read from the graduated cylinder. For each powder type, measurements were done in triplicate.

Quantitative analysis of swelling behaviour of powder mixtures

Powder mixtures as described above were analysed on their swelling behaviour. For this a powder layer was prepared by evenly spreading approximately 2 g of powder onto a glass microscope slide (VWR®) and pressing this layer with a 300 g weight for 5 min. Subsequently, a droplet of 5 μL of prepared binder was deposited onto the powder layer in a Tracker™ Drop Tensiometer (Teclis Scientific, Civrieux d'Azergues, France). The degree of swelling or collapse after droplet deposition of the powder layer was measured using a ZEISS SmartZoom microscope (Carl Zeiss Microscopy GmbH, Jena, Germany). 3D analysis was done using SmartZoom software to acquire a 2D height profile of the wetted powder surface. The vertical distance between the unwetted and the wetted powder surface was calculated by the SmartZoom software. For each powder type, measurements were done in triplicate.

Powder bed printing

In total ten powder mixtures were powder bed printed. Five CaCas-starch powder mixtures were prepared by mixing different CaCas content (33, 40, 50, 60, 67 wt%) and corresponding

starch content (67, 60, 50, 40, 33 wt%) together. Five CaCas-MCT-starch powder mixtures were also prepared by manually mixing. All CaCas-MCT-starch powder mixtures contained 25 wt% starch, but varied in CaCas content (18.75, 25, 37.5, 50, 62.5 wt%) and corresponding MCT powder content (56.25, 50, 37.5, 25, 12.5 wt%). Mixing was done using a spatula to mix powders together followed by a sieving processing through a 250 µm mesh size. The sieving process was supposed to better separate powder particles, which allowed for a better mixing process. The spatula blending and sieving process were repeated three times to reach appropriate powder blends.

Powder bed printing was performed with a Spectrum Z510 3D printer (Z Corporation, Rock Hill, USA) at Oceanz B.V. (Ede, the Netherlands). The prepared binder (1 mM Tween 20 solution) was filled into an HP11 (type C4810A) printing cartridge using a cartridge refilling set to replace the original ink. Twelve cylinder-shape samples with a dimension of 10 mm in diameter and 10 mm in height were designed for printing. The layer thickness was always chosen as 0.1 mm, and the core saturation level was always set twice the amount of the shell saturation level. The amount of binder used for printing was varied with the shell-core saturation level in the printer software and depended on the powder mixture used. The exact binder amounts of each selected printing setting were measured to quantify the actual binder amount inside the final printed cylinders. Table 1 shows an overview of printing settings used in this study. Exactly 12 cylinders were printed for each printing setting. The printed cylinders were removed from the powder bed shortly after printing and excessive powder was carefully brushed away. The obtained cylinders were sealed in closed 50 mL containers and stored for further analysis at room temperature. Binder content in the printed sample was calculated as the ratio between deposited binder amount per printed cylinder and weight of per printed cylinder.

Post processing

Part of the printed cylinders was post-treated by heating the next day after printing. A heating step was applied to better consolidate powder particles and to prevent microbial growth. These cylinders were inserted into a custom-made aluminium mould that can be tightly closed, and the mould was further sealed inside a vacuum-sealed bag to avoid moisture loss during the heating process. The mould loaded with cylinders was heated in water bath at

80°C for 20 min and subsequently it was placed in cold water for immediate cooling. Just before texture analysis the cylinders were taken out from the mould to prevent moisture loss.

Table 3.1. Printing settings and corresponding binder amount.

Powder mixtures	Powder type (non-food)	Shell-core saturation level (%)	Binder amount (g/cylinder)
CaCas-starch	ZP150	140-280	0.18
		170-340	0.23
		200-400	0.25
	ZP102	120-240	0.28
CaCas-MCT-starch	ZP150	35-70	0.02
		70-140	0.05
		100-200	0.1
		200-400	0.25

Texture profile analysis

Texture profile analysis was carried out on both non-treated and heat-treated cylinders using a TA.XTPlusC (Stable Micro systems, Surrey, UK) texture analyser equipped with a cylindrical 40 mm diameter probe. In case the samples had a hardness exceeding the upper limit (50 N) of the TA.XTPlusC, the samples were measured using an Instron 5564 (Illinois Tool Works Inc, Glenview, USA) texture analyser. The height and diameter of each cylinder were measured before conducting texture profile analysis. Compression speed was set as 5 mm/s until a compression strain of 50% of the original height was reached throughout the whole experiment. The post-test speed was set as 5 mm/s. A holding time of 5 s was applied between two compression cycles. Samples were measured in triplicate one day after being printed. Hardness, cohesiveness and springiness were obtained from the force-distance curve. Hardness is determined as the maximum force of the first compression. Cohesiveness is calculated as the area of work during the second compression divided by the area of work during the first compression. Springiness is calculated as the distance of the sample height

before the second compression divided by the original compression distance. Measurements were done in triplicate.

Scanning electron microscopic (SEM) analysis

Scanning electron microscopic analysis was done using a FEI Magellan 400 XHR SEM (FEI company, Eindhoven). The structures were fixated in 2.5% glutaraldehyde for 48 h, and then for another 48 h in 1% osmium. After this the samples were dehydrated using ethanol (30, 50, 70, 80, 90, 100%). Finally, samples were dried using critical point drying. The samples were further vacuum dried for 48 h and consequently glued to the sample holder. Both the gel samples and powder samples were coated in 12 nm tungsten. The samples were analysed with magnifications ranging from 250 x to 20000 x.

3.3. Results and discussion

3.3.1. Particle size distribution, circularity and powder flowability

Powder flowability is one of the keys determining factors for making an even powder layer during powder bed printing (Spierings et al., 2016). Powder properties such as particle size, powder morphology, and moisture content are relevant for powder flowability. Table 3.2 shows the particle size distribution and circularity of CaCas, MCT, and starch powders. CaCas powder particles were larger in size than MCT and starch powder particles, which is related to the degree of agglomeration of this powder. Circularity was used to quantify how close a particle shape is close to a perfect circle. Starch granules were more spherical than CaCas and MCT powders.

The measured average angle of repose of CaCas, MCT, and starch powders was 21.6°, 37.7°, and 38.0°, respectively. A smaller repose angle can be related to a higher flowability (Beakawi Al-Hashemi & Baghabra Al-Amoudi, 2018). The higher flowability of CaCas powder may be explained by its larger particle size compared to that of MCT and starch powders. This is because the contact area between larger particles is relative smaller, which leads to less cohesive forces, e.g., van der Waals forces, and thus higher flowability (Fitzpatrick et al., 2004; Goh et al., 2018; Lavoie et al., 2002). Preliminary powder printing trials with the three different powders showed that CaCas could be best evenly distributed, which is in line with the presented results on flowability. The use of only MCT or starch

powder led to clear uneven distribution of these powders. It is noted that flowability of the powder during printing is the result of both material properties and the specific flow conditions applied during handling the powder in the printer (Prescott & Barnum, 2000). Therefore, there is no flowability testing method that can fully predict the spreading process during powder bed printing. Nevertheless, the angle of repose measurement provided a good indication of handling the selected powders during powder bed printing.

Table 3.2. Particle size distribution and circularity of CaCas, MCT and starch powders.

		CaCas	MCT	Starch
Volume based size distribution (µm)	D_{10}	70.3	38.69	18.7
	D_{50}	151.6	93.32	29.9
	D_{90}	302.0	132.2	50.0
	D [4.3]	172.4	92.32	35.9
Circularity	D_{10}	0.59	0.552	0.68
	D_{50}	0.92	0.907	0.96
	D_{90}	0.98	0.982	0.99
	D [4.3]	0.85	0.827	0.89

3.3.2. Starch addition reduces powder swelling upon hydration

Initial printing trials with CaCas powder showed significant swelling upon deposition of the binder onto the powder bed hampering subsequent application of powder layers. To visualize the swelling of CaCas powder upon hydration, optical microscope images were taken of a single CaCas powder particle during hydration as function of time (Fig 3.1). The CaCas particle swelled almost instantly upon binder addition and continued swelling throughout the entire 120 s measurement period. Similar swelling behaviour of native casein and caseinate powders during hydration has been reported in several previous studies as quantified by turbidity, rheology, or particle size measurement (Felix da Silva et al., 2018; Gaiani et al., 2006, 2007; Ji et al., 2016).
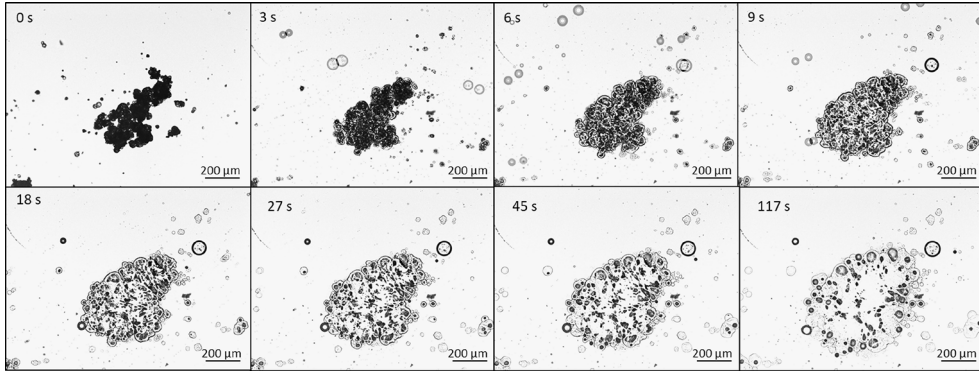
Figure 3.1. Swelling of a CaCas powder particle during hydration as function of time as visualized with an optical microscope.

To reduce the swelling of the powder bed upon binder addition, native wheat starch was mixed with CaCas powder in different ratios. A droplet of binder was dispensed onto a prepared powder layer and the distance between the wetted surface and dry powder bed surface was measured to assess the degree of swelling (Fig 3.2A). The wetted surface of pure CaCas powder mixtures was approximately 150 μm higher than the original dry powder bed surface, indicating the swelling of CaCas powder bed upon binder addition. Mixing starch with the CaCas effectively led to less swelling of the powder upon hydration. With more than 33% starch in the powder mixture, the wetted powder surface dropped below that of the original dry powder bed, indicating a collapse of the powder at the spot where the binder was deposited.

To understand the influence of starch addition on swelling behaviour we measured the tapped specific volume of CaCas and starch mixtures, which is shown in Figure 3.2B. The specific volume reduced with increasing starch content, indicating that a more compact structure is obtained in the presence of more starch. This can be explained because the small starch granules can fill interstitial voids of a randomly packed CaCas powder bed. The particle size ratio of CaCas-starch mixture is approximately 5:1 (Table 3.2). If we assume that starch does not contribute to the specific volume, then the assumed powder mixture volume ($V_{assumption}$) would be the same as the specific volume occupied by CaCas (V_{CaCas}).

$$V_{CaCas} = V_{pure\_CaCas}\emptyset_{CaCas} \tag{3.1}$$

Where V_{pure_CaCas} represents the powder volume of CaCas, and $Ø_{CaCas}$ is the mass fraction of CaCas in the CaCas-starch powder mixtures. The calculated powder volume based on the CaCas only is shown in Figure 3.2B next to the measured specific volume of the mixtures. Below 33% starch addition, the starch does not contribute to the specific bed volume. Above 33% starch the specific volume of the mixture became smaller than the volume based on CaCas only, which indicates that starch particles are not only 'hidden' in the voids but also add to the specific volume. We hypothesize that when a small amount of binder is added to starch powder, liquid bridges are formed at the contact points between the granules due to surface tension (Kudrolli, 2008). The formed liquid bridges induce cohesion between granules and cause agglomeration and dense packing of starch particles into geometric clusters. As a result, starch granules are likely to position themselves into more ordered arrangements, which reduces total volume. In contrast to starch particles, CaCas particles absorb water during hydration and grow in size. It is thus expected that starch powder particles cluster and collapse upon hydration and thus compensate swelling of CaCas particles.
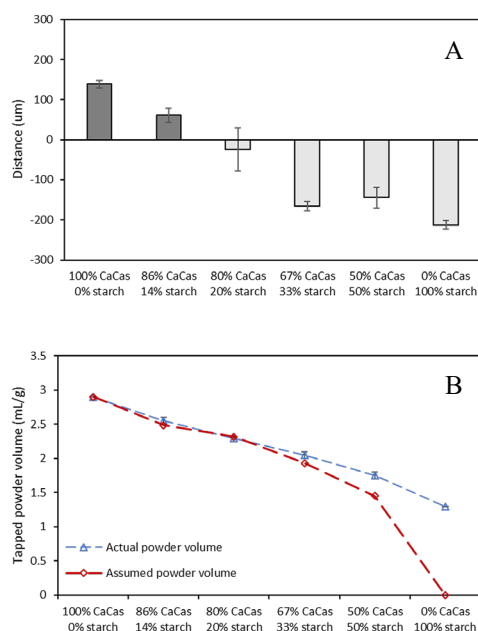

Figure 3.2. Relative distance of wetted powder bed surface compared to (A) original powder bed surface and (B) tapped powder volume of CaCas-starch powder mixtures (B).

Figure 3.3 shows a schematic drawing of how the volume of CaCas-starch powder mixtures changed when binder is added. Pure CaCas powders swell when a binder is deposited onto the prepared powder bed. When a small amount (14%) of starch is included in the powder mixture, starch granules fill the voids of CaCas powders. Upon binder addition, liquid bridges are formed in between starch granules causing only some local aggregated starch clusters. When more starch (33%) is present, agglomeration of starch granules causes more volume reduction, which compensates for the swelling of CaCas particles. When a binder is deposited onto a powder bed of pure starch granules, a cavity forms due to agglomeration and clustering of starch granules. The reasoning further suggests that the formation of liquid bridges in between starch granules is faster than the hydration and swelling process of CaCas particles. It is worth to mention that the minimum amount of starch needed in CaCas powder mixtures to reduce swelling of powder bed upon binder addition is very likely to depend on botanical source of starch. Native starch granules obtained from different botanical source have large variation in both shapes (spheres, ellipsoids, polygons, platelets, irregular tubules) and sizes (from 0.1 to over 200 µm). The shape and size of granules will influence surface area, packing density and internal voids of powder mixtures, which can further influence binder penetration behavior (Hapgood et al., 2002) and shrinkage rate (Mirzababaei and Pasebani, 2019).

To sum up, the addition of over 33% starch powder to CaCas powder reduced swelling upon binder addition due to two reasons: 1). more necking sites were available in between particles due to the added starch filling the voids of coarse CaCas powder particles; 2). starch granules formed a continuous phase in powder mixtures in which larger CaCas particles were trapped.
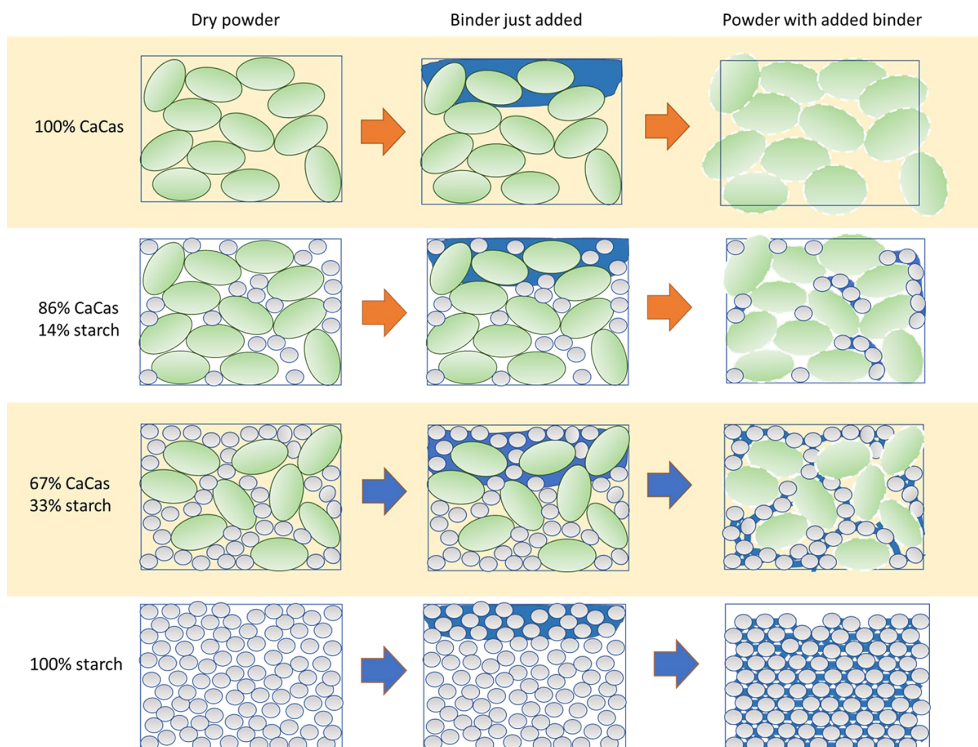
Figure 3.3. Schematic drawing of volume change of CaCas, starch and their mixtures upon binder addition.

3.3.3. Printing using CaCas-starch mixtures

Deposition of binder on powder mixtures with too much CaCas causes swelling of the top powder layer, which affected the application of the subsequent powder layer during printing and thus impaired the process such that the printed object became distorted. For the cylinders that were successfully printed the swelling of printed cylinders took primarily place after printing and continued during overnight storage. Figure 3.4 shows the heights of the printed cylinders after one day storage. Clearly, not all cylinders had the final pre-designed height of 10 mm. The height of printed structures depended both on CaCas and binder contents. A reduction in height of printed cylinders is observed when reducing CaCas content in powder mixtures. This observation is probably also related to the swelling of the CaCas particles. Even though the heights of cylinders printed with 60 and 67% CaCas were more than 10 mm, no observable swelling was observed during the printing process. This could be possibly due

to moisture redistribution inside printed objects, which led to delayed swelling of CaCas particles. More binder resulted in decreased cylinder height, which may be explained by the enhanced agglomeration and rearrangement of starch granules, also assisted by gravity (Kudrolli, 2008).
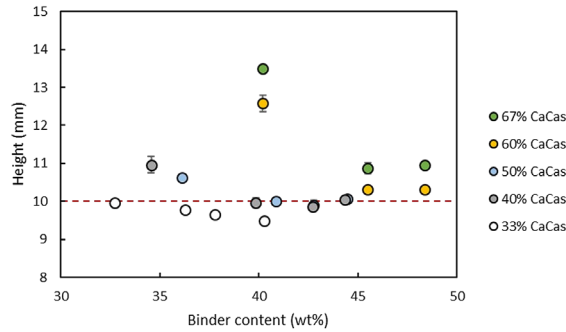

Figure 3.4. Heights of powder bed printed cylinders using CaCas-starch mixtures after 1-day storage. Red dashed line is the designed cylinder height. Legends indicate the CaCas content in the CaCas-starch powder mixtures.
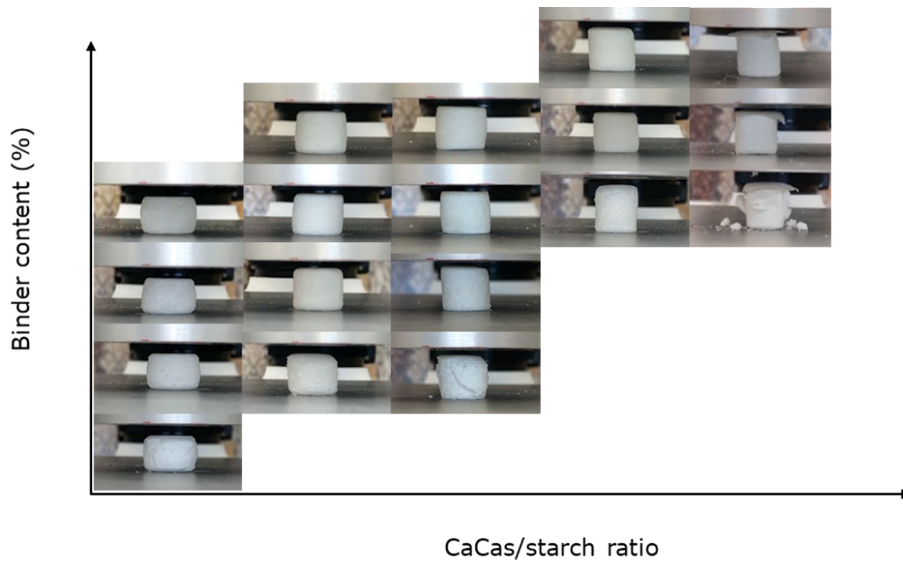

Figure 3.5. Visual overview of cylinders printed with CaCas-starch mixtures after performing texture profile analysis.

Figure 3.5 shows an overview of cylinders printed with CaCas-starch mixtures after performing texture profile analysis. Most of the printed cylinders remained intact after the

double compression and were springy. Textural properties of printed cylinders are shown in Figure 3.6. The cohesiveness of printed cylinders was strongly influenced by the deposited binder amount (Fig 3.6-A1). A higher binder content led to increased cohesiveness of printed cylinders. The cohesiveness of cylinders printed with 33-60% CaCas increased linearly with increasing binder content, while a lower cohesiveness was found for cylinders printed with 67% CaCas at a lower binder content of 40%. It is assumed that 40% binder content was not enough to form strong liquid bridges between the starch granules. It was not possible to print with a powder mixture containing 67% CaCas with a lower binder amount due to severe swelling during the printing process. Heat treatment increased the cohesiveness of printed cylinders (Fig 3.6-A2).

The CaCas content affected the springiness of printed cylinders (Fig 3.6-B1). Cylinders printed with powder mixtures containing 40-67% CaCas had comparable springiness and were more springy than those printed with powder mixtures containing 33% CaCas. (Thomar et al., 2013) studied rheology properties of CaCas over a wide range of concentrations. They reported a sharp increase in elastic modulus of CaCas at a concentration between 160 g/L and 200 g/L due to the formation of a viscoelastic suspension, which was caused by sudden connectivity between the dense protein domains or micelles present in CaCas. A further increase of CaCas concentration only slightly increased the elastic modulus of the studied solution. In our case, it is hard to calculate the actual mass concentration of CaCas in printed cylinders due to the porous structure. However, a rough estimation based on CaCas content and printed cylinder volume suggests that the mass concentration of CaCas in printed cylinders using powder mixtures containing 40-67% CaCas was indeed higher than 200 g/L. This concentration was not achieved in powder mixtures containing 33% CaCas or less. Figure 3.6-B2 shows the influence of heat treatment on the springiness of printed samples. A decrease in springiness was observed for cylinders printed with a powder mixture with 40-67% CaCas after heating. It is known that native starch granules swell upon heating (Choi & Kerr, 2004). Starch granules competed for water with CaCas during the heating step and the size change of swelled starch granules possibly influenced the rheological properties of the mixture. Alternatively, we may expect rehydrated CaCas powders to undergo plastic deformation upon heating, which may also contribute to a decreased springiness after heating.

The hardness of printed cylinders was influenced both by the deposited binder amount and CaCas content (Fig 3.6-C1). The heating process had a large influence on sample hardness (Fig 3.6-C2). An increase in hardness was observed for all printed samples after heat treatment. Heat-treated samples with higher CaCas content were found to be harder than those printed with powder mixtures containing less CaCas content. Besides, the hardness was also found to be negatively correlated with binder content in the heat-treated samples.

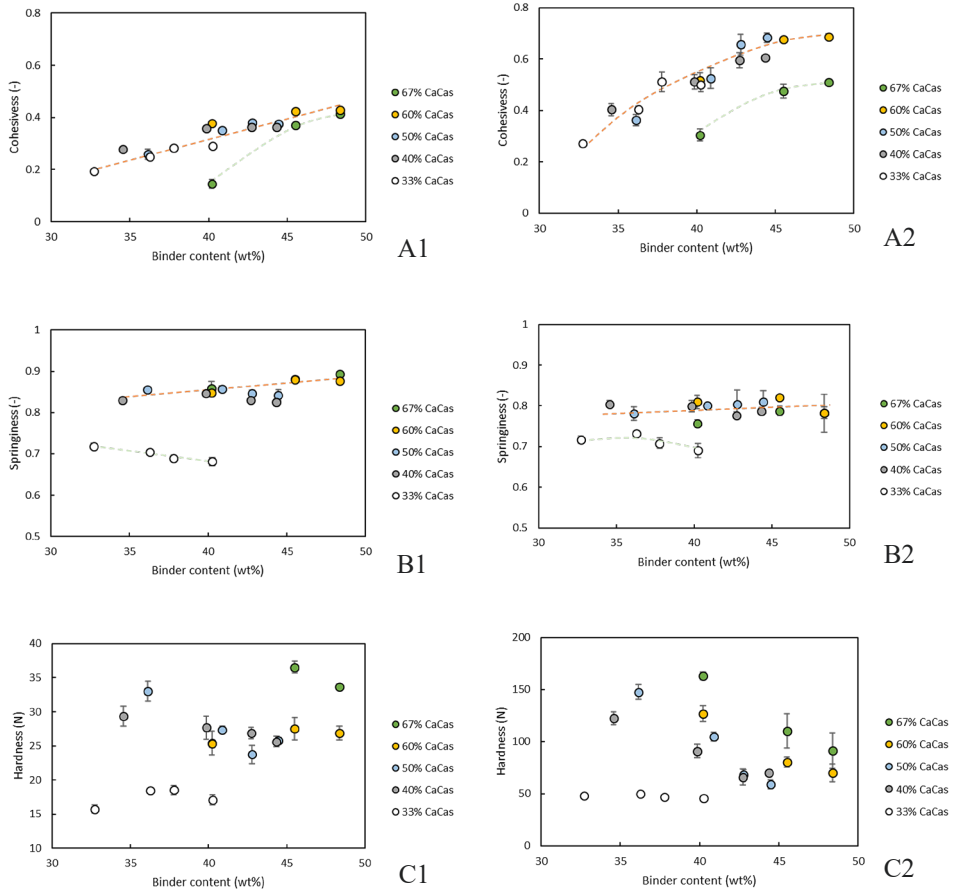**Figure 3.6.** Texture properties of powder bed printed cylinders using CaCas and starch mixtures. A1, B1 and C1 represent cohesiveness, springiness and hardness of freshly printed samples, respectively; A2, B2 and C2 represent cohesiveness, springiness and hardness of printed samples after additional heating. Dashed lines are drawn for guiding the eye. Legends indicate the CaCas content in the CaCas-starch powder mixture on dry basis.

3.3.4. Printing using CaCas-MCT-starch mixtures

Fat, one of the main macronutrients in the human diet, is not only an important source of energy, but also acts as a carrier for flavour and vitamin, and provides consumers desirable mouthfeel (Sanders, 2016). Commercial protein-rich foods such as protein bars often contain MCT as a main fat source. Therefore, it is interesting to investigate how MCT influences the texture of printed samples.

Printing with powder mixtures containing only CaCas and MCT powder was found to be rather challenging. Initial experiments suggested that despite the printing significantly improved by adding MCT to CaCas powder, printed objects were all distorted in shape to a certain extent. Liquid oil was likely to be released from MCT powder once wetted with binder, after which the released oil helped 'gluing' neighbouring CaCas particles. The oil acts in that sense also as a binder and agglomerates particles together (Písecký, 2012). The partial distortion of printed structures was probably mainly again due to the gradual swelling of CaCas, which affected the printing process negatively. By adding starch (25%) in the powder mixtures, we were able to obtain non-distorted printed cylinders. Therefore, all subsequent experiments were carried out with powder mixtures having 25% starch on dry basis.

Figure 3.7 shows the heights of printed cylinders using CaCas-MCT-starch powder mixtures. All printed cylinders had heights exceeding the designed dimension (10 mm). Similar to CaCas-starch mixtures, the increase in height took place after completion of the printing process. The maximum CaCas content for successful printing was 62.5%, and further increasing CaCas content lead again to distortion of printed structures. Printed cylinder heights with low protein content (25% and 18.75% CaCas) were not much influenced by binder content in printed objects, while cylinder heights with high protein content (above 37.5% CaCas) mixtures were largely affected by binder amount. The ones printed with high protein content mixtures showed maximum cylinder height at around 10% binder content and then reduced in height as binder content increased.
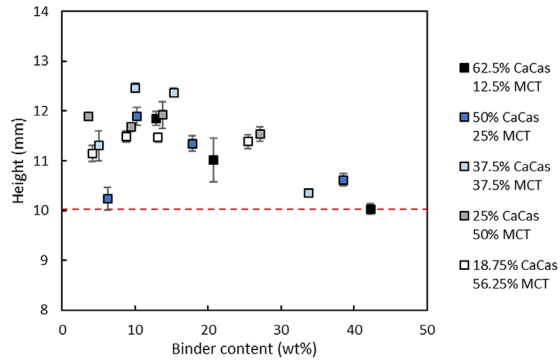
Figure 3.7. Heights of powder bed printed cylinders using CaCas-MCT-starch powder mixtures. All samples contained 25% starch in the dry powder mix. Red dashed line is the designed cylinder height.
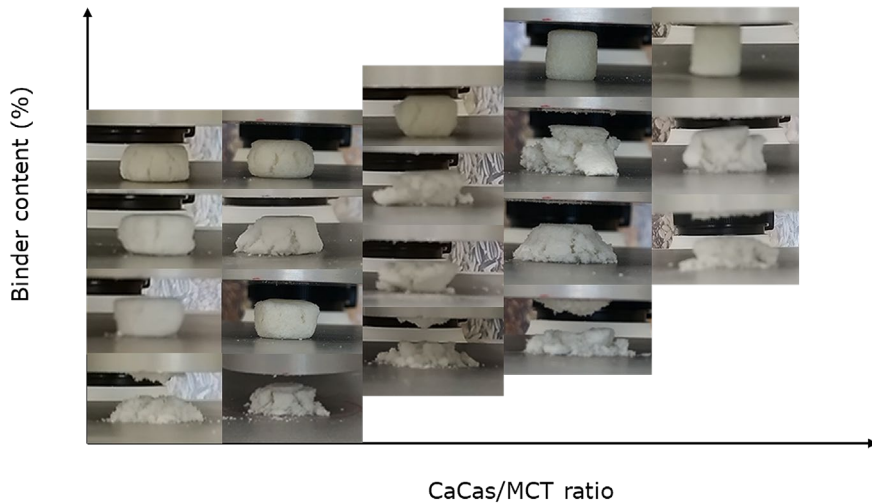
Figure 3.8. Visual overview of cylinders printed with CaCas-MCT-starch mixtures after performing texture profile analysis.

Figure 3.8 shows an overview of samples printed with CaCas-MCT-starch mixtures after performing texture profile analysis. Textures of printed cylinders can be either powdery, crumble, or springy depending on the CaCas content and binder amount. Textural properties of cylinders printed with CaCas-MCT-starch mixtures are shown in Figure 3.9. A higher binder content contributed to a more cohesive structure (Fig 3.9-A1). Cylinders printed using low CaCas content mixtures showed a different trend of increase in cohesiveness compared to those printed with high CaCas content mixtures. When the binder content was below 30%,

cylinders printed with low CaCas content mixtures were more cohesive than those printed with high CaCas content powder mixtures. This might be due to the presence of more MCT powder in powder mixtures containing less CaCas. As mentioned before, MCT powders likely released oil when wetted by the binder, and the released oil led to agglomeration of CaCas powders. The latter assisted the agglomeration caused by the binder. Figure 3.10 shows an example of the microstructure of a printed cylinder with CaCas-MCT-starch mixtures. It is likely that the oil acted as a glue between the neighbouring powders. Therefore, more wetted MCT powders were likely to lead to a more cohesive structure. The additional heat treatment did not have a large impact on the cohesiveness of the printed cylinders, except for those printed with high CaCas content mixtures at binder contents between 13-40% (Fig 3.9-A2). Figure 3.10 shows microstructural changes for printed cylinders before and after heat treatment. For samples printed with 18.75% CaCas content powder mixtures, no obvious structure change could be observed upon heat treatment (Fig 3.11-A1&A2). Samples printed with 62.5% CaCas had a more granular structure (Fig 3.11-B1) compared with samples printed with 18.75% CaCas (Fig 3.11-A1) when they both contained 13% binder amount. It is likely that such a binder amount was not enough to fully release the oil from the MCT powder, and thus starch and CaCas powders were not well bound. After the heat treatment, a denser structure was observed (Fig 3.11-B1). CaCas powder particles were deformed and filled the voids of the printed structure during heat treatment. Samples printed with 62.5% CaCas powder mixtures with 21% binder content (Fig 3.11-C1) were denser in structure compared to that with 13% binder content (Fig 3.11-B1). The increased binder amount seemed to wet or even plasticize more of the MCT powder.

Similar to cohesiveness, a higher binder content also contributed to a springier texture (Fig 3.9-B1), and different trends of increase in springiness were observed between cylinders printed using low CaCas content and high CaCas content mixtures. The heating process did not have much influence on the springiness of printed samples, except for the cylinders printed with powder mixtures containing 50% and 62.5% CaCas with a binder content less than 15% (Fig 3.9-B2).

The hardness of cylinders printed with high CaCas content depended largely on binder content (Fig 3.9-C1). A sharp increase in hardness was observed for these samples with increased binder content up to 20%. Further increasing binder content did not seem to

influence hardness. Hardness increased dramatically for cylinders printed with high CaCas content after heat treatment (Fig 3.9-C2). The hardness of these samples first increased with increasing binder content up to 20%. Further increasing binder content reduced the hardness of heat-treated samples.
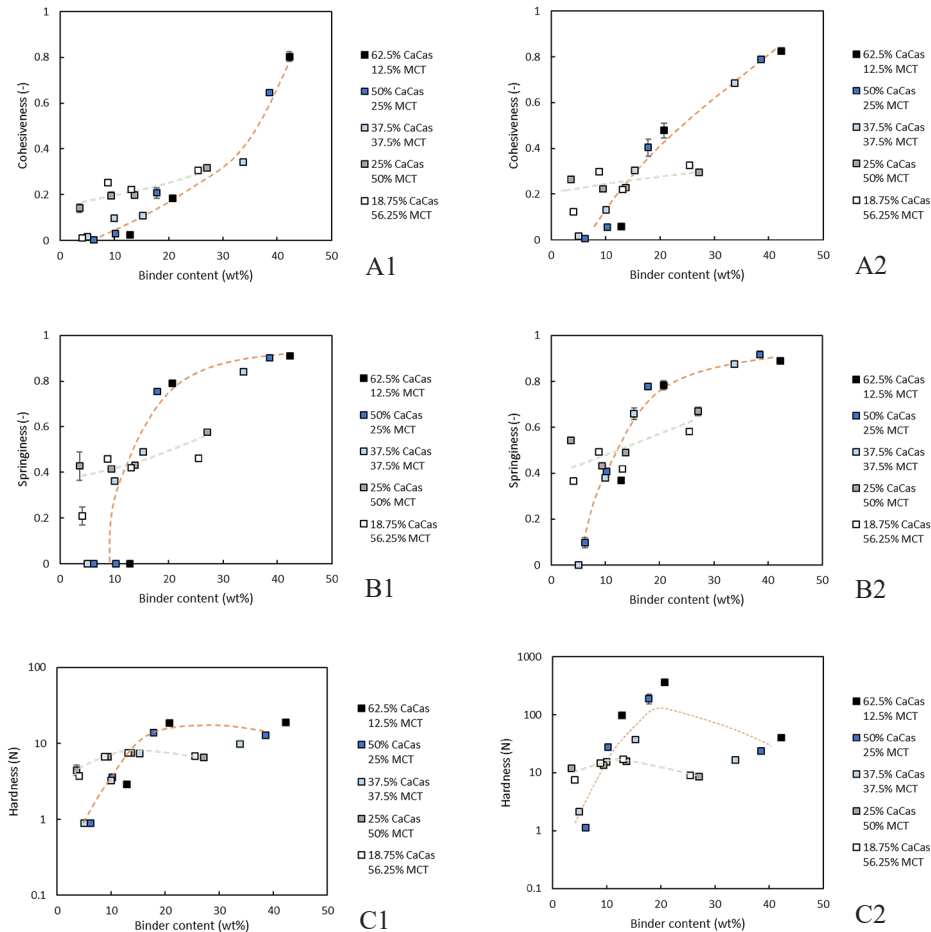
Figure 3.9. Texture properties of powder bed printed cylinders using CaCas-MCT-starch mixtures. All powder mixtures contained 25% starch on dry basis next to MCT and CaCas as indicated in the legend. A1, B1 and C1 represent cohesiveness, springiness and hardness of freshly printed samples, respectively; A2, B2 and C2 represent cohesiveness, springiness and hardness of printed samples after heating, respectively. Dashed lines are drawn to guide the eye.
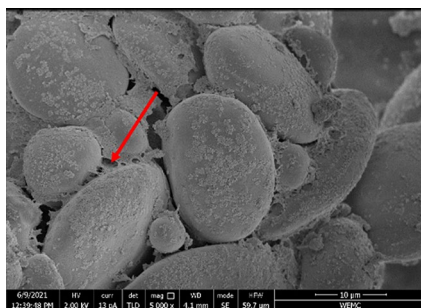
Figure 3.10. Scanning electron microscope image of printed sample using a powder mixture of 18.75% CaCas, 56.25% MCT and 25% starch, and the deposited binder content was 13% based on the total sample weight. The red arrow most probably indicates released MCT oil acting as a glue.
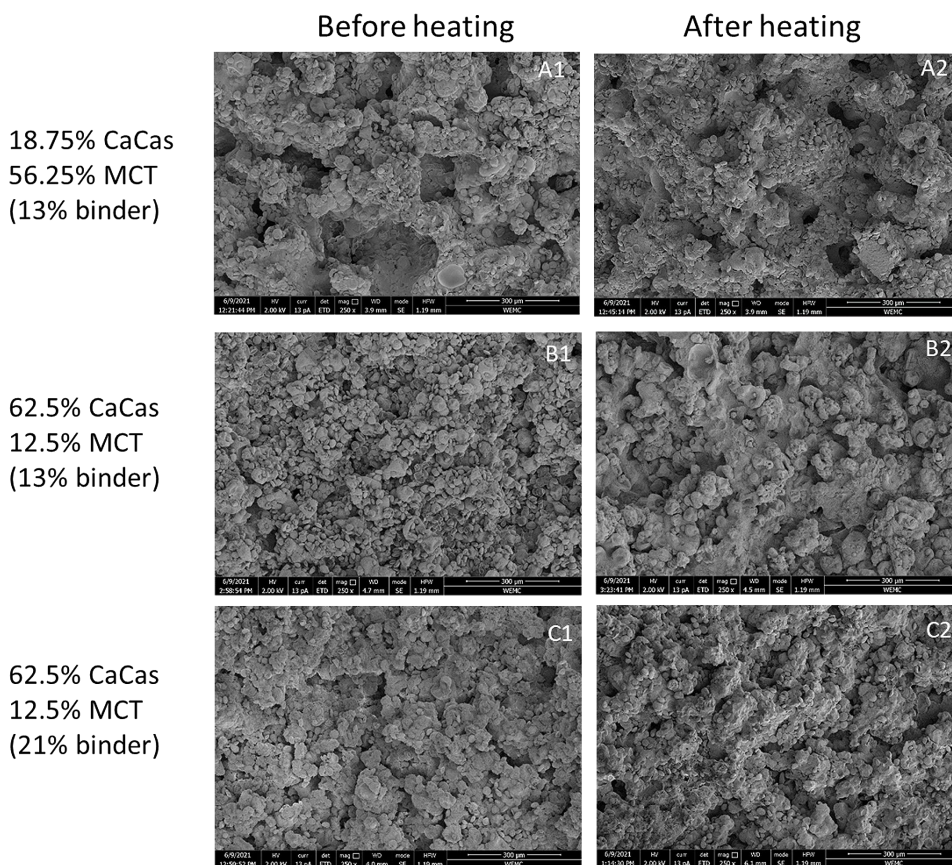
Figure 3.11. Scanning electron microscope images of selected powder bed printed cylinders using CaCas-MCT-starch powder mixtures. All samples contained 25% starch in the dry powder mix.

3.4. Conclusions

This study demonstrated the feasibility of using CaCas to create printed protein-rich structures using binder jet 3D printing. Both CaCas-starch and CaCas-starch-MCT powder mixtures were varied in CaCas content and printed with different binder amounts. Starch addition was found to effectively enable printing of CaCas formulations without distortion of the printed objects. It was found that increasing binder content in printed products always led to a more cohesive sample, and that protein content in dry powder mixtures greatly influenced the springiness of the final product. By changing the deposited binder amount and CaCas content in the dry powder mixtures, a broad range of structures such as crumble cake-like or springy wine gum-like structures can be achieved as printed structures. This study investigated the role of different components for optimal binder jet 3D printing of protein-rich formulation and demonstrated preparation of protein-rich product prototypes that can be made with binder jet 3D printing. This technology provides new opportunities for preparation of for example personalized protein-rich products, such as protein bars having a springy wine-gum like texture. It also enables us to think outside the box and create protein-rich foods with customized shape, texture, colour, and unconventional mouthfeel. Since binder jet 3D printing has not been widely studied using food materials, we hope this work can inspire researchers and provide opportunities for the application of this technology in the food sector.

Chapter 4

Shear-induced structuring of phase-separated sodium caseinate - sodium alginate blends using extrusion-based 3D printing: Creation of anisotropic aligned micron-size fibrous structures and macroscale filament bundles

Abstract

3D food printing is considered a promising method to prepare personalised foods having unique macroscopic design and composition. It is still challenging to create 3D printed foods with tailored microstructure, e.g., fibrous microstructures, to print meat-like foods. In this study we aimed at the preparation of 3D printed model food gels that have macro- and microscale aligned fibrous structures using sodium caseinate - sodium alginate (SC/SA) blends. A bath containing an agar fluid gel was used to allow precise deposition and solidification of the SC/SA blend after the printing process. Besides, the influences of nozzle type and printing speeds on texture were assessed. We successfully created aligned micron-size fibrous structures and macroscale aligned filament bundles. Filaments extruded using tapered nozzles had finer fibrous structures compared to those extruded using straight nozzles. Both printing speed and nozzle type significantly influenced Young's moduli of 3D printed model food gels. A higher printing speed resulted in smaller Young's moduli of individual printed filaments. This study shows that anisotropic structures can be created by extrusion-based 3D printing of phase-separated sodium caseinate - sodium alginate blends. The results of this study could become relevant when striving for meat analogues made by 3D-printing.

4.1. Introduction

Driven by health awareness and environmental concerns among consumers, the global market of meat analogues shows rapid growth in recent years (Ismail et al., 2020). Various food manufacturing technologies such as extrusion cooking and shear cell technology have been studied to create whole cut types of meat analogues that display both microscale and macroscale anisotropic fibrous structures (Kyriakopoulou et al., 2018). The underlying texturizing mechanism is known as the solidification of phase-separated food systems in which a liquid dispersed phase is deformed and aligned under shear flow (Dekkers et al., 2018; Tolstoguzov, 2006). Dekkers et al., (2016) obtained fibrous structures with a blend of pectin and soy protein isolate using shear cell technology. The authors observed that elongated pectin filaments being oriented in the direction of shear flow were entrapped in a continuous soy protein phase. In both extrusion cooking and shear cell technology, the solidification process of phase-separated systems was achieved through cooling, where the continuous, soy protein rich phase transits from a viscous state to a more elastic state (Pietsch et al., 2019; Schreuders et al., 2021). Shear-induced structuring of phase-separated food blends can also be achieved using other technologies that generate desired shear flow. Examples of those technologies include microfluidic devices (Takayama & Kato, 2018), spinning and extrusion-based 3D printers.

Extrusion-based 3D printing is an emerging food manufacturing technique that allows layer by layer deposition of three-dimensional structures according to a digital design (Sun et al., 2015). 3D printing has the potential to create foods with complex shapes (BluRhapsody, 2022), personalized nutrition (Escalante-Aburto et al., 2021) and to alter sensory perception of foods (Khemacheevakul et al., 2021; Kistler et al., 2021; Zhu et al., 2021). To date, only few studies have investigated the creation of aligned fibrous structures that might be considered meat-like structures using 3D printing technologies (Kim et al., 2021; Ko et al., 2021). In these studies, the 3D printed aligned fibrous structures had mostly a diameter around 1 mm, which is much larger than that of real muscle fibres (20-100 µm) (Feher, 2017). In order to create 3D printed micro-scale fibrous structures, new printing formulations and adapted printing methods are required. A promising approach is the use of protein-polysaccharide blends, e.g., caseinate-alginate mixtures that were recently employed to create micron size fibril bundles (Takayama & Kato, 2018). Caseinate-alginate mixtures were extruded with a co-flow microfluidic device during which fibrous micro-structures were formed. Subsequently, the structures were solidified in calcium chloride solutions. The influence of the shear profile during the extrusion process on

micro fibrillar structure formation is unknown. Additionally, it is not known whether or how the extruded fibres can be bundled into larger macroscopic structures.

3D printing of viscous liquids, i.e., caseinate-alginate mixtures, can be challenging since the extruded viscous liquids do not hold their shape after deposition onto a platform. 3D printing of caseinate-alginate mixtures into calcium-containing solutions is also not possible because the printed filaments are easily dragged by the moving print head, which causes printing failure. Recently, a 3D bioprinting technique termed "Freeform Reversible Embedding of Suspended Hydrogels (FRESH) has been developed to enable deposition of hydrogels (Hinton et al., 2015). The FRESH technique applies a supporting bath consisting of thermo-reversible gelatine microparticles that can initiate gelling of printed bio-ink due to the presence of crosslinking compounds. Such gel systems are often referred to as fluid gels, i.e., a suspension of gelled particles that are dispersed in a non-gelled continuous medium (Garrec & Norton, 2012). The advantage of fluid gels is that they behave as a fluid when sheared but as a solid in rest.

In this study we investigated the use of extrusion-based 3D printing to prepare fibre bundles using caseinate-alginate blends and create macroscale fibrous structures via layer-by-layer deposition. We investigated the influence of extrusion conditions on the microstructural change of caseinate-alginate (SC/SA) blends and the feasibility of creating both macroscale and microscale aligned fibrous structures using extrusion-based 3D printing technology. First, SC/SA blends were prepared and extruded with different extrusion speeds and nozzle types, and the obtained structures and textures were assessed by microscopic and tensile mechanical analysis. To enable accurate deposition and solidification of the extruded SC/SA fibre bundles, the extrudate was deposited into an agar fluid gel bath. Finally, the solidification process and textural properties of the structures were studied to identify the conditions to obtain macroscopic anisotropic fibrous structures.

4.2. Materials and methods

4.2.1. Materials

A concentrated sodium caseinate dispersion (48% dry matter content) was kindly provided by Royal FrieslandCampina. Sodium alginate powder (Rudin®ProVega, Netherlands) was kindly provided by Ruitenberg Ingredients. Calcium chloride ($CaCl_2$) (Sigma-Aldrich, Netherlands) and Agar powder (Sigma-Aldrich, Netherlands) were purchased from MilliporeSigma.

4.2.2. Preparation of SC/SA blend

SC/SA blends were prepared according to (Capron et al., 2001; Takayama & Kato, 2018) with slight modifications. A 10 wt% sodium caseinate dispersion was prepared by mixing concentrated sodium caseinate with Milli-Q water and stirred at 80°C for 30 min. The 10 wt% sodium caseinate dispersion was centrifuged at 15000 G at 20°C for 60 min to remove any undissolved aggregates. A 4 wt% sodium alginate solution was prepared by mixing sodium alginate powder with Milli-Q water. The sodium alginate solution was stirred at 80°C for 30 min followed by additional stirring at room temperature for 30 min to ensure dissolution of sodium alginate. A mixture of sodium caseinate and sodium alginate (SC-SA stock solution) was prepared by mixing 660 g of 10 wt% sodium caseinate dispersion with 220 g of 4 wt% sodium alginate solution and stirring at room temperature for 60 min. The SC-SA stock solution was centrifuged at 15000 g at 20°C for 2 hours to separate the alginate-rich phase (top) from the caseinate-rich phase (bottom). The SC/SA blend was obtained by mixing 30 g SC-rich phase with 70 g SA-rich phase at 300 rpm for 2 min using a planetary mixer (Thinky ARV 310, Japan).

4.2.3. Preparation of agar fluid gels

A 1% agar solution was heated at 90 °C for 30 min to allow dissolution. To obtain agar fluid gels, the heated agar solution was passed through a lab-scale colloid mill (IKA magic LAB®, IKA Staufen, Germany) with circulating cooling water of 5°C. The gap width was set to 0.159 mm and a rotational speed of 20,000 rpm was applied. The shearing-cooling process was repeated until the agar fluid gel reached a temperature of 15°C. $CaCl_2$ was added to agar fluid gel in order to crosslink printed SC/SA blend. To study the influence of $CaCl_2$ on the rheological properties of the agar fluid gel, $CaCl_2$ was either added to a heated agar solution before the shear-cooling process or directly mixed into the obtained agar fluid gel. $CaCl_2$ was added to heated agar solution or already prepared agar fluid gel at various concentrations (0.12, 0.25, 0.33, 0.55 and 1.1 wt%).

4.2.4. Rheology characterization of the agar fluid gel

Rheological measurements were conducted with a MCR 502 rheometer (Anton Paar, Austria) equipped with a concentric cylinder (CC17). A Step test with pre-set oscillation for three test

intervals was used to assess the breakdown of the agar fluid gel under shear and its subsequent recovery. A pre-set shear strain (1%) was applied for the first and third test intervals to simulate the behaviour at rest before and after high shearing. For the second test interval, the strain was set to 100% to simulate the flow behaviour when moving the printing nozzles inside a fluid gel. Measurements were performed for 30 s each for the first and second test interval, and 120 s for the thirst test interval. All measurements were done at 20°C using a frequency of 1 Hz. The storage modulus (G') at the end of the first interval was obtained, and structural regeneration was determined as the percentage of recovery of G' at 60 s in the third interval compared with the G' at the end of first interval.

4.2.5. Single string extrusion of SC/SA blends

To study the influence of shear profiles on microstructure of SC/SA blends during the extrusion process, SC/SA blends were loaded into a 30 mL syringe barrel and extruded into 0.12 wt% $CaCl_2$ solution using a Harvard PHD 4400 syringe pump (Harvard apparatus, USA). Four nozzle tips with an outlet diameter of 0.84 mm were used for extrusion, among which three straight tips (Optimum® general purpose dispense tips, Nordson EFD) that vary in length (6.35, 25.4, and 38.1 mm) and had a tapered tip (Optimum® SmoothFlow™ tapered dispensing tips, Nordson EFD) (31.2 mm). The SC/SA blends were extruded at 3 different volumetric flow rates (19.94, 49.85, and 99.20 mL/h) which was achieved by applying three different printing speeds (10, 25, 50 mm/s) during the 3D printing process. The extruded strings were kept in $CaCl_2$ solution for 30 min and then heated in a water bath for 10 min at 90°C. Subsequently, strings were washed with Milli Q water to remove excess $CaCl_2$ and stored for further analysis.

Figure 4.1. Nozzle tips used for extrusion and printing. Nozzles from left to right: long straight nozzle (metal part 38.1 mm), medium straight nozzle (metal part 25.4 mm), short straight nozzle (metal part 6.35 mm) and tapered nozzle (31.2 mm). All nozzles have an outlet diameter of 0.84 mm.

4.2.6. 3D printing of the SC/SA blend

Printing experiments were performed using a byFlow 3D printer (byFlow B.V., the Netherlands). A printing design of a cuboid with a dimension of $70 \times 80 \times 1.8$ mm (l × w × h) was used for printing. Layer height for the printed structure was set as 0.6 mm and the infill pattern was set as 'aligned rectilinear'. The cuboid-shaped structure was made with three printing speeds (10, 25, and 50 mm/s) using both a straight nozzle (25.4 mm in length) and a tapered nozzle (31.2 mm in length). All experiments were performed at room temperature.

The SC/SA blends were extruded inside a fluid agar gel printing bath. Printed samples were kept at ambient temperature overnight to allow crosslinking of alginate with calcium ions. The printed samples were steamed for 10 min while leaving in the fluid agar gel bath. The heating led to melting of the agar fluid gel facilitating removal of the printed sample. Afterwards, the printed samples were washed using Milli Q water and stored for further analysis.

4.2.7. Composition analysis

The protein content of the SC-SA stock solution, SC-rich phase, SA-rich phase, and SC/SA blend were determined using a Nitrogen Analyser (Rapid N cube, Elementar Analysensysteme GmbH) with a nitrogen-to-protein conversion factor of 6.25. The alginate content was calculated

as the difference between the dry matter content and the measured protein content. All measurements were performed in duplicate.

4.2.8. Microscopic analysis

Scanning electron microscope (SEM) (Phenom™ G2 pure, Phenom-world BV, the Netherlands) was performed for visualizing the microstructures of single string samples and 3D printed samples. All samples were dried overnight in a 40°C oven before SEM analysis.

Confocal Scanning Laser Microscope (CSLM) analysis was performed to visualize the location of caseinate in SA-rich phase, SC-rich phase, SC/SA blend, and single string samples. Rhodamine B (Sigma R 6626, Sigma Aldrich) was diluted with demi water to a concentration of 0.002 wt% and was used for staining sodium caseinate. Samples were visualized with Confocal Scanning Laser Microscope type 510 (Zeiss, Oberkochen, Germany) using a 543 nm HeNe laser and a 405 nm Blue/Violet diode laser. The images were analysed with the software ZEN, the blue edition (Carl Zeiss Microscopy).

4.2.9. Tensile analysis

The mechanical properties of single strings and 3D printed samples were measured using a texture analyser (Stable Micro System, Godalming, UK). The diameters of strings were measured before the tensile test using a calliper. Young's moduli of samples were obtained via a uniaxial tensile test, which was performed at room temperature with a constant deformation speed of 2.5 mm/s.

Rectangular pieces were cut from 3D printed samples in a shape of 5×30 mm both in parallel and perpendicular to the filaments aligning direction. The thickness of the cut rectangular pieces was measured using a digital calliper (Mitutoyo, Kawasaki, Japan) to calculate the initial cross-sectional area. The edges of the cut rectangular pieces were fixed into tensile grips, resulting in an initial length of 24 mm for the sample. The Young's modulus was calculated as the slope of the initial stress-strain curve in the tensile strain range from 0.2 to 0.5. Measurements were done in triplicate.

4.2.10. Data analysis

Statistical data analysis was done using IBM SPSS statistics (version 25.0). Significant differences among samples were determined using two-way ANOVA followed by Tukey post-hoc tests. A significance level of $p < 0.05$ was chosen for all data analysis. Means together with standard deviation are reported unless stated otherwise.

4.3. Results and discussion

4.3.1. *Microstructure and composition of SC/SA blend*

When sodium caseinate and alginate are mixed in water, aqueous phase separated blends are obtained, creating so called "water in water emulsions" (Capron et al., 2001; Pacek et al., 2000). The two aqueous phases were separated via centrifugation and re-combined to obtain defined SC/SA blends comprising an SC and SA-rich phase. Figure 4.2 shows microscopic images of the SA-rich phase and SC-rich phase after centrifugation and the SC/SA blend after recombination. Both the SA-rich phase (Fig 4.2a) and the SC/SA blend (Fig 4.2c) consist of dispersed caseinate droplets, while the SC-rich phase (Fig 4.2b) consists of dispersed alginate droplets. Since the SC/SA blend is a combination of the SC-rich phase and the SA-rich phase from the SC-SA stock solution at a 3:7 ratio, larger caseinate droplets can be expected in SC/SA blends (Fig 4.2c) compared to the SA-rich phase (Fig 4.2a).

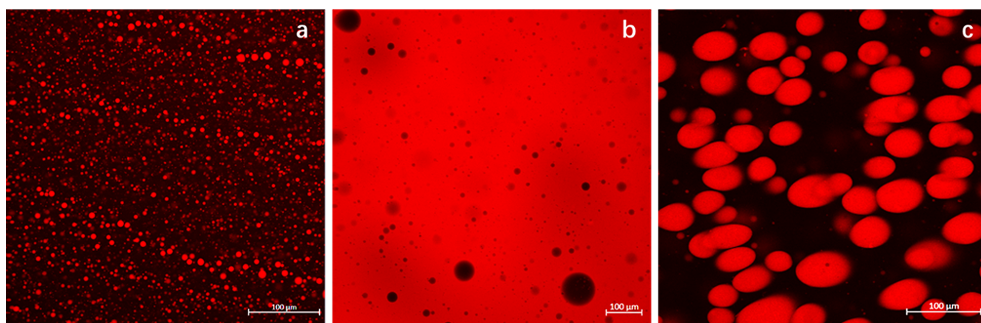**Figure 4.2.** CSLM images of (a) SA-rich phase, (b) SC-rich phase, and (c) the obtained SC/SA blend. Caseinate is stained in red.

Table 4.1 shows the composition of the original SC-SA stock solution, SC-rich phase, SA-rich phase, and recombined SC/SA blend. The difference in composition between our blends (Table 4.1) compared to the blends described previously by (Capron et al., 2001) was likely

due to the use of ingredients provided by different suppliers and the application of different methods to quantify composition.

Table 4.1. Compositions of the SC-SA stock solution, SC-rich phase, SA-rich phase, and SC/SA blend

Composition (wt%)	SC-SA stock solution	SC-rich phase	SA-rich phase	SC/SA blend
Sodium Caseinate	7.04 ± 0.01	10.08 ± 0.02	1.03 ± 0.01	3.63 ± 0.00
Sodium Alginate	1.33 ± 0.01	1.11 ± 0.02	2.20 ± 0.01	1.79 ± 0.00

4.3.2. Extrusion of single strings

4.4.2.1 Young's modulus of single printed strings

To investigate shear-induced structures of SC/SA blends during the 3D printing process, we first extruded the SC/SA blends into a 0.12 wt% calcium chloride solution. Figure 4.3 shows Young's moduli of single strings prepared at different extrusion speeds and using different nozzle types. In general, it was observed that Young's moduli of single strings decreased with increasing extrusion speed.

For the strings prepared using straight nozzles, nozzle length did not have significant effect on the Young's modulus ($F_{(2, 27)} = 2.065$, $p = 0.146$), while extrusion speed had a significant effect on the Young's modulus ($F_{(2, 27)} = 17.397$, $p < 0.001$). The Young's moduli of strings extruded at low speed (10 mm/s) were significantly higher than those extruded at medium speed (25 mm/s) ($p = 0.003$) and at high speed (50 mm/s) ($p < 0.001$). No significant difference was found between strings extruded at medium (25 mm/s) and high speed (50 mm/s) ($p = 0.094$). There was no significant interaction between the effects of nozzle length and extrusion speed on Young's modulus ($F_{(4, 27)} = 0.98$, $p = 0.435$). From the results one may conclude that fibre strength is not affected by the residence time but more by the velocity profile inside the nozzle affecting the alignment of the emulsion droplets in a different way.

A comparison of the strings prepared using a tapered nozzle and middle straight nozzle revealed that nozzle type did not have a significant effect on Young's modulus ($F_{(1, 18)} = 0.074$, $p = 0.788$), while extrusion speed had a significant effect on Young's modulus (F (2,

18) = 16.170, p < 0.001). Young's moduli of strings extruded at high speed (50 mm/s) were also here significantly lower than those extruded at low speed (10 mm/s) (p < 0.001) and those extruded at medium speed (25 mm/s) (p = 0.008). No significant difference was found between strings extruded at low speed (10 mm/s) and those extruded at medium speed (25 mm/s) (p = 0.095).
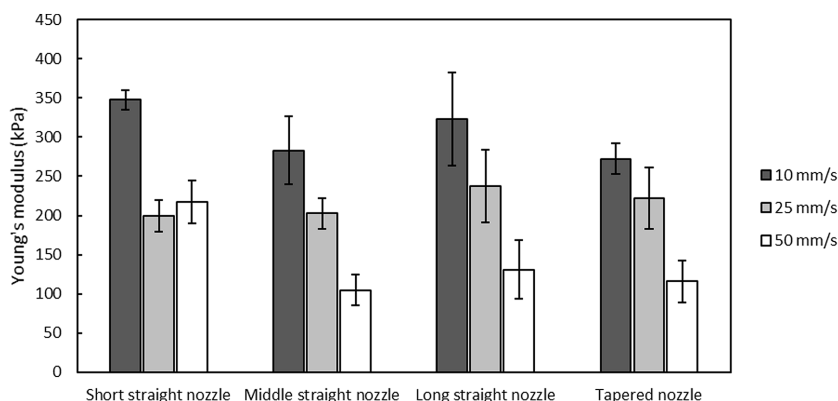

Figure 4.3. Young's moduli of single strings prepared at different extrusion speeds (corresponding to realistic printing speeds) with different nozzle types in a 0.12 wt% $CaCl_2$ solution. Means are shown together with standard deviations.

4.4.2.1 Microstructure of single extruded strings

Figure 4.4 shows SEM images of the surface structures of prepared single strings. All prepared single strings appeared to have a micron-sized fibrous structure. As can be observed from Figure 4.4, morphologies of strings extruded with the tapered nozzle were finer than those of strings extruded with straight nozzles. This difference is possibly due to the different radial velocity profiles when extruding with either straight or tapered nozzles. In straight nozzles the velocity profile remains stable along the entire flow direction, whereas in tapered nozzles the velocity gradually increases until the SC/SA blend reaches the nozzle outlet (Reina-Romo et al., 2021). Moreover, during extrusion through straight nozzles we have simple shear flow (laminar flow), while in tapered nozzles also elongational flow is expected. Since elongational flow is more effective to extend droplets than shear flow (Coussot, 2014), caseinate droplets present inside SC/SA blends may be more prone to break up into smaller droplets when extruded using a tapered nozzle. During the extrusion process, the small

droplets were stretched into elongated shape in the principal flow direction (Arrigo et al., 2021; Coussot, 2014).
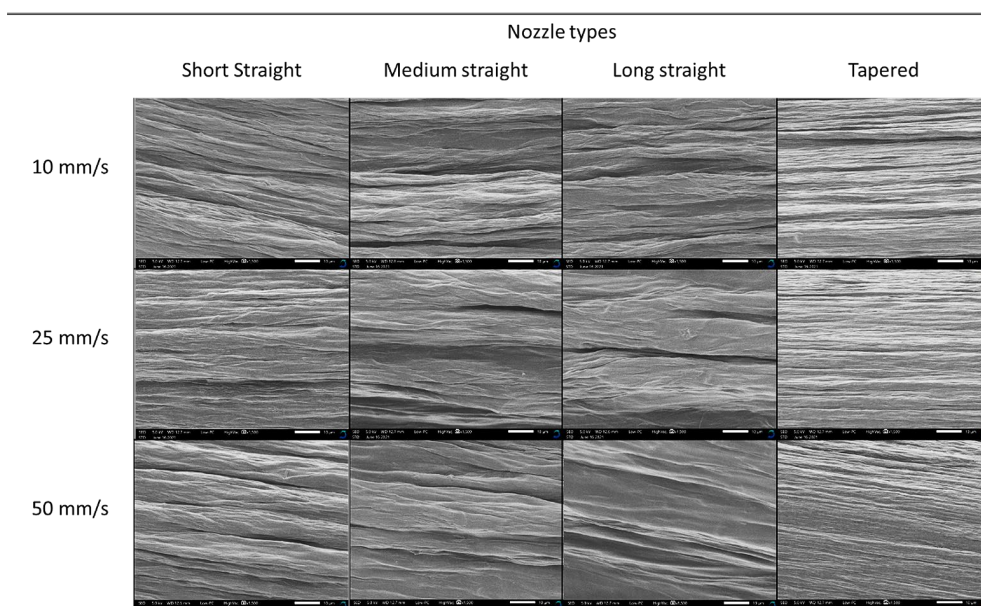

Figure 4.4. SEM images of single strings prepared at different extrusion speeds (corresponding to realistic printing speeds) and with different nozzle types. SEM images were taken at 1500 x. Scale bars in the picture correspond to 10 μm.

Another explanation for the "thicker" fibres observed in strings extruded from straight nozzles is the formation of several "bands" that were stacked in the vorticity direction. During laminar flow in a straight nozzle, the SC/SA blend moves faster near the centre of the nozzle and remains stationary next to the wall, resulting in a strong velocity gradient perpendicular to the flow direction. Though the exact mechanism is not well understood, various studies have reported the so-called 'vorticity banding' phenomenon in emulsions (Caserta et al., 2008; de Vita et al., 2020; Dhont & Briels, 2008). In this study, bands of clustered deformed droplets inside extruded strings were observed using CSLM (Fig 4.5b).

Figure 4.5 shows CLSM images of a single string extruded using a straight nozzle scanned in different depths. The structure of printed strings consists of elongated caseinate droplets (red) trapped inside crosslinked alginate gel. The elongated caseinate droplets near the string surface were smaller (Fig 4.5a-c) compared to those close to the centre of the extruded string (Fig 4.5d-f). It is possible that small caseinate droplets were also elongated close to the centre

of the extruded string during extrusion process, but they slowly coalesced into bigger droplets within the time of diffusion of calcium ions used for crosslinking surrounding alginate phase.
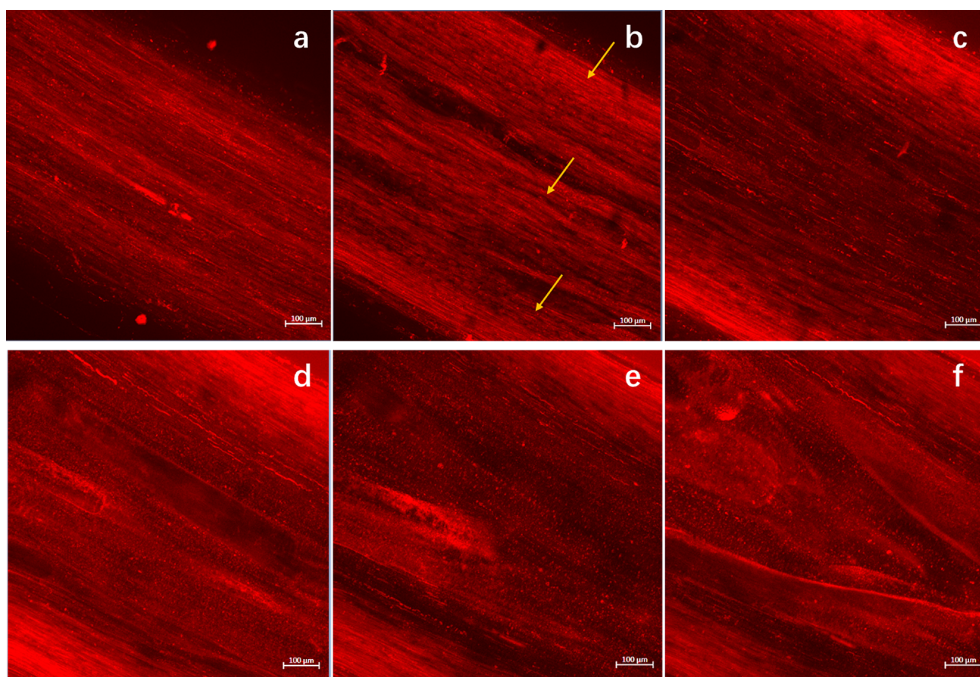

Figure 4.5. CLSM images of a single string extruded using a straight nozzle. Structures were scanned in depths of 20 μm (a), 90 μm (b), 150 μm (c), 220 μm (d), 260 μm (e) and 300 μm (f) from surface to the inner part of a string. Red colour indicates SC-rich phase. Yellow arrows in Figure 4.5b indicate three bands of clustered deformed droplets.

4.3.3. 3D Printing in a fluid gel supporting bath

In the current study, we used an agar fluid gel bath to 3D print SC/SA blends. Successful printing was achieved by depositing extruded SC/SA blends and allowing in situ solidification of printed filaments through crosslinking via calcium ions in the agar fluid gel bath.

4.4.3.1. Influence of $CaCl_2$ addition procedure on agar fluid gel rheology

The rheological properties of agar fluid gels were largely influenced by the procedure of $CaCl_2$ addition. The influence of $CaCl_2$ addition, either added before the shear-cooling process or mixed afterwards into the prepared agar fluid gel, on storage modulus and recovery behaviour of agar fluid gel can be found in Figure A.4.1 (Appendix). Agar fluid gels with

$CaCl_2$ addition before the shear-cooling process had lower G' and less recovery compared to those with $CaCl_2$ directly mixed into already obtained fluid gels. According to (Yu et al., 2020), the addition of ions like calcium reduces the viscosity of agar solutions. If we assume the shear rate to be constant during the shearing-cooling process, the shear stress being proportional to the viscosity of agar solution is likely to decrease with the presence of calcium ions. The reduced shear stress experienced by the growing nuclei may influence the morphology of the final afar gel particles, and both particle size and shape have been reported to have an impact on the rheological behaviour of agar fluid gel (Ghebremedhin et al., 2021; Norton et al., 1999).

Higher G' and recovery percentage of agar fluid gel supporting bath appeared to ensure better entrapment of printed strings. Figure 4.6 shows the printed structures in different agar gel supporting baths. When printing was performed using a fluid agar gel bath with addition of $CaCl_2$ before the shear-cooling process, printed SC/SA filaments were not able to stay in place and were dragged backward when the printing head changed its moving direction (Fig 4.6a). Better results were obtained when using a fluid agar gel bath that had $CaCl_2$ addition after fluid gel production (Fig 4.6b). Therefore, a supporting bath of fluid agar gel with afterwards added $CaCl_2$ is preferred for 3D printing experiments.
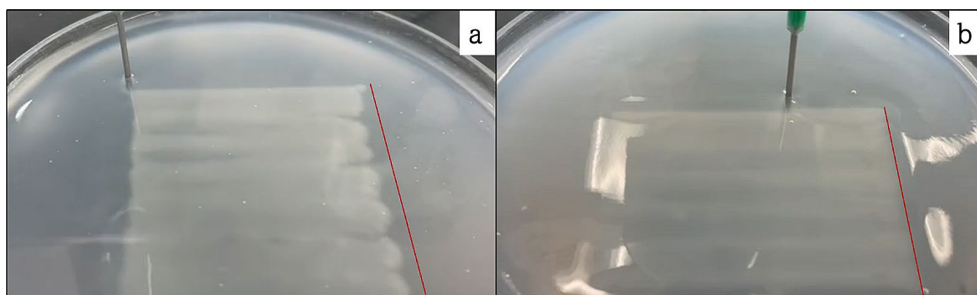

Figure 4.6. 3D printing of SC/SA blend in agar fluid gel supporting baths containing 0.25 wt% $CaCl_2$. $CaCl_2$ was either added to hot agar solution before the shear-cooling process (a) or added afterwards to obtained agar fluid gel (b). Red lines indicate the edges of designed printing figures.

4.3.3.2. Influence of $CaCl_2$ concentration on the texture of printed structures

To determine the suitable $CaCl_2$ concentration in the agar fluid gel bath, the Young's moduli of 3D printed structures were measured parallel and perpendicular to the filament orientation. The results are shown in Figure 4.7. It can be observed that the Young's moduli measured in parallel direction were higher than those measured in a perpendicular direction. In the parallel

direction, the Young's moduli of printed structures increased with increasing $CaCl_2$ content in agar fluid gel bath. The increased Young's modulus may be due to an increased crosslinking density (Li et al., 2016) related to the higher $CaCl_2$ content.

In the perpendicular direction, the Young's moduli of printed structures increased with increasing $CaCl_2$ content up to 0.3%. It was impossible to measure the Young's modulus of the structures printed in the fluid gel bath containing 0.55% $CaCl_2$ since the printed structures easily broke apart in the perpendicular direction when handling. A explanation could be that at this high $CaCl_2$ concentration crosslinking of the surface of extruded filaments is fast and thus fusion with neighbouring filaments is prevented. Based on the tensile test results shown in Figure 4.7, the agar fluid gel containing 0.25% $CaCl_2$ was chosen for later study.
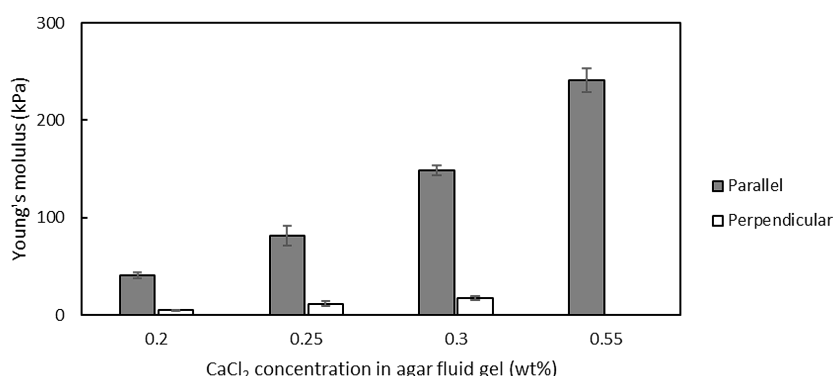

Figure 4.7. Young's moduli of 3D printed structures measured in both parallel and perpendicular directions with respect to the filament orientation. 3D printing was performed using a straight medium nozzle with a printing speed of 25 mm/s.

4.3.3.3. 3D printed structures with various shearing profile

The printed structures reduced in size after crosslinking and steaming. A higher degree of size reduction was found in the parallel direction than in the perpendicular direction for all printed samples. The higher degree of size reduction in the parallel direction was probably due to relaxation of the SC/SA blend. The study of Ko et al. (2021) observed the same phenomenon when they post-processed (by oven heating) printed meat analogues that consisted of soy protein paste, sodium alginate and other hydrocolloids. Interestingly, we also observed more size reduction in samples printed with the straight medium nozzle than for the ones printed with the tapered nozzle in both parallel and perpendicular directions.

Figure 4.8 shows the Young's moduli of 3D printed samples with either the straight medium nozzle or tapered nozzle at different printing speeds. For samples printed with straight nozzles, the Young's moduli in the parallel direction were much larger than those measured in the perpendicular direction. Differences in Young's moduli in the two directions were less pronounced for samples printed with the tapered nozzle.

In the parallel direction, the nozzle type significantly influenced the Young's modulus ($F_{(1, 12)} = 18.968$, $p = 0.001$). It is worth mentioning that although the nozzle type did not seem to influence Young's moduli of strings that were extruded into $CaCl_2$ solutions (Fig 4.3), nozzle type significantly influenced Young's moduli of 3D printed structures. A possible explanation for this is that the number of filaments in printed structures subjected to tensile test were different depending on the nozzle type used for printing. As mentioned above, more shrinkage was found in samples printed using the medium straight nozzle than in samples made with the tapered nozzle in a perpendicular direction. The larger size reduction in structures printed with the straight nozzle resulted thus in a higher fibre density for the defined sample width used in the tensile test. Therefore, although the nozzle type did not influence the Young's moduli of individual strings (Fig 4.3), higher Young's moduli were found for structures 3D printed using straight nozzles (Fig 4.8). Printing speed also appeared to have a significant influence on Young's modulus ($F_{(2, 12)} = 4.582$, $p = 0.033$), where those of the samples printed at 50 mm/s were significantly smaller than those printed at 25 mm/s ($p = 0.029$).

In perpendicular direction, the nozzle type significantly influenced the Young's modulus ($F_{(1, 12)} = 76,335$, $p < 0.001$). This may be due to a better fusion between neighbouring filaments when printing was done using the tapered nozzle (Appendix: Fig A.4.2). The better fusion suggests less complete crosslinking of alginate at the surface of individual filaments that were extruded using the tapered nozzle allowing subsequent fusion of filaments.
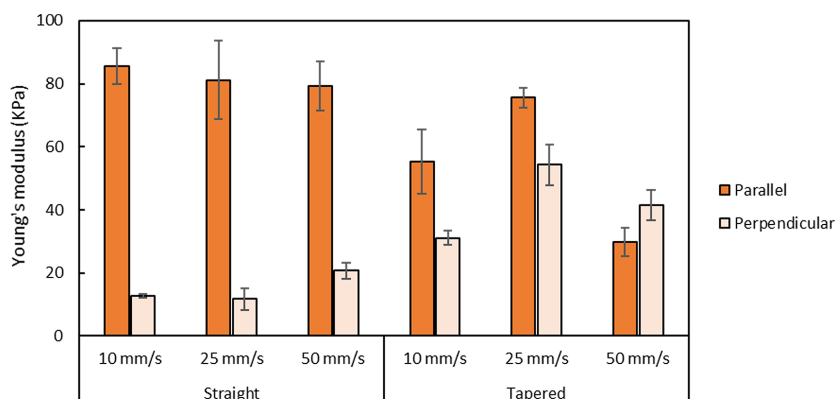
Figure 4.8. Young's moduli of samples 3D printed using different printing speeds and nozzle types. Means are shown with standard deviations.

4.3.4. Potential of 3D printing for making meat-like structures

The 3D printing of SC/SA blends appeared promising to make aligned structures that might be further explored to prepare meat-analogues (Ramachandraiah, 2021). Figure 4.9 shows some examples of 3D printed SC/SA anisotropic structures. The appearance of 3D printed SC/SA blends, depending on the calcium content applied for crosslinking, ranged from transparent to turbid and white. The appearance might be easily tuned using colouring agents. Individual strings can be distinguished in 3D printed samples, and the higher the calcium content applied for crosslinking the easier the individual filaments can be visually observed.

The protein content of 3D printed SC/SA blends in this study was around 3.6%, which is lower than that of meat (usually about 20%). A higher protein concentration may be achieved when printing with SC/SA mixtures with a higher caseinate content or using other protein-polysaccharide combinations.

Structures of 3D printed SC/SA blends had both microscale and macroscale fibre alignment which in principle resembles the structure of animal muscle tissue. Texture analysis also indicated that the gel strength was higher in the parallel direction than the perpendicular direction of filament orientation. According to (James & Yang, 2011), the Young's moduli of a steak (both raw and cooked) is between 70 and 260 kPa. Although the Young's moduli of the printed structures are at the lower end of this range, it should not be too difficult to increase the Young's moduli of 3D printed SC/SA blends further by e.g., adjusting blend

composition, printing nozzle type, printing speed, and concentration of calcium ions. Another challenge is to translate those results to plant proteins like those from soy or pea.
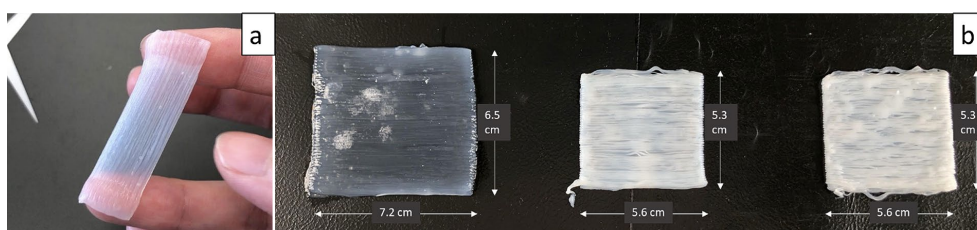

Figure 4.9. Examples of 3D printed SC/SA blend samples. (a) a single layer of a 3D printed sample (b) 3D printed structures prepared in agar fluid gel bath containing different $CaCl_2$ content (from left to right: 0.12, 0.3, and 0.55 wt%).

4.4. Conclusions

This study investigated the influence of shearing profiles on microstructure change of SC/SA blends during the extrusion process and the feasibility of creating both macroscale and microscale aligned fibrous structures using extrusion-based 3D printing technology. We successfully created aligned micron-size fibrous structures and macroscale aligned filament bundles using SC/SA blends. Morphology of extruded filaments differed when using different types of nozzles, and Young's moduli of extruded filaments were significantly influenced by extrusion speed. Calcium-containing agar fluid gel was used as a supporting bath during the 3D printing process, allowing precise deposition and solidification of extruded SC/SA blends. The rheological properties of calcium-containing fluid gels were influenced by the procedure of $CaCl_2$ addition. The addition of $CaCl_2$ directly to agar fluid gels led to a higher storage modulus and recovery percentage. Both nozzle types and extrusion speed were found to influence Young's moduli of 3D printed samples. Compared to the structures printed using a straight nozzle, better fusion among neighbouring strings was observed in structures printed with a tapered nozzle. This study shows the possibility to create multiscale anisotropic structures using a phase-separated system (e.g., SC/SA blend) by extrusion-based 3D printing technology and can become relevant when striving for products such as 3D printed meat analogues.
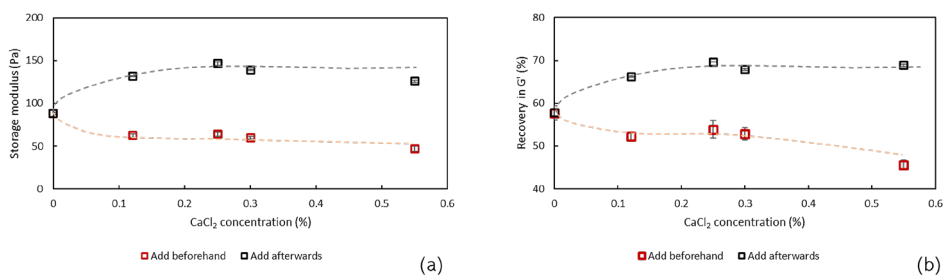
4.5. Appendix

(a)

(b)

Figure A.4.1. Storage modulus G' (a) and recovery percentage (b) of agar fluid gel prepared with different $CaCl_2$ addition procedures, either $CaCl_2$ was added before the shear-cooling process (red) or mixed afterwards into the obtained agar fluid gel (black). The recovery percentage was determined as the ratio of G' at 60 s in the third interval compared to the G' value at the end of the first interval. Means are shown with standard deviations. Data points were shown with dashed line as a guide to the eye.

Medium Straight nozzle
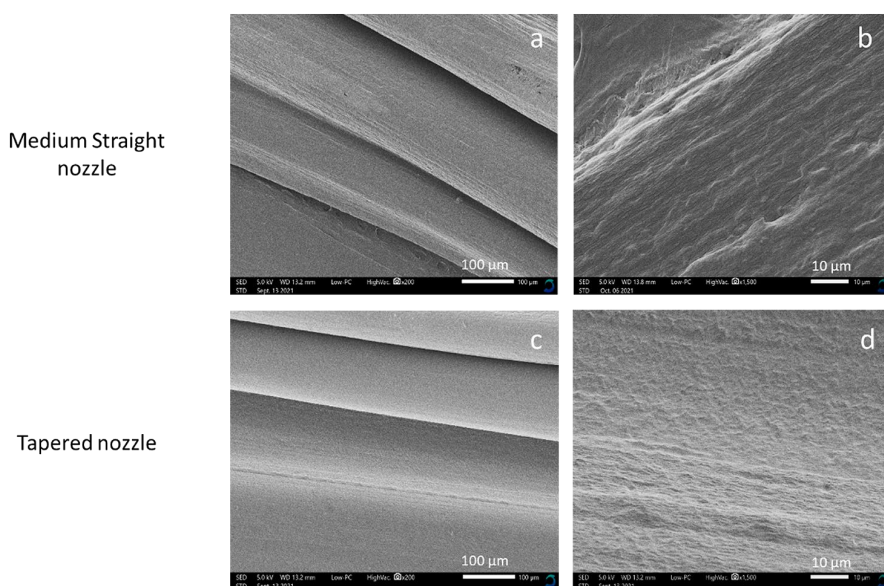
Tapered nozzle

Figure A.4.2. SEM images of 3D printed structures using a medium straight nozzle (a, b) and a tapered nozzle (c, d) at a printing speed of 10 mm/s. SEM images were taken at either 200× (a, c) or 1500× (b, d). The aligned extruded filaments can be seen in figures (a, c). The surface of the printed filaments is smoother for the tapered nozzle (c, d) compared to the medium straight nozzle (a, b), indicating a better fusion.

Chapter 5

Modifying sensory perception of chocolate coated rice waffles through bite-to-bite contrast: an application case study using 3D inkjet printing

Abstract

Consumers expect perceptual constancy between multiple bites of the same food. In this study, we investigated how sweetness, creaminess, expected fullness and liking of chocolate coated rice waffles can be modified by bite-to-bite variation in chocolate thickness. 3D inkjet printing was used to accurately deposit chocolate layers varying in thickness (0.8, 1.6 and 3.2 mm) onto rice waffles. In the first study, single bites of homogeneous coated chocolate rice waffles were evaluated. With increasing thickness of chocolate coating, sweetness, creaminess, expected fullness increased significantly. In the second study, we evaluated seven chocolate coated rice waffles containing constant total chocolate amount but differing in the chocolate thickness between three sequential bites. The order of chocolate thickness between bites had significant, but small effects on sweetness, expected fullness and liking. Interestingly, homogenous coated rice waffles were preferred over inhomogeneous coated ones. Neither recency nor primacy effects were sufficient to explain sweetness perception in this study. We conclude that sweetness of chocolate coated rice waffles can be modified by bite-to-bite variation of chocolate thickness. This study demonstrates that 3D inkjet printing allows to produce foods with bite-to-bite contrast, which possibly might be used for healthier food product design.

5.1.Introduction

The Western diet, high in saturated fats and sucrose, is associated with increased occurrence of metabolic diseases such as diabetes and obesity (Lustig et al., 2012; Statovci et al., 2017). In order to promote healthier dietary patterns, food manufactures continue to develop reduced sugar and fat products without sacrificing sensory properties such as taste and texture. During the past years, several studies explored how an inhomogeneous distribution of tastants in foods can be used to enhance sensory perception of single bites of foods as an approach to design healthier foods. Noort et al. used encapsulated salt in bread to create taste contrast (M. W. J. Noort et al., 2012). Saltiness intensity was maintained even though the total amount of salt was reduced by 50%. Emorine et al. observed a significant enhancement of saltiness in hot snacks with a heterogeneous salt distribution (Emorine et al., 2013, 2015). They demonstrated that a large contrast in salt concentrations within one bite was required to enhance saltiness, and that salt-associated aromas (ham aroma) could contribute to saltiness enhancement. The enhancement of sweetness has also been described in several other studies, using layered gels with sucrose concentration differences between layers (Holm et al., 2009; Mosca et al., 2010, 2013). Bitterness is also influenced by inhomogeneous distribution of bitter compounds. In the study of Hutchings et al. (2015) the effect of an inhomogeneous distribution of quinine in gelatine-agar gels on bitterness was explored. They concluded that a homogeneous distribution of bitter compounds is the most suitable structure for minimizing bitterness perception. Comparable results were also found for perception of fat related sensory attributes in emulsion filled gels. Mosca et al. reported an enhancement of fat related mouthfeel attributes (e.g., spreadable and melting) in gels with inhomogeneous fat distribution (Mosca et al., 2012). All studies thus reveal the possibility to modulate saltiness, sweetness, bitterness and fattiness by manipulation of the spatial distribution of tastants in foods within a bite.

Another strategy to manipulate consumer's sensory perception of foods is by designing "between bites heterogeneity", in other words by changing the composition of a food between bites. Mosca et al. investigated sweetness perception of gels and custards by varying the sucrose concentration between bites and the order of bites differing in sucrose concentration (Mosca et al., 2014). Compared with homogeneous stimuli (all bites of gels and custards had same sucrose concentration), sweetness enhancement was observed in sequences that ended

with stimuli with high sucrose concentration, suggesting that recency effects influenced overall sweetness perception. Dijksterhuis et al. performed a study using sandwiches which contained three regions differing in salt concentrations that were consumed in three sequential bites (Dijksterhuis et al., 2014). Sandwiches containing more salt in the first bite were perceived to be overall saltier compared to sandwiches with constant salt concentration throughout three bites, suggesting that an "initial boost" effect (primacy effect) occurred. Another study done by Le Berrre et al. used chocolate ice creams to which theobromine was added at different concentration to vary bitterness between bites (Le Berrre et al., 2013). When the first bite of the ice cream was of low bitterness, perception of subsequent bites tended to have lower bitterness intensity as well. This suggests that consumers expected bitterness perception to be consistent and constant from the first to the third bite (perceptual consistency). These three studies demonstrate that sensory perception of multiple bites of foods can be altered by changing the concentration of tastants between bites. Overall perception of taste and texture attributes can be enhanced or suppressed. Different psychological mechanisms (e.g., primacy effects, recency effect, perceptual consistency) have been suggested to explain the observed effects.

Preparation of foods with taste contrast from bite to bite is not trivial. Mosca et al. used separate spoons with custards, or gel cubes to realize differences in tastant concentration between successive bites (Mosca et al., 2014). While this approach allows to control tastant concentration per bite, the approach cannot be put into practice for consumers eating foods at home. Dijksterhuis et al. manually prepared sandwiches with different salt concentrations in spreads in different regions of the sandwiches (Dijksterhuis et al., 2014). In the study of Le Berrre et al. (2013), ice creams were also shaped manually to obtain different bitter compound concentrations in different regions. These studies demonstrated how tastant concentration differences between bites influences sensory perception in a variety of manually prepared foods. The question remains how to achieve tastant concentration differences between bites of foods in a more realistic production environment. Future applications in food industry that involve foods with gradients in composition or tastants require alternative and more automated processing technologies. Therefore, in this study we introduced 3D inkjet printing technology to facilitate production of foods with bite-to-bite contrast in composition. 3D inkjet food printing technology was developed by de Grood et al. and commercialized by the name of FoodJet printing (De Grood & De Grood, 2013). 3D

inkjet food printing uses an array of pneumatic membrane nozzle-jets which can jet droplets of foods with low viscosity (e.g., molten chocolate, jams, sauces) onto a moving object (Godoi et al., 2016). Thicker layers of deposited materials can be obtained by going through multiple "printing-cooling-printing" cycles. As mentioned above, only few studies explored the effect of tastant concentration difference between bites on sensory perception, and none of them applied 3D printing technology for sample preparation. To the best of our knowledge, this study is one of the first studies that explores sensory perception of 3D printed foods.

The objective of this study was to investigate how bite-to-bite variation in chocolate content of chocolate coated rice waffles influences consumers' sensory perception and liking. We hypothesized that changes in sensory intensity between successive stimuli plays a role in overall sensory perception of the whole chocolate coated rice waffle. To prepare chocolate coated rice waffles with accurate and differing amounts of chocolate between bites, we used 3D inkjet printing. We characterized various chocolates and chocolate mixtures to obtain chocolates with desired flow properties of molten chocolate and solidification behaviour to ensure a proper printing process. First, we determined sensory perception and liking of single bites of chocolate coated rice waffles differing in chocolate thickness. Secondly, we investigated how bite-to-bite variation in chocolate content of chocolate coated rice waffles influenced overall sensory perception and liking.

5.2. Materials and methods

5.2.1. Materials

Milk fountain chocolate (Barry Callebaut, Wieze, Belgium) was purchased from a local retailer. Dark chocolate "Easymelt compound coating dark" (Barry Callebaut, Wieze, Belgium) was kindly provided by FoodJet B.V.. Biological rice waffles with quinoa (Albert Heijn B.V, the Netherlands) were purchased from a local supermarket.

5.2.2. Sample preparation

Milk fountain chocolate, dark chocolate, and a mixture of dark chocolate and milk fountain chocolate (2:1 ratio) were preheated and kept at 52°C for at least 1 hour before rheological measurements. For sensory studies, the chocolate mixture (Easymelt dark chocolate: milk fountain chocolate at 2:1 ratio) was printed on the rice waffles using a 3D FoodJet Pilot

Depositor at FoodJet B.V. (Nijmegen, the Netherlands). The equipped depositor (FJ22.48) had a straight row of 48 nozzles to enable jetting of low-viscosity foods at high frequency. The chocolate mixture was premixed and kept molten in a big pot before transferring to the printing tank. Chocolate was circulated in water-jacketed hoses which was heated using water bath at 48°C before printing. After printing, chocolate coated rice waffles were immediately placed in 4°C cooling room for 10 minutes to solidify the chocolate.

5.2.3. Rheological characterization

Rheological measurements were done using a MCR301 rheometer (Anton Paar, The Netherlands). Viscosity of molten chocolates was determined in rotational mode with a cylindrical geometry CC17 (16.7 mm probe diameter). 50 g of chocolates were preheated in a water bath of 52°C for minimal 1 hour, based on the ICA standards. Viscosity measurements were done according to IOCCC guidelines at 40 °C. A pre-shear of 5 s^{-1} was applied for 5 min in order to homogenize the temperature throughout the sample, and then shearing was stopped for 10 s. Flow curves were measured by increasing the shear rate from 2 s^{-1} to 50 s^{-1} in 3 min, maintaining the shear rate of 50 s^{-1} for 1 min, and then decreasing the shear rate from 50 s^{-1} to 2 s^{-1} in 3 min. All samples were measured in duplicate.

Solidification curves were determined in oscillatory mode using the same testing geometry as for the viscosity measurements. Temperature was decreased from 40°C to 20°C at a rate of 1°C/min. Storage modulus (G') and loss modulus (G'') were determined at a frequency of 1 Hz and a strain amplitude of 0.5%. The solidification temperature (T_S) was defined as the temperature at which the storage modulus (G') was equal to the loss modulus (G'') (Mezger, 2015). Measurements were performed in duplicate.

5.2.4. Single bite sensory evaluation of chocolate coated rice waffles

Stimuli

Single bites of rice waffles with homogeneous thickness of chocolate coating were inkjet printed by depositing chocolate onto 7.5 × 5 × 0.66 cm rice waffles. Chocolate coatings were printed onto the rice waffles with chocolate thickness of 0.8, 1.6 or 3.2 mm. Printed waffles were cut into four pieces of 3.75 × 2.5 × 0.66 cm for single bite sensory evaluation (Fig 5.1A).

Examples of 3D inkjet printed chocolate coated rice waffles with homogeneous and heterogeneous chocolate thickness are shown in Figure 5.1A and 5.1B.
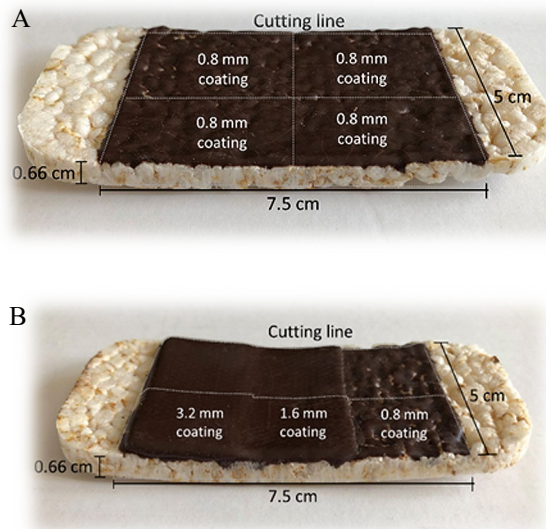

Figure 5.1. Examples of 3D inkjet printed chocolate rice waffles. (A) Example of chocolate coated rice waffle with homogeneous chocolate coating of 0.8 mm. (B) Example of chocolate coated rice waffle with chocolate coating thickness of 3.2, 1.6 and 0.8 mm from left to right. Dashed lines represent the cutting lines for preparation of samples used in sensory evaluation.

Subjects

A total of n = 75 subjects (64 females; average age: 24 years; SD = 6) were recruited via flyers and social media to participate in this study. Subjects were generally of good health (self-reported) and did not have any taste or smell disorders (self-reported). Subjects were naive with respect to the purpose of the study and were not trained. Subjects were mainly students from Wageningen University. All subjects provided written informed consent. Subjects were reimbursed after completion of the study.

Procedure

Sensory study was performed in a meeting room at Wageningen University with separators on tables. Three rice waffles with either 0.8, 1.6 or 3.2 mm chocolate coatings were evaluated by all subjects in a session of 15 minutes. Subjects were instructed to consume a single bite of a chocolate coated rice waffle (3.75 × 2.5 × 0.66 cm) with the chocolate coating facing downwards. A pilot study was performed with n = 15 participants to determine bite size of

chocolate coated rice waffles. The pilot study showed that participants consumed chocolate coated rice waffles (3.75 × 5.0 × 0.66 cm) typically with two bites. Based on the pilot study, we selected a bite size of 3.75 × 2.5 × 0.66 cm for the single bite sensory evaluation of this study. The thickness of the chocolate coating was therefore not visible for the subjects during sensory evaluation. After consumption of one bite of the rice waffle, subjects were asked to evaluate sweetness, creaminess, expected fullness and liking on 100 mm line scales anchored with "Not" to "Very" at the end of the scale. Sweetness was defined as the basic taste sensation typically induced by sugars. Creaminess was defined as having a thick and smooth mouthfeel. Expected fullness was defined as the expected feeling of being full. Liking was defined as the feeling of enjoyment. Between the different waffles, a break of 3 min was given, and participants were asked to rinse their mouth with water to clean the palate. Serving order of samples was fully randomized over subjects. Samples were coded with three-digit codes. Data collection was done on paper.

5.2.5. Multiple bite sensory evaluation of chocolate coated rice waffles with bite-to-bite variation in chocolate content

Stimuli

Seven types of chocolate coated rice waffles containing the same total amount of chocolate were designed. Rice waffles differed in the way the thickness of the chocolate coating was distributed on the rice waffles between first, second and third bite. The schematic design of the seven chocolate coated rice waffles is shown in Figure 5.2. 3D inkjet printed waffles were cut into pieces of 7.5 × 2.5 × 0.66 cm for multiple bite sensory evaluation, so that each bite was approximately 2.5 × 2.5 × 0.66 cm. Figure 5.1B shows an example of a 3D inkjet printed chocolate coated rice waffle differing in chocolate thickness between bites.
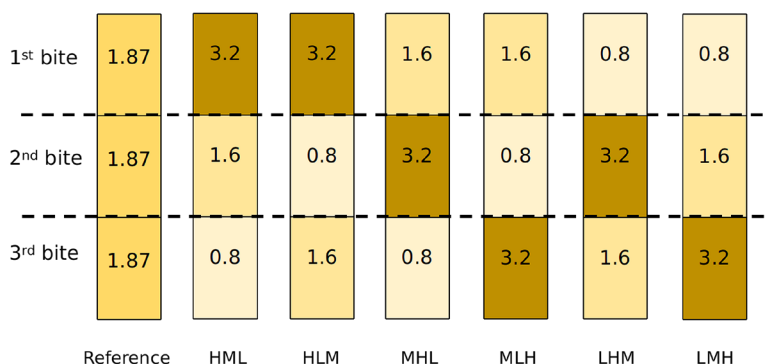
Figure 5.2. Schematic representation of the seven chocolate coated rice waffles used in the multiple bite sensory evaluation. Each rice waffle consisted of three regions differing in amount of chocolate coating. Numbers in the figure indicate thickness of chocolate coating per region (mm). Total amount of chocolate per samples was constant. The three letter sample codes denote the amount of chocolate from first to third bite as L = Low (0.8 mm), M = Medium (1.6 mm) and H = High (3.2 mm).

Subjects

A total of n = 70 subjects (56 females; average age: 24 years; SD = 6) were recruited via flyers and social media to participate in this study. N = 64 out of the n = 70 subjects also participated in the single bite evaluation of rice waffles with chocolate coatings. Subjects were generally of good health (self-reported) and did not have any taste or smell disorders (self-reported). Subjects were naive with respect to the purpose of the study and were not trained. Subjects were mainly students from Wageningen University. All subjects provided written informed consent. Subjects were reimbursed after completion of the study.

Procedure

Sensory study was performed in sensory booths at Wageningen University. Seven chocolate coated rice waffles with various bite-to-bite designs (Fig 5.2) were assessed by all subjects in a sensory session of 30 minutes. Subjects were instructed to consume the rice waffles (7.5 × 2.5 × 0.66 cm) with the chocolate coating facing downwards. The thickness of the chocolate coatings of the multiple bites was therefore not visible for the subjects during sensory evaluation. When observing some of the subjects performing the sensory evaluation, it became apparent that subjects followed the instructions well eating the waffles with the chocolate facing downwards. While we cannot provide experimental proof with absolute certainty that participants could not see the chocolate, we think that the vast majority of participants did not see the chocolate. Subjects were instructed to consume the entire waffle

in three equal bites and to swallow after each bite. After the consumption of the whole rice waffle in three bites, subjects were asked to evaluate overall sweetness, creaminess, expected fullness and liking on 100 mm line scales anchored with "Not" to "Very" at the end of the scale. Sweetness, creaminess, expected fullness and liking were defined as described in section 5.2.4. Between the different waffles, a break of 3 min was given, and participants were asked to rinse their mouth with water to clean the palate. Serving order of samples was fully randomized. Samples were coded with three-digit codes. Data collection was done on paper.

5.2.6. Data analysis

All data analysis (single bite and multiple bite sensory evaluation of chocolate coated rice waffles) was done in R (version R 3.6.1). Sweetness, creaminess, expected fullness and liking were reported as mean values with standard error. Mixed-linear models were used with sweetness, creaminess, expected fullness and liking as response variables (fixed effects), sample as predictor variable and subject as random effect. A significance level of $p < 0.05$ was chosen and Tukey's HSD test was used for post hoc analysis.

5.3. Results and discussion

5.3.1. Rheology

Figure 5.3A shows the flow curves for molten dark chocolate, milk chocolate and mixture of dark chocolate and milk chocolate (2:1 ratio) at 40°C, and Figure 5.3B shows the solidification curves of the temperature sweeps. All three molten chocolates show shear-thinning behaviour. Molten dark chocolate had the lowest viscosity of 810 mPa·s at 50 s^{-1}, while milk chocolate had the highest viscosity of 1040 mPa·s at 50 s^{-1}. The viscosity of the chocolate mixture was 930 mPa·s at 50 s^{-1}, thus between the viscosities of dark and milk chocolate. The difference in viscosity between dark chocolate, milk chocolate and chocolate mixture could be due to different particle sizes and distribution, surface characteristics, addition of emulsifiers, and the amount and the nature of the lipid phase (Windhab, 2006). Probably in this study, the fat content of the used chocolates/chocolate mixtures explains to a large extend the differences in viscosity between molten chocolates. Fat content of dark chocolate, chocolate mixture and milk chocolate were 37.3%, 38.2%, and 40.3%,

respectively. Hartel et al. described that chocolate viscosity increases with increasing fat content (Hartel et al., 2018). This was explained as with more fat the distance between the fine solid particles present in chocolate is increased and their interactions during shear decrease. According to Guo et al., shear thinning behaviour is desirable during inkjet printing, where high shear rate within the printhead facilitates jetting of the liquid (Guo et al., 2017). Once the drop detaches from the nozzle, the increased viscosity at decrease shear rate suppresses satellite drop formation.
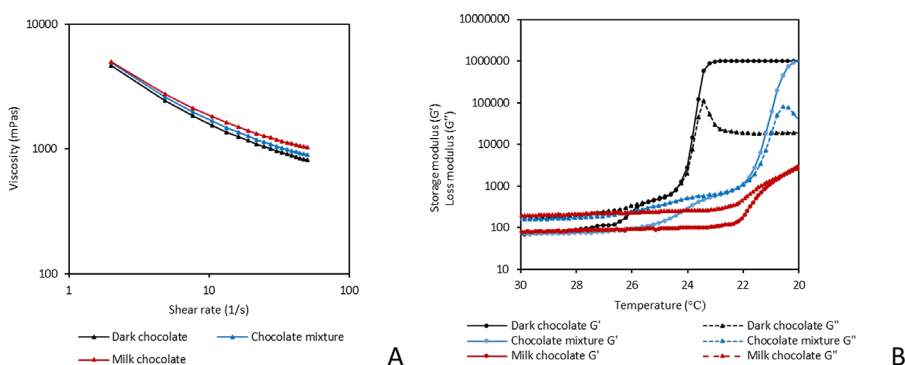

Figure 5.3. Flow curves of (A) molten chocolates at 40°C, and (B) temperature-dependent G' and G'' of dark chocolate (black), milk chocolate (red), and mixture of dark chocolate and milk chocolate at 2:1 ratio (blue).

Temperature sweeps were performed to characterize the solidification process of dark chocolate, milk chocolate and their mixture (Fig 5.3B). Dark chocolate had the highest solidification temperature ($T_S = 24.2°C$), followed by the chocolate mixture ($T_S = 22.8°C$) and milk chocolate ($T_S = 20.4°C$). It is widely known that milk fat has an inhibitory effect on crystallization of cocoa butter (Hartel & Rao, 1998). In this study, the milk chocolate contained 5.6% milk fat, while the dark chocolate had no milk fat in the composition, which may explain the lower crystallization temperature of milk chocolate. Apart from the milk fat, the cocoa butter composition also can be expected to affect crystallization temperature and rate (Hartel & Rao, 1998).

Even though milk chocolate may be more palatable to use as waffle coating compared with dark chocolate, it was not chosen in this study. The reason for this was that accurate inkjet printing with milk chocolate was not possible due to chocolate run-off from the waffle surface because of its low solidification temperature and slow solidification process. The rheological

properties (i.e., faster solidification) of dark chocolate were better suited for inkjet printing. Considering that the final product was expected to be preferred when it is sweet and creamy, it was decided to use the 2:1 mixture of dark and milk chocolate as coating material rather than the dark chocolate. This 2:1 mixture exhibited increased shear thinning behaviour and faster solidification compared to the milk chocolate, thus better printability than the milk chocolate, and was perceived as sweeter and creamier than dark chocolate (feasibility study, data not shown).

5.3.2. Sensory perception and liking of single bites of rice waffles differing in amount of chocolate coating

To evaluate the effect of chocolate coating thickness on sweetness, creaminess, expected fullness and liking, single bites of the three homogeneously coated chocolate waffles were evaluated by the consumer panel (n = 75) (Fig 5.4). Chocolate thickness had a significant effect on sweetness ($\chi^2(6) = 154.65$, p < 0.001), creaminess ($\chi^2(6) = 189.71$, p < 0.001), expected fullness ($\chi^2(6) = 161.51$, p < 0.001) and liking ($\chi^2(6) = 34.53$, p < 0.001). Sweetness, creaminess and expected fullness increased significantly with increasing chocolate layer thickness and differed significantly between all samples. This demonstrates that the variation in amount of chocolate deposited on the rice waffle (thickness) was clearly sufficient to lead to changes in sensory perception. With increasing thickness of the chocolate coating, the amount of sugar and fat consumed per bite increased, which consequently led to an increased intensity of sweetness, creaminess and expected fullness. These results are in line with the study of Prinz et al. (2006), who observed that increasing bite size of custards increased fatty and creamy sensations. Increased perceived sensory intensity can be explained by a spatial summation process, where intensity is a function of the concentration of the compound and the area being stimulated (Division et al., 2007). In this study, the relative concentrations of sugar and fat in the chocolate coating were kept constant, but the total amount of consumed chocolate per bite was increased by increasing the chocolate coating thickness. For liking, significant differences were only observed between 0.8 and 1.6 mm chocolate coated waffles (p < 0.001), and between 0.8 and 3.2 mm chocolate coated waffles (p < 0.001). No significant difference was observed between 1.6 and 3.2 mm chocolate coated waffles (p = 0.143).
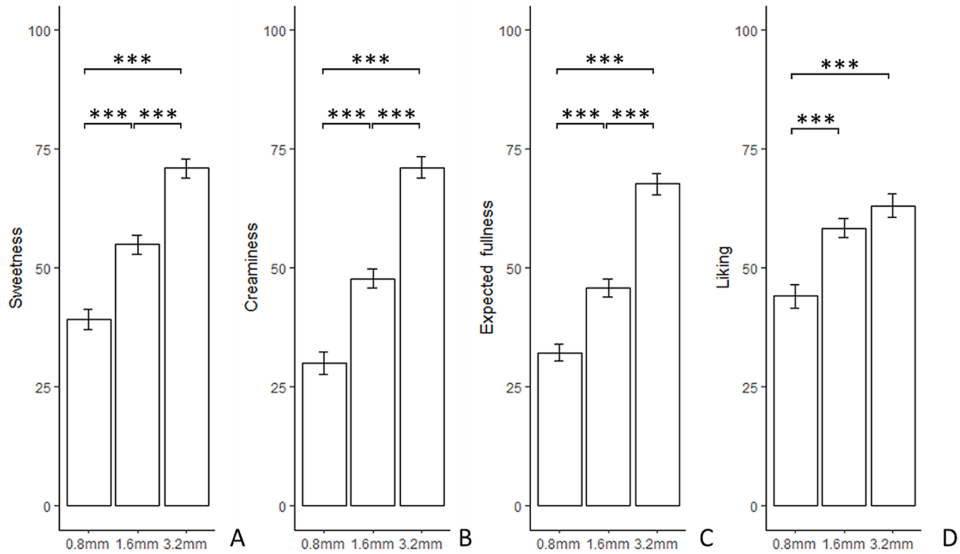
Figure 5.4. Sweetness (A), creaminess (B), expected fullness (C), and liking (D) of rice waffles evaluated by n = 75 naive subjects. Rice waffles were coated with 0.8, 1.6 and 3.2 mm thick chocolate. Error bars indicate standard error. Significant differences are indicated by *** (p < 0.001).

5.3.3. Sensory perception and liking of multiple bites of rice waffles with bite-to-bite variation in chocolate amount

Figure 5.5 shows sweetness, creaminess, expected fullness and liking scores of the homogeneous waffle and the six rice waffles with bite-to-bite variation in chocolate content. Distribution of chocolate coating from first to third bite significantly influenced sweetness ($\chi^2(10) = 17.52$, p = 0.008), expected fullness ($\chi^2(10) = 14.60$, p = 0.02), and liking ($\chi^2(10) = 19.02$, p = 0.004). No significant effect of distribution of chocolate coating from first to third bite on creaminess ($\chi^2(10) = 9.34$, p = 0.15) was observed. While we observed several significant differences in sweetness, expected fullness and liking between chocolate coated rice waffles differing in chocolate thickness from first to third bite, we emphasize that the magnitude of the differences between samples was small. It is noted that all averaged intensity scores of the four attributes ranged from 50-60, indicating that participants used only a very narrow range of the scale. This is in sharp contrast to the single bite evaluations which showed average intensity scores ranging from 25 to 75. We suggest two possible explanations for these observations. The results might indicate that the waffles coated with chocolate varying in thickness from bite-to-bite were actually perceived fairly similar, so that

91

variation in chocolate thickness from bite-to-bite has only a minor effect on sweetness, creaminess, expected fullness and linking. It should be noted that the total chocolate content consumed with three bites was the same for all waffles, only the distribution between bites differed. This is in contrast to the single bite evaluations, where the total chocolate content differed between waffles. This might explain why the differences in sweetness, creaminess, expected fullness and liking were small in the multiple bite evaluations. Alternatively, the results might show that it was difficult for the naive consumers to integrate their sensory response over multiple subsequent bites into one overall intensity score. Participants tasted three subsequent bites of which each bite tasted differently (Fig 5.2), but participants were asked to provide only one intensity score per attribute after tasting three bites. It is possible that the task of averaging perceived intensity over three consecutive bites was difficult to perform for the participants. Participants might have been uncertain how to report their response and how to integrate intensity differences between bites into a single intensity score. Therefore, participants might have avoided to use the entire line scale and might have tended to use only a relatively small part around the middle of the scale. Mosca et al. also observed that participants tended to use the middle part of the line scale when asked to assess overall sweetness intensity of multiple bites with bite-to-bite variation in sweetness (Mosca et al., 2014). In contrast, when performing Time-Intensity evaluations, Mosca et al. observed clear differences between separate bites and participants used a broader range of the scale to report their perception (Mosca et al., 2014).

For sweetness, HML was significantly sweeter than HLM (p = 0.006), MHL (p = 0.018), and MLH (p = 0.028); LHM was significantly sweeter than HLM (p = 0.014), MHL (p = 0.038); LMH was significantly sweeter than HLM (p = 0.003), MHL (p = 0.011), and MLH (p = 0.016). No significant difference in sweetness was observed between the homogeneously distributed chocolate coating waffles and samples with bite-to-bite variation in chocolate thickness. Recency effects were not observed for sweetness, since not all samples with the thickest chocolate as third bite were perceived as the sweetest (e.g., MLH was perceived less sweet than HML). Primacy effects were not observed either, since sequences starting with high chocolate amounts at the first bite (e.g., HLM) were not consistently evaluated as sweeter than the ones starting with less chocolate (e.g., LMH).
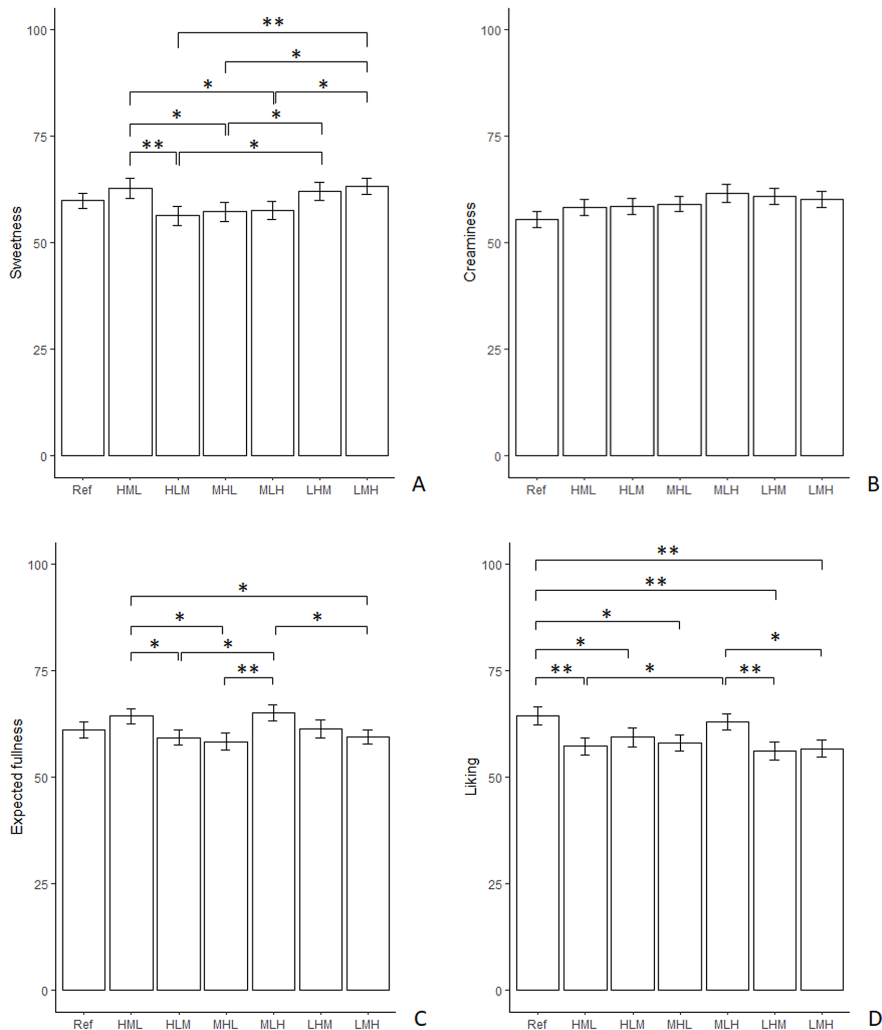
Figure 5.5. Sweetness (A), creaminess (B), expected fullness (C), and liking (D) of rice waffles with bite-to-bite variation in chocolate content evaluated by naive consumers (n=70). The three letter sample codes denote the amount of chocolate from first to third bite as L = Low (0.8 mm), M = Medium (1.6 mm) and H = High (3.2 mm). Error bars indicate standard error. Significant differences are indicated by * (p < 0.05) and ** (p < 0.01).

Another way to interpret the obtained results is to consider changes in sweetness, creaminess, and expected fullness intensity between bites and to consider whether these changes influence overall perception. With the results described in section 5.3.2, we applied another way of coding the six rice waffles with bite-to-bite variation in chocolate thickness (Table 5.1). The

new coding is based on expected changes of sensory intensity and liking between first, second and third bite.

Table 5.1. Chocolate coated rice waffles with bite-to-bite variation in chocolate thickness (L: 0.8 mm; M: 1.6 mm; H: 3.2 mm). Symbols (↗, ↘, =) represents the intensity differences (increase, decrease, no change) between first and second bite and between second and third bite, based on the results of the single bite evaluations (section 5.4.2). Green/red arrows indicate small/large differences.

	sweetness, creaminess, fullness	liking
HML	↘↘	=↘
HLM	↘↗	↘↗
MHL	↗↘	=↘
MLH	↘↗	↘↗
LHM	↗↘	↗=
LMH	↗↗	↗=

We noticed that the sweetness intensity decreased when there was an abrupt decrease in sweetness either between first and second or between second and third bite (HLM (↘↗) and MHL (↗↘)), compared to waffles having a more gradual change in sweetness between bites (LMH (↗↗) and HML (↘↘)). This may be explained by a "contrast effect" which suggests that a stimulus might be perceived as less intense in the presence of a stronger stimulus (Schifferstein & Oudejans, 1996). When a thin layer of chocolate is consumed right after a thicker layer, the bite with the thin layer could be perceived less sweet than it would normally have been, and this may possibly influence the sweetness perception of the entire rice waffle.

For creaminess, even though no significant differences between samples were observed, we tend to observe a non-significant trend that creaminess of MLH and LHM might be higher than the homogenous reference waffle (Fig. 5.5B). If that was a significant effect, the increased creaminess of LMH and MLH could be due to a recency effect. According to Bireta et al., recency effects dominate over primacy effects when the retention interval is short (Bireta et al., 2018). It could be that intervals between the three bites were sufficiently short in our study, and therefore only recency effects were observed. Taking bite-to-bite contrast into consideration, it seems that waffles tend to be perceived creamier (not significant) when chocolate thickness between the bites increased sharply (LHM (↗↘) and MLH (↘↗)). A perceptual contrast mechanism may be used to explain our observations, as suggested by de Wijk *et* al. who reported similar observations in thickness perception of desserts (de Wijk et

al., 2003). Panels were asked in that study to first consume five bites of thin low-fat custards before another five bites of thick full fat custards. An enhancement in thickness rating of thick full fat custards was observed in their study.

For expected fullness, HML is perceived as significantly more full than HLM (p = 0.031), MHL (p = 0.010), and LMH (p = 0.034). MLH is perceived as significantly more full than HLM (p = 0.012), MHL (p = 0.004), and LMH (p = 0.014). No significant differences in expected fullness were observed between the waffle with homogeneously distributed chocolate coating and other waffles. Even though significant differences were found, we do not observe a consistent pattern in the data and can therefore not provide a reasonable explanation. The inconsistent pattern in the data is probably due to the difficulty for subject to assess expected fullness based on consuming three small bites of rice waffles, as was mentioned by several subjects after evaluation.

For liking, waffle with homogeneously distributed chocolate coating was significantly more liked than HML (p = 0.005), HLM (p = 0.049), MHL (p = 0.012), LHM (p = 0.001), and LMH (p = 0.002); MLH was significantly more liked than HML (p = 0.023), LHM (p = 0.007) and LMH (p = 0.012). In general, consumers liked rice waffles with homogeneous chocolate coatings over waffles with bite-to-bite variation in chocolate content (except for MLH which was not significantly different from the waffle with homogeneously distributed chocolate coating). Coatings with higher liking score in the first bite and last bite (MLH (↘ ↗)) were preferred over coatings of either low liking score in first bite (LHM (↗=) and LMH (↗=)) or coatings of low liking score in last bite (HML (=↘) and MHL (=↘)). Results of the single bite evaluation (Fig 5.4) indicate significant differences in liking only between 0.8 and 1.6 mm chocolate thickness, and between 0.8 and 3.2 mm thickness; no significant differences were found in liking between 1.6 and 3.2 mm chocolate thickness. It seems that the combination of an "initial boost effect" as well as a "recency effect" played an important role in one's preference toward the chocolate coated rice waffles.

In this study, 3D inkjet printing showed its advantages in preparing food products of different compositional designs. Conventionally, one can only achieve various chocolate layer thickness by manual shaping foods. Such procedures are usually time consuming, material demanding (e.g., requires molds) and not always precise. Here we demonstrated that 3D

inkjet food printing can be a powerful tool to prepare foods with modified composition between bites having the potential to be used for healthier product design.

5.4. Conclusions

Sweetness, expected fullness and liking of chocolate coated rice waffles were influenced by bite-to-bite variation in chocolate content without changing the overall amount of chocolate consumed. No clear recency nor primacy effects was able to explain the variation in sweetness perception, while a contrast effect seems to play a role. A combination of an initial boost effect as well as a recency effect played an important role in scoring liking. Results suggest that sweetness perception can be modified by different bite-to-bite variations. Compared to a homogeneous coated chocolate rice waffle, waffles with bite-to-bite variations in coating thickness were less preferred (except for MLH), though they had similar sweetness and creaminess as a homogeneous coated waffle. This study shows the potential application of 3D inkjet printing for making advanced food designs with variations in composition between bites.

Chapter 6

How macroscopic structure of 3D printed protein bars filled with chocolate influences instrumental and sensory texture

Abstract

The aim of this study was to determine the influence of the macroscopic structure of 3D printed protein bars with chocolate fillings on instrumental texture properties and sensory perception. Protein bars with different printing patterns (layered, rectilinear and concentric) were prepared by extrusion-based 3D printing. We found that protein bars with concentric chocolate infill pattern were significantly harder than bars with a chocolate layer, despite their similar chocolate content. Protein bars with a chocolate layer were significantly more cohesive than bars with a rectilinear pattern. Differences in instrumental texture were explained using spring models. Results of sensory ranking tests (n=70 participants) were in good agreement with those of instrumental texture analysis. For protein bars with 16 g/100g chocolate content, protein bars with concentric pattern were perceived as the hardest. For protein bars with 25 g/100g chocolate content, protein bars with concentric and rectilinear patterns were both perceived significantly harder than bars with a chocolate layer. No significant differences were found between bars that differed in infill pattern for perceived chewiness and liking. We conclude that by changing the macroscopic structure (printing pattern) of 3D printed protein bars with chocolate fillings, the instrumental and sensory properties can be modified without affecting liking.

6.1. Introduction

3D food printing is a process that employs layer by layer deposition of food materials according to a predesigned digital pattern. It offers multiple advantages for food preparation such as shape customization, personalization of nutrition (Godoi et al., 2016; Liu et al., 2017), and the potential to modify the structure and texture of foods in a precisely defined manner. The use of 3D printing techniques facilitates the modification of food structures on a macroscopic length scale (> 1 mm), which can affect food texture. Various studies (Derossi et al., 2020; Liu, Bhandari, et al., 2018; Liu et al., 2020; Mantihal et al., 2019; Noort et al., 2017; Vancauwenberghe et al., 2018) demonstrated how macroscopic modifications of food structure by 3D printing can be used to alter mechanical food properties. Mantihal et al. (2019) investigated how variations in infill percentage influenced instrumental hardness of 3D printed dark chocolates. The study concluded that a higher infill percentage resulted in harder chocolate bars. Derossi et al. (2020) used 3D printing to vary the pore size and void fraction in cereal snacks and demonstrated that 3D printed snacks with differences in hardness can be obtained by modulating the number and position of cubical-shaped pores. Liu et al. (2020) showed that instrumental hardness and fracturability of air-fried potato snacks decreased with decreasing infill level and dependent on infill patterns. Apart from solid foods such as chocolates, cookies, cereal and potato snacks, the influence of printing design on texture properties was also studied in semi-solid food pastes (Liu, Bhandari, et al., 2018; Vancauwenberghe et al., 2018). Liu et al. (2018) printed pastes of mashed potatoes and demonstrated that instrumental hardness and gumminess changed upon changing the infill level.

Only very few studies (Chow et al., 2021; Fahmy et al., 2021; Kistler et al., 2021; Mantihal et al., 2019; Punpongsanon et al., 2020; Zhu et al., 2020) investigated how structural modifications created by 3D printing impact consumer and sensory perception of foods. These studies explored sensory and oral behavioural responses (sweetness perception, texture preference and mastication behaviour) rather than texture perception of 3D printed foods. In contrast to numerous studies about the impact of structure modifications on instrumental texture properties of 3D printed foods, no study to date described the impact of structure modifications on texture perception. This lack of data is especially surprising given that

modifications of shape and structure by 3D food printing to tailor texture perception are often described as the major benefit of 3D food printing.

Commercially available protein bars consist of a core of a protein paste coated by a chocolate layer. The protein paste of these bars is often perceived as chewy and cohesive. The addition of chocolate to protein bars not only provides consumers with a more indulgent feeling but also provides more diverse and pleasurable texture sensations to the product. In commercial protein bars, typically the entire protein paste is covered with a thin chocolate layer. With 3D printing, one has the opportunity to distribute the chocolate differently in the protein paste. This allows to explore the impact of the infill pattern of solid materials (chocolates) on instrumental and sensory texture of paste like foods (protein bars).

The aim of this study was to determine the influence of the macroscopic structure of 3D printed protein bars with chocolate fillings on instrumental texture properties and texture perception. Protein bars were designed, formulated and printed with different chocolate infill patterns and infill percentages. Texture profile analysis (TPA) was performed to quantify the instrumental texture properties. Ranking tests were performed to determine texture perception (hardness, chewiness) and liking. Instrumental texture properties were correlated to sensory texture.

6.2. Materials and methods

6.2.1. Materials

Spray-dried instant lecithinated calcium caseinate (CaCas), whey protein concentrate (WPC), high-fructose corn syrup (HFCS) (Tereos, Aalst, Belgium) and medium-chain triglyceride (MCT) oil were kindly provided by Royal FrieslandCampina N.V. (Wageningen, The Netherlands). Glycerol was purchased from VWR International (Leuven, Belgium). High protein chocolate (XXL Nutrition, Eindhoven, The Netherlands) was purchased online. High protein chocolate had a protein content of 27 g/100g and was used in this study as a filler for the protein bars.

6.2.2. Protein paste preparation

The protein paste consisted of 18 g/100g CaCas, 23 g/100g WPC, 49 g/100g HFCS, 5 g/100g glycerol, and 5 g/100g MCT oil, which closely resembles the formulation of commercially available protein bars. Protein pastes were made in 500 g batches. HFCS was put in a 50ºC water bath for at least 15 min to lower viscosity and facilitate mixing with other ingredients. Then HFCS was mixed with glycerol in a N50 Mixer (Hobart Corporation, USA) equipped with a stainless-steel flat beater at the lowest speed for 30 s. MCT oil was then added to the mixture and mixed at the second speed for 30 s. The dry ingredients (WPC and CaCas) were sieved before weighing to avoid lump formation during mixing. WPC and CaCas was added to the mixture of wet ingredients and mixed at the lowest speed until a homogeneous paste was obtained. The paste was then manually shaped into a ball and flattened and then pressed into a stainless-steel mould designated for the syringes used in 3D printer. The moulded pastes were pushed into syringes, which were used afterwards for 3D printing. Before printing, syringes were heated for at least 15 min at 60ºC using a water bath.

6.2.3. Production of protein bars

3D printing process

A TNO in-house manufactured single head 3D printer (Paolillo et al., 2021) was used in this study. The preheated syringes were loaded into a 3D printer (TNO, The Netherlands) which is shown in Figure 6.1. Syringes were kept at 60ºC throughout the printing process. The nozzle diameter was 2.5 mm, and the layer height was 1 mm. A printing speed of 4 mm/s was used for printing.
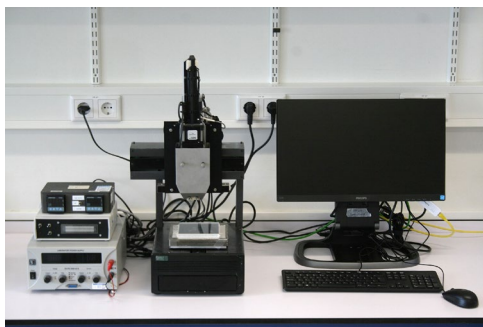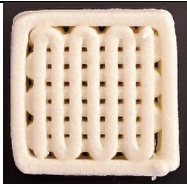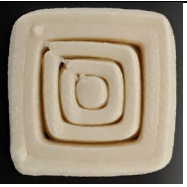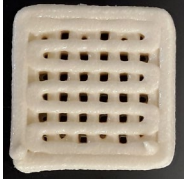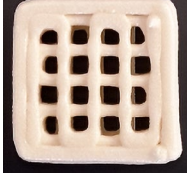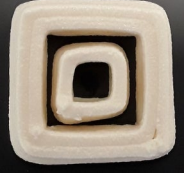

Figure 6.1. Single head 3D printer (TNO, The Netherlands) used in this study.

Feasibility study: protein bars with air filling

A feasibility study was done to investigate the instrumental texture properties of 3D printed protein bars with air fillings, so porous protein bars. Table 6.1 shows different designs of printed protein pastes with air fillings. These porous protein bars did not maintain their shape over time due to the paste-like flow properties of the protein paste and were easily deformed when handling. Even though texture differences (e.g., hardness) among different filling densities were observed by instrumental measurements (data not shown), the texture differences were hardly perceivable when protein bars were evaluated by panellists (preliminary study, data not shown). The apparent lack of sensory discrepancy among different infill patterns and infill densities was probably caused by the highly chewy, paste-like protein material. Porosity in protein bars disappeared quickly during mastication so that texture differences become unnoticeable. Therefore, chocolate was chosen as a solid filling material instead of air for the protein bars used in this study.

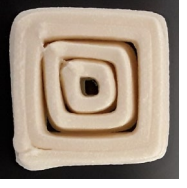**Table 6.1.** Photos of top view of porous protein bars with different air infill densities and air infill patterns used in the feasibility study. All 3D printed protein bars were 30 × 30 × 10 mm.

Infill density	Rectilinear	Triangle	Concentric
70%			
60%			
40%			

Protein bars with chocolate filling

Table 6.2 shows the different digital printing designs and the printed protein bars with chocolate used in this study. The 3D printing designs were made and converted into G-Codes by using Slic3r software version 1.3.0 (Alessandro Ranellucci, Italy). The protein bar geometry was customized and kept constant for all bars as $30 \times 30 \times 10$ mm. Weight of protein paste and filled chocolate are listed in Table 6.2. Two protein paste infill patterns (rectilinear and concentric) and infill densities (60 and 40 g/100g infill density, which corresponds to a chocolate content of the protein bar of 16 and 25 g/100g) were chosen for 3D printed protein bars. Two protein bars with chocolate layers were also prepared to mimic the design of commercial protein bars (Table 6.2). Infill density was set in Slic3r and was defined as the amount of protein paste inside a print design without taking into account the amount of protein paste used for the perimeter. Digital top views show digital designs of perimeters (yellow strings) and infills (red strings) of printed protein pastes.
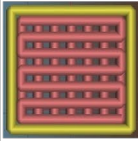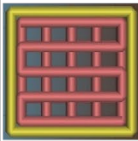
Protein bars were printed as described above. The printed bars were stored in individual 50 mL plastic cover cups and transferred to the 4ºC fridge for cooling. The high protein chocolate was melted in a 60ºC water bath before it was transferred to a 10 mL plastic syringe having a 0.84 mm diameter nozzle (Nordson EFD). Once the printed protein bars were cooled down, a syringe was used to add the melted chocolate manually into the voids of the printed protein pastes.

In addition, two protein bars with a chocolate coating layer were made. A preheated protein paste was extruded from the same 3D printer at 60ºC, and afterwards manually shaped and pressed into moulds having the same geometry as the other 3D printed protein bars. The protein paste was extruded using the 3D printer to obtain a uniform heating and extruding profile similar to the rectilinear and concentric protein bars. To be time efficient, the protein paste was then manually pressed into moulds rather than 3D printed into solid cubes. Protein pastes were cooled to 4ºC in the fridge before the chocolate layer was added. The chocolate coatings were applied in one layer on top of the bars to reach a chocolate content of 16 or 25 g/100g based on the total weight of chocolate protein bar.

Finally, protein bars without chocolate and chocolate bars were prepared. The protein and chocolate bars were manually moulded into the same dimension as the other chocolate

protein bars. These two bars were only used as reference materials for the instrumental texture analysis.

Table 6.2. Overview of protein bars with chocolate fillings. All 3D printed protein bars with chocolate were 30×30×10 mm. Protein and chocolate weight are reported per printed bar.

	16 g/100g chocolate Rectilinear	25 g/100g chocolate Rectilinear	16 g/100g chocolate Concentric	25 g/100g chocolate Concentric	16 g/100g chocolate Layered	25 g/100g chocolate Layered
3D printing infill density (%)	60	40	60	40	-	-
Weight protein paste (g)	9.2	7.9	9.2	7.9	9.2	7.9
Weight chocolate (g)	1.7	2.7	1.7	2.7	1.7	2.7
Digital top view of printed protein paste					-	-
3D printed protein bars with chocolate						

6.2.4. Texture profile analysis (TPA)

Printed protein bars that were prepared according to the procedure described in section 6.2.3 were stored at 4ºC overnight and were taken out of the fridge 1 h before TPA measurements. TPA measurements were carried out using an Instron 5564 texture analyser (Illinois Tool Works Inc, Glenview, USA). Protein bars (30 × 30 × 10 mm) were compressed twice by a cylindrical probe (50 mm diameter). The TPA was conducted using a 2000 N load cell with a pre-test speed of 10 mm/min, and a trigger force of 0.1 N. A compression distance of 5 mm was chosen corresponding to 50% strain. The testing speed during TPA analysis was set at 60 mm/min with a holding period of 5 s between first and second compression. The Young's modulus was defined as the slope of the initial linear portion of the stress-strain curve. Hardness was determined as the maximum force of the first compression, cohesiveness as the area of work during the second compression divided by the area of work during the first compression. Chewiness was defined as in equation 6.1, where springiness was distance of the sample height before the second compression divided by the original compression distance. Triplicate measurements were performed for each protein bar.

$$\text{Chewiness} = \text{Hardness} \times \text{Cohesiveness} \times \text{Springiness} \qquad (6.1)$$

To better understand the influence of the spatial distribution of chocolate in the protein pastes on Young's modulus and hardness, different spring models were developed. The compression Young's modulus (E) is given by:

$$E = \frac{\sigma}{\varepsilon} \qquad (6.2)$$

where σ denoting compressive stress and ε describing strain in the linear elastic region. The compressive stress is given as:

$$\sigma = \frac{F}{A} \qquad (6.3)$$

where F is the applied compressive force and A denotes contact surface area to which the force is applied. The compressive strain is defined as:

$$\varepsilon = \frac{\Delta h}{h} \qquad (6.4)$$

where Δh is the change in height and h describes the original height of the object. Combining equations 6.2, 6.3, and 6.4 we obtain:

$$E = \frac{Fh}{A\Delta h} = \frac{h}{A}\, k \qquad (6.5)$$

where k is the spring constant. Equation 6.5 shows that Young's modulus of an ideal elastic material is proportional to the spring constant of an object with a defined height and cross-sectional area.

It is well known that the equivalent spring constant of two springs in series (k_{eq_series}) is:

$$\frac{1}{k_{eq\_series}} = \frac{1}{k_1} + \frac{1}{k_2} \qquad (6.6)$$

and the equivalent spring constant of two springs in parallel ($k_{eq\_parallel}$) is:

$$k_{eq_{parallel}} = k_1 + k_2 \qquad (6.7)$$

where k_1 and k_2 represent the spring constants of individual springs.

6.2.5. Sensory study – Ranking tests

Participants

A total of $n = 70$ untrained participants (43 females, 27 males; average age: 26 ± 5 years) were recruited via flyers and social media. Participants were mainly students from Wageningen University and were required to be not allergic to soy or dairy products. Participants were naive to the purpose of the study. Participants were financially reimbursed for their participation. All participants gave written informed consent. The study was conducted in accordance with the Declaration of Helsinki (2013). The study did not fall within the remits of the Medical Research Involving Human Subjects Act (WMO) as outlined by the Central Committee on Research Involving Human Subjects (CCMO) of The Netherlands.

Stimuli

Three 16 g/100g chocolate protein bars (layered, concentric, and rectilinear pattern), and three 25 g/100g chocolate protein bars (layered, concentric and rectilinear pattern) were

offered to the participants in the sensory study (Table 6.2). Protein bars were prepared one day before sensory evaluation according to section 6.2.3 and stored overnight at 4°C. Protein bars were removed from the fridge 1 h before the sensory sessions. Protein bars were cut into half using a scalpel to obtain two pieces with dimensions of 30 × 15 × 10 mm. This sample dimension was chosen to standardize bite size during the sensory evaluations. The standardized bite size was determined in a pilot study ($n = 25$). All samples were labelled with random 3-digit codes.

Procedure

Participants attended one sensory session of 30 min. Two series of ranking tests were performed in a meeting room at Wageningen University. In the first series, three 16 g/100g chocolate protein bars (layered, rectilinear, concentric) were provided to the participants. Participants were instructed to put the whole piece (30 × 15 × 10 mm) into their mouth, with the chocolate layer/pattern facing upwards, and bite with their molars. Between samples, participants were asked to rinse their mouth with water to clean the palate. After tasting three protein bars, participants were asked to rank the three protein bars for liking, hardness and chewiness from most (1st rank) to least (3rd rank). Ties were not allowed, so participants had to assign each sample to one rank. Liking was defined as overall preference for a protein bar. Hardness was defined as the force required to bite through the bar in the first few chews. Chewiness was defined as the mastication effort needed to chew the bar to a state that is ready for swallowing. Participants could re-taste a protein bar if needed. The serving order of bars in each round was fully randomized over the participants. In the second series of ranking tests, three 25 g/100g chocolate protein bars, (layered, rectilinear, concentric) were evaluated by the participants. The same procedure was followed as in the first ranking series.

Data analysis

Data analysis was done in IBM SPSS statistics (version 25). Significant differences among samples for the TPA parameters (Young's modulus, hardness, cohesiveness, chewiness) were determined using one-way ANOVA followed by Tukey post-hoc test for 16 and 25 g/100g chocolate content protein bars separately. Significant differences between 16 and 25 g/100g chocolate content protein bars with same infill pattern were determined by independent samples t-tests. Results of the ranking tests (liking, hardness, chewiness) were reported as mean ranks. Significant differences between samples in ranks of liking, hardness and

chewiness were determined using Friedman tests followed by post-hoc Wilcoxon signed-rank tests. Spearman-Rho correlation tests were performed to determine significant correlations between different attributes (liking, hardness and chewiness). A significance level of $p < 0.05$ was chosen for all data analysis.

6.3. Results and discussion

6.3.1. Texture profile analysis of protein bars

Figure 6.2 shows the results of the instrumental texture analysis of the 16 and 25 g/100g chocolate protein bars with layered, rectilinear and concentric pattern. For the 16 g/100g chocolate protein bars, the differences in Young's moduli were not significant ($p = 0.13$) despite small differences in their means (Fig 6.2A). A trend is apparent that suggests that the Young's modulus might increase from layered to rectilinear to concentric pattern (Fig 6.2A). Section 6.3.2 describes different spring models which were developed to understand and predict the texture properties, especially the Young's modulus, of the 3D printed protein bars filled with chocolate. Protein bars with concentric pattern had significantly higher hardness than protein bars with rectilinear pattern ($p < 0.01$) and protein bars with a chocolate layer ($p < 0.01$) (Fig 6.2B). It can be seen in Figure 6.2A and 6.2B that a higher Young's modulus corresponded to higher hardness. It is worth mentioning that the hardness of protein bars with a concentric pattern was higher than that of protein bars with a rectilinear pattern. (Liu, Bhandari, et al., 2018) observed that hardness of mashed potatoes filled with air was not influenced by filling pattern. A possible explanation for this discrepancy is that the infill materials for the pastes were different in both studies. Here, the filling material for the protein paste was chocolate, which was harder than the protein paste matrix, while (Liu, Bhandari, et al., 2018) used air as a filling material for mashed potatoes. The cohesiveness of protein bars with a chocolate layer was significantly higher than that of protein bars with a rectilinear pattern ($p < 0.01$) and a concentric pattern ($p < 0.01$) (Fig 6.2C). The cohesiveness of pure protein paste bars and pure chocolate bars were 0.075 (-) and 0.038 (-), respectively. The higher cohesiveness of the pure protein paste indicated a higher strength of internal bonds compared to those in chocolate (Tuoc & Glasgow, n.d.). It is likely that the distribution of chocolate in the protein bars with a rectilinear or concentric pattern disrupted the integrity of the protein paste leading to a reduced number of the strong protein paste internal bonds

compared to protein bars with a chocolate layer. Protein bars with a chocolate layer had the highest chewiness, which was significantly higher (p < 0.05) than that of protein bars with a rectilinear pattern (Fig 6.2D). The higher chewiness of protein bars with a chocolate layer was largely attributed to its higher cohesiveness.
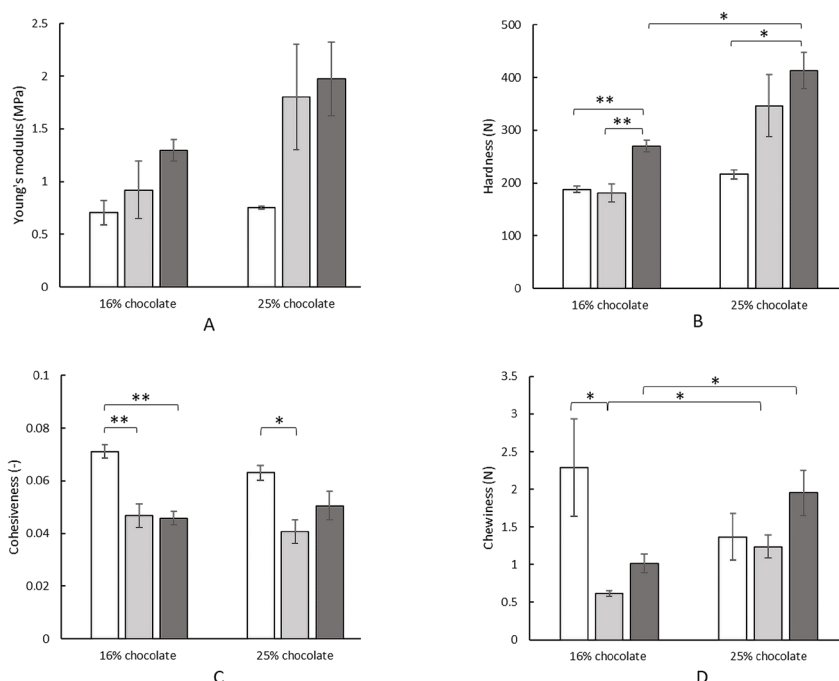
Figure 6.2. Young's modulus (A), hardness (B), cohesiveness (C), and chewiness (D) of 16 and 25 g/100g chocolate protein bars with layered (white), rectilinear (light grey) and concentric (dark grey) filling pattern. Error bars indicate standard error of the mean. Significant differences are indicated by * (p < 0.05) and ** (p < 0.01). Significant differences between samples differing in infill pattern but with same chocolate content (16 or 25 g/100g) were determined separately using one-way ANOVA followed by Tukey post-hoc tests. Significant differences between 16 and 25 g/100g chocolate content protein bars with same infill pattern were determined by independent samples t-tests.

For the 25 g/100g chocolate protein bars, no significant differences in Young's moduli (p = 0.097) were observed between layered, rectilinear and concentric pattern. Young's moduli of protein bars with concentric and rectilinear pattern tended to be higher than that of protein bars with a chocolate layer (Fig 6.2A). Protein bars with a concentric pattern were significantly harder than protein bars with a chocolate layer (p < 0.05) (Fig 6.2B). The cohesiveness of protein bars with a chocolate layer was significantly higher than that of protein bars with a rectilinear pattern (p < 0.05) (Fig 6.2C). As discussed above, chocolate

distributed in protein bars with a rectilinear pattern disrupted the protein paste phase, resulting in a reduced cohesiveness. No significant differences were found in chewiness among the 25 g/100g chocolate protein bars (Fig 6.2D).

An increase of the chocolate content from 16 to 25 g/100g did not significantly change Young's modulus of protein bars with layered (p = 0.695), rectilinear (p = 0.197) or concentric (p = 0.136) pattern (Fig 6.2A). 25 g/100g chocolate content protein bars with concentric pattern were significant harder (p = 0.017) than 16 g/100g chocolate content protein bars with concentric pattern. No significant differences were observed for hardness of protein bars with a chocolate layer (p = 0.052) and with rectilinear pattern (p = 0.055) when an increase of chocolate content from 16 to 25 g/100g, yet a trend towards increased hardness with higher chocolate content was apparent (Fig 6.2B). Cohesiveness of protein bars was hardly influenced by chocolate content, regardless of the chocolate distribution pattern (Fig 6.2C). A significant increase in chewiness was found for protein bars with rectilinear (p = 0.018) and concentric (p = 0.044) patterns when increasing chocolate content from 16 to 25 g/100g, while chewiness of protein bar with a chocolate layer was not significantly influenced (p = 0.269). The Young's modulus of the protein paste without chocolate and the Young's modulus of pure chocolate bar were 1.22 ± 0.32 MPa and 4.32 ± 0.60 MPa, respectively.

6.3.2. Explanation and discussion of instrumental texture properties using spring models

Figure 6.3 shows a schematic drawing of spring models and side-cut images of layered and concentric protein bars with 16 and 25 g/100g chocolate content. These spring models were developed to understand and predict the Young's modulus of the 3D printed protein bars filled with chocolate described in section 6.3.1. If we assume that the protein paste and chocolate have a similar density, the volume fractions of protein paste were 84% and 75% for protein bars with 16 and 25 g/100g chocolate content, respectively. For protein bars with a top chocolate layer, the overall spring constant can be approximated as two springs in series with a small spring representing the chocolate and a larger spring representing the protein paste (Fig 6.3A). Table 6.3 shows calculated spring constants for the chocolate, protein paste and the total spring constant for protein bars with different chocolate content (16 and 25

g/100g) and chocolate distribution patterns (layered and concentric). Spring constants of protein bars with layered structures were calculated based on equation 6.6. The calculated theoretical Young's moduli were 0.68 MPa and 0.74 MPa for 16 and 25 g/100g chocolate content protein bars, respectively. For protein bars with chocolate distributed in a concentric pattern, the overall spring constant can be considered to depend on two separate springs representing the protein paste and chocolate filling acting in parallel (Fig 6.3B). Spring constants of protein bars with concentric structures were calculated based on equation 6.7. The calculated theoretical Young's moduli were 1.71 MPa and 2.00 MPa for 16 and 25 g/100g chocolate content concentric protein bars, respectively. These calculated theoretical Young's moduli values matched with experimentally determined Young's moduli.
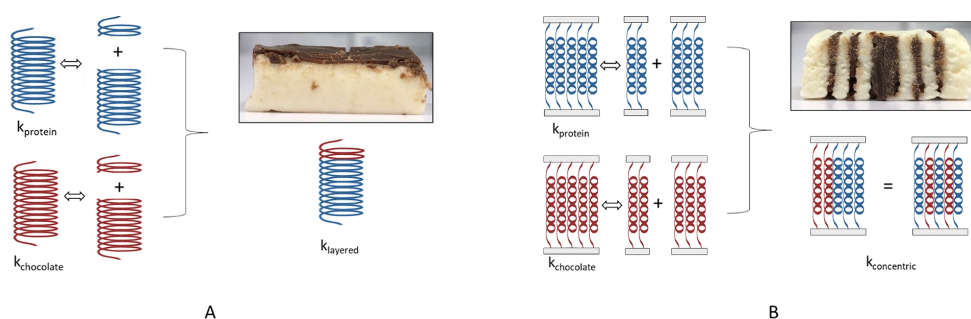
Figure 6.3. Schematic drawing of spring models and side-cut images of protein bars. (A) In-series spring model and side-cut image of 16 g/100g chocolate protein bar with a chocolate layer, and (B) in-parallel spring model and side-cut image of 16 g/100g chocolate protein bar having a concentric pattern.

For protein bars with a rectilinear pattern, the filled chocolate could flow in both perpendicular and parallel directions between printed protein paste strings. Therefore, the spring model for rectilinear protein bars would probably be a combination of in-series springs and in-parallel springs. The theoretical Young's modulus of the rectilinear protein bar probably has a value in between that of protein bars with layered and concentric pattern.

Table 6.3. Calculated spring constants for chocolate, protein paste and total spring constants for protein bars with different chocolate content (16 and 25 g/100g) and different chocolate distribution patterns (layered and concentric).

	Layered 16 g/100g chocolate	Layered 25 g/100g chocolate	Concentric 16 g/100g chocolate	Concentric 25 g/100g chocolate
$k_{chocolate\_part}$ (MPa)	0.72	0.81	1.02	0.92
$k_{protein\_part}$ (MPa)	13.5	8.64	0.69	1.08
k_{total_theory} (MPa)	0.68	0.74	1.71	2.00
$E_{experimental}$ (MPa)	0.70	0.75	1.30	2.00

6.3.3. Sensory evaluation

Comparison of protein bars with 16 g/100g chocolate content

The mean ranks of liking, perceived hardness and perceived chewiness of 16 g/100g chocolate protein bars with layered, rectilinear and concentric pattern are shown in Table 6.4. No significant differences were observed for liking between protein bars ($\chi2(2) = 4.229$, $p = 0.121$). Protein bars with a concentric pattern tended to be perceived harder than protein bars with layered and rectilinear patterns ($\chi2(2) = 5.943$, $p = 0.051$). The perceived hardness of protein bars is in good agreement with the instrumentally determined hardness (Fig 6.2B). Protein bars with layered structure had comparable instrumental hardness as protein bars with rectilinear pattern. Similarly, to perceived hardness, instrumental hardness values of layered and rectilinear bars were lower than instrumental hardness of protein bars with concentric pattern. No significant differences were observed for chewiness between protein bars ($\chi2(2) = 0.343$, $p = 0.842$). Unlike hardness, perceived chewiness was not in agreement with instrumental chewiness determined instrumentally (Fig 6.2D). This discrepancy between perceived and instrumental chewiness is not surprising. Perceived chewiness was defined as the mastication effort needed to chew a bar to a state ready for swallowing, while the

determination of chewiness using the instrumental texture analysis was based on two compression cycles of 50% strain. It is very unlikely that a protein bar could reach a state ready for swallowing with only two mastication cycles. Oral mastication is a more complex process since saliva is incorporated into the protein bar bolus upon mastication leading to lubrication of the bolus (van Vliet et al., 2009). These processes are not mimicked by the instrumental texture analysis.

Table 6.4. Mean ranks and p-values of ranking tests (n=70) of 16 g/100g chocolate protein bars differing in infill pattern. Lower mean ranks indicate protein bars that are perceived as more liked, harder and chewier.

	Layered	Rectilinear	Concentric	p-value
Liking	2.09	2.11	1.80	0.121
Hardness	2.17	2.06	1.77	0.051
Chewiness	2.03	2.03	1.94	0.842

A significant but weak, negative correlation was found between liking and chewiness (ρ = -0.136, p = 0.05), indicating that a chewier protein bar was less preferred by consumers. A significant but weak, positive correlation was observed between hardness and chewiness (ρ = 0.193, p = 0.005), which suggests that harder protein bars were perceived as chewier. No significant correlations were found between liking and hardness (ρ = -0.014, p = 0.084).

Comparison of protein bars with 25 g/100 g chocolate content

The mean ranks of liking, perceived hardness and perceived chewiness of 25 g/100g chocolate protein bars are shown in Table 6.5. No significant differences were observed for liking between protein bars ($\chi2(2)$ = 3.543, p = 0.17). Significant differences in perceived hardness were found between protein bars ($\chi2(2)$ = 37.829, p = 0.000). Protein bars with a layered pattern were perceived significantly less hard than protein bars with a rectilinear (Z = -4.802, p = 0.000) and a concentric pattern (Z = -5.000, p = 0.000). Perceived hardness did not significantly differ between protein bars with rectilinear and concentric pattern (Z = -0.186, p = 0.852). It seems that the sensory results of hardness perception did not fully comply

here with the results from the instrumental texture measurements in the sense that instrumental hardness did not significantly differ between protein bars with layered and rectilinear pattern (p = 0.130) (Fig 6.2B). Nevertheless, it is apparent that a large difference in average hardness (>100 N) existed between these two protein bars. The lack of significance of the instrumental hardness measurements might be caused by the fact that only three replicate measurements were performed. No significant differences were observed for perceived chewiness between protein bars ($\chi 2(2)$ = 4.2, p = 0.122).

Table 6.5, Mean ranks and p-values of ranking tests of 25 g/100g chocolate protein bars differing in infill pattern. Lower mean ranks indicate protein bars that are perceived as more liked, harder and chewier.

	Layered	Rectilinear	Concentric	*p*-value
Liking	2.14	2.03	1.83	0.170
Hardness	2.60[a]	1.69[b]	1.71[b]	<0.001
Chewiness	2.19	1.84	1.97	0.122

A significant but weak, negative correlation was found between liking and chewiness (ρ = -0.171, p = 0.013) for the protein bars with 25 g/100g chocolate, which aligns with results obtained with protein bars containing 16 g/100g chocolate. A consumer study done by Lundahl (2014) also suggested that a chewy texture of energy bars was less preferred by consumers. In addition, a significant but also weak, positive correlation was found between hardness and chewiness (ρ = 0.193, p = 0.005). No significant correlation was found between liking and hardness (ρ = -0.064, p = 0.354).

As mentioned previously, modifications on instrumental texture properties of 3D printed foods have been demonstrated by numerous studies, yet no study explored the impact of these structure modifications on sensory texture perception. To the best of our knowledge, this study reports for the first time results of analytical sensory texture evaluations of 3D printed foods. Results from this sensory study demonstrated that 3D printing is a promising tool to control sensory perception of protein bars filled with chocolate for different texture attributes.

By modifying the spatial distribution of solid chocolate in paste-like protein bars, sensory texture can be modified without affecting consumers liking. For paste-like, chewy foods like protein bars, the approach to use solid materials rather than air as filling material to modify texture perception is promising.

6.4. Conclusion

The aim of this study was to determine the influence of the macroscopic structure of 3D printed protein bars with chocolate fillings on instrumental texture properties and texture perception. We demonstrated that instrumental and sensory texture of semi-solid, paste-like foods can be modified by filling them with solid foods like chocolate. Protein bars with a composition that closely resembles formulations of commercially available recipes were used in this study. The instrumental texture analysis revealed significant differences among protein bars with different patterns. We proposed different spring models to better understand the impact of the spatial distribution of chocolate on Young's modulus and hardness of protein bars with different patterns. Such spring models can be used to predict texture properties of semi-solid materials in the future. Results of the sensory study were in good agreement with instrumental texture analysis results. To the best of our knowledge, this is the first study that explored sensory properties of 3D printed food pastes. This study demonstrated that by changing the macroscopic structure (printing pattern) of 3D printed foods, so by modifying the spatial distribution of solid chocolate in paste-like protein bars, both instrumental and sensory texture can be modified without affecting consumers liking. Thus, modifications of shape and structure by 3D food printing can be used to tailor texture perception of 3D printed foods. While this is not unexpected, to the best of our knowledge this is the first time that this benefit of 3D food printing has been demonstrated and supported with experimental data.

Chapter 7

General discussion

7.1. Introduction

The technique of 3D food printing is gaining increased interest thanks to its ability to create unique food designs that cannot be made with conventional manufacturing techniques. Many recent food printing studies focused on formulation of printable food materials and evaluation of printed food structures. However, these studies did not design guidelines for formulation and printing conditions to obtain desired product properties, nor performed research on applications with clear added value for consumers in terms of perceived taste and texture. The aims of this thesis were therefore (1) to understand the relationships between material properties, printing conditions and physical properties of printed foods, and (2) to determine how 3D food printing can be effectively used to modulate food structure and whether these modulations affect texture and taste perception of foods. In this chapter, we first summarize the main findings of the thesis. Then, a reflection on the main findings is given and finally, an outlook of future research about 3D food printing will be described.

7.2. Main findings

The research of this thesis started with investigating the relationships between formulation and 3D printing conditions to create foods of desired structural design (**Chapter 2 & 3**). **Chapter 2** reports about tomato paste as a model material to investigate the correlations between the rheological properties and printability (dispensability and stability) of a material during the extrusion-based printing process. The flow point has been established as a material property that has a strong impact on paste printability. The flow point of food inks determined by amplitude sweep oscillatory rheology experiments appeared strongly related to printing stability of model foods (tomato pastes) and commercial food pastes (aqueous- or fat-based), while the flow point was related to dispensability for aqueous food formulations. Based on the findings, a guideline was proposed to develop and realize printable recipes and printing designs more efficiently. As suggested by the guideline, the maximum height of an object during figure design and the extrusion force a printer should reach can be estimated based on the flow point of a printing material. In **Chapter 3**, the role of different components (CaCas, starch and MCT) for optimal binder jet 3D printing of protein-rich formulations was investigated. The addition of starch to CaCas formulations effectively enabled the binder jet printing process. Deposited binder content positively influenced cohesiveness of printed foods, while CaCas content in dry powder mixtures contributed to the springiness of the final

product. This study demonstrated that it is possible to create unique textures of protein-rich products using binder jetting 3D printing technology that are difficult to obtain by other means. Results from both **Chapter 2 & 3** reveal the importance of understanding material properties (e.g., flow behaviour of food pastes, binder-powder interactions) to achieve good printability.

Chapters 4, 5, and **6** describe how 3D printing can be used to modify food structures at the micro- and macroscale, and how the structure modifications alter sensory perception. In **Chapter 4** the extrusion-based printing of SC/SA blends into fibrous multi-scale structured model foods is described. At the macro-scale a fibrous structure was created by designing a parallel printing path in the longitudinal direction. Both the calcium content in the fluid gel bath and the geometry of printing nozzles influenced the fusion of neighbouring printed filaments. It was discovered that both printing speed and nozzle geometry could be used to steer the morphology of the smaller micro-scale fibrous filaments.

The feasibility to apply 3D printing to alter sensory perception is evaluated in **Chapters 5 and 6**. In **Chapter 5,** the distribution of chocolate coatings on rice waffles was achieved by using inkjet printing technology in order to create variation in sensory perception from bite to bite. The study showed that sweetness of chocolate coated rice waffles can be modified without changing the overall amount of chocolate consumed. **Chapter 6** investigated the influence of the macroscopic structure of 3D printed protein bars with chocolate fillings on instrumental texture properties and sensory perception. Among protein bars with different printing patterns, the ones with concentric chocolate infill pattern were the hardest, both for instrumental and sensory hardness. Liking and perceived chewiness of printed protein bars were not influenced by the spatial distribution of the chocolate infill pattern. The study demonstrated that by changing the macroscopic structure (printing pattern) of 3D printed protein bars with chocolate fillings, the instrumental and sensory properties can be modified.

7.3. Understanding the interplay between material properties, printing conditions and physical properties of 3D printed foods

7.3.1. Extrusion-based printing

Extrusion-based printing is the most widely used 3D food printing method. In this thesis, room-temperature printing of food materials was investigated that are either self-standing after extrusion (**Chapter 2**), or solidify upon chemical crosslinking (**Chapter 4**). Elevated-temperature printing was applied to process more solid-like food materials such as dense protein pastes, which solidified upon cooling after printing (**Chapter 6**). To achieve good printability, the combination of two material properties turned out to be critical: extrudability and stability/buildability.

Extrudability

Extrudability, sometimes referred to as dispensability, is defined as the force needed to extrude foods through a printing nozzle. For a material to be extrudable, the extrusion force for self-supporting food pastes/slurries builds up gradually while the piston pushes downwards and ultimately attains a constant value while the material is smoothly extruded. This raises the questions whether extrudability of a food can be predicted based on rheological properties during extrusion-based printing or that other factors should be considered to predict to extrusion-based printability?

Several recent studies demonstrated that the Herschel–Bulkley model (i.e., a generalized model for non-Newtonian fluids) with consistency index (K) and the flow index (n) can be well used to assess extrudability of food pastes (Liu, Zhang, et al., 2018; Ma et al., 2021). Liu et al. suggested pastes with a relatively small K and n value are preferred for extrusion. Chen et al. showed that starch pastes need to have a relatively low flow stress in order to be easily extruded. In **Chapter 2**, flow stress was indeed determined as the critical rheological property that determines extrudability of food pastes. A strong linear relationship between flow stress and extrusion force was observed for tomato pastes, and this held also for several other aqueous-based food pastes (vegepate, mayonnaise, kippate). Thus, for aqueous-based food pastes extrudability can be predicted based on flow stress. Printing conditions such as printing temperature, speed and nozzle geometry are also known to affect extrudability (Ma et al., 2021; Udofia & Zhou, 2019). Many studies printed food materials at elevated

temperature which was effective in lowering viscosity of food materials and required extrusion force (Ross et al. 2021; Hao et al. 2010).

Ideally, the extrusion force for self-supporting food pastes or slurries builds up gradually while the piston pushes downwards after which the force reaches a constant value during smooth extrusion. However, even though the measured flow point from oscillatory rheology measurements can be used to predict the overall force needed to extrude a food ink as suggested in **Chapter 2**, it does not assure that food materials can always be smoothly extruded. While normally food inks should be extrudable, in practice during development of new inks it may be a struggle to formulate food inks that can be smoothly extruded. This is partly because most food inks are dispersions that contain for example solid particles, crystals or oil droplets. Suspensions are hard to remain homogenous over time. The dispersed phase may aggregate or sediment leading to clogging of the nozzle and thus disturbing a flow and thus severely limiting printability. Besides, shearing during extrusion can induce separation of the dispersion into zones that are particle-rich and other zones that are particle-depleted (Coussot, 2014). Dispersed particles can form a percolating network during extrusion, where the dispersed particles act as a filter allowing for drainage of the liquid which leads to compaction (Mascia et al., 2006). Due to clogging, the pressure inside the barrel can build up until a critical pressure is reached, after which the accumulated particles leading to the clogging are suddenly pushed out. A straightforward way to predict whether a paste can be smoothly extruded, is to assess possible segregation of particles in a food paste by means of centrifugation. Segregation is most likely to occur in the presence of free water and can thus be associated to risk of clogging during extrusion.

An example of assessing the extrudability of a food paste consisting of pea protein isolate (PPI), oil, starch, and fibre is provide here. The extrusion force of food inks containing 10% and 18% PPI during extrusion from a syringe connected to a texture analyser are shown as function of piston displacement in Figure 7.1A. The extrusion force of 10% PPI inks fluctuated strongly during the extrusion process, which indicates clogging during the extrusion leading to uneven extrusion and thus to poor control of the shape of the printed food. A straightforward way to assess whether inks of PPI, oil, starch and fibre can be smoothly extruded is via centrifugation of the ink. Inks that showed particle segregation (the white starch particles are clearly on top) after centrifugation (10% PPI) could not be printed (Fig 7.1B). In contrast, inks that showed no segregation after centrifugation (18% PPI) were extrudable and printable into objects of well-defined shape.

(A)   (B)
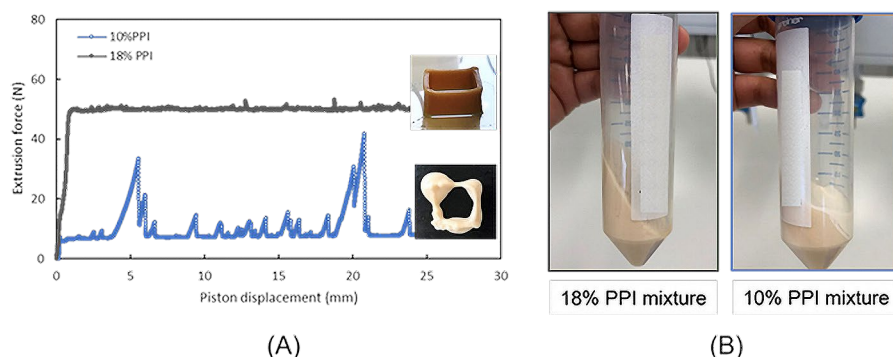
Fig 7.1 (A) Extrusion force of pastes containing 10% or 18% pea protein isolate, 8% sunflower oil, 3% pea starch, and 3% pea fibre. (B) Pastes containing either 10% or 18% pea protein isolate, and with 8% sunflower oil, 3% pea starch, and 3% pea fibre after centrifugation at 20,000 g for 20 min.

There are several strategies to prevent clogging of nozzles during extrusion of food formulations with dispersed particles. The first one is to formulate food inks with a more "jammed" structure by increasing solid content or removing free water, as shown in the example described above (Fig 7.1). An increase of the volume fraction of the solid phase keeps particles in the flow trajectory during extrusion due to the restricted moving space. Another strategy is to add hydrocolloids to increase the viscosity of the liquid phase to slow down sedimentation or aggregation of particles. Other ways to avoid clogging are for instance

using printing nozzles with a larger outlet diameter or tuning particle properties such as size or shape to reduce the risk of clogging. These solutions seem reasonable from an operational perspective but may not always be possible due to practical restrictions such as required printing resolution or required macronutrient composition. On top of that extrudability is also restricted by the maximum extrusion force that a printer can achieve.

In short, extrudability of food pastes is correlated to rheological parameters such as consistency index, flow index and flow stress. Since a linear correlation was found between flow stress and required extrusion force during printing processes (**Chapter 2**), one may derive the required extrusion force of an aqueous-based food paste from its flow point. Nevertheless, more research is needed to extend and further substantiate this guideline. For food materials that are difficult to extrude at room temperature, printing at elevated temperature can lower the viscosity and flow stress and reduce the required force needed for printing. Moreover, to assess the potential risk for clogging of aqueous-based food pastes, one may apply simple centrifugation.

Stability/Buildability

In addition to extrudability, stability/buildability is critical to achieve good printability. Some studies defined stability as the moment of reduction in height during the printing process (Rando and Ramaioli 2021), while other studies defined stability as the ability to remain the height of a printed structure after a defined storage period (Kim, Bae, and Park 2017; Chow et al. 2021). A general definition of stability is difficult to provide because the printing stability depends on the application case. In **Chapter 2,** stability was assessed via measurement of the stress at the collapsing moment of the printed food.

Stability may be expected closely related to the yield stress of a printable food paste (Wilms et al., 2021), which is defined as the stress that must be applied to a material before it starts to flow. Yield stress depends on the internal structure of a material. For concentrated suspensions such as food pastes, electrostatic interactions and direct contact between the suspended particles play a crucial role in determining a material's yield stress (Coussot, 2014). So far, there is no universal approach to determine yield stress. While traditionally yield stress is determined via mathematical curve-fitting models of flow curves (Rando and Ramaioli 2021), many studies determined yield stress as the initial drop of the storage modulus obtained from stress ramp measurements (Chen et al., 2019; Chow et al., 2021; Lille

et al., 2018). In **Chapter 2**, we demonstrated that the yield stress (flow stress) determined by oscillatory amplitude sweep at which storage modulus and loss modulus crossover has a linear relationship with the stability/buildability of a 3D printed object. It is important to point out that neither yield stress nor flow stress are material constants, and they both depend on the measuring and analysis method used (Mezger, 2015; Wilms et al., 2021). For food pastes such as doughs and chocolate spreads the time-dependent flow behaviour influences printing stability/buildability. Therefore, thixotropy behaviour of a printing material needs to be taken into consideration in future research. Besides flow stress, Chapter 2 also shows that zero shear viscosity can be a good indicator of stability/buildability of printed objects, and similar conclusions have been reported recently by Zheng et al. (2021).

As stated above, food pastes with a higher zero shear viscosity and flow stress allow building of higher objects. Besides material properties, more factors such as printing design, post processing method can all influence the stability of a printed product. For instance, a proper printing design can also help to improve printing stability. In **Chapter 2**, we printed a hollow column, which by itself is not very stable compared to printing designs with more solid infill. For materials that are printed at an elevated temperature (e.g., protein paste in **Chapter 6**) or require crosslinking, one needs to consider cooling rate or crosslinking kinetics to rapidly solidify the material to achieve good stability.

To summarize, both extrudability and stability/buildability are critical to assess whether a food material is printable in extrusion-based 3D printing. Extrudability and stability/buildability of a food material can be derived from simple rheological parameters such as flow stress and zero-shear viscosity. To ensure a smooth printing process and stable printed products, possible flow-induced segregation in a food dispersion system during printing as well as thixotropic behaviour of printed materials could be considered.

7.3.2. Powder bed printing

A major challenge in food powder bed printing is to find a proper powder mixture and suitable binder. A printable powder should flow freely upon spreading in the printer (Holland et al., 2019). Particle size, morphology, and surface cohesiveness influence powder spreadability. There is currently no flowability testing method available that can fully predict the spreading process during powder bed printing. A simple method that characterizes the

spreadability of food powders is the angle of repose, which is described in **Chapter 3**. Therefore, particle size analysis together with angle of repose measurements are recommended for future applications to have a better prediction of spreadability of a food powder in powder bed printing.

Powder bed printing using food powders is not widely investigated (Diaz et al., 2017; Holland, Foster, et al., 2018; Holland, Tuck, et al., 2018) and mostly powders that contain substantial amounts of sugar or maltodextrin are used. This is because many food powders tend to swell upon hydration after binder deposition. The swelling impairs the powder bed printing process as a wet layer emerges above the powder bed surface, which causes misalignment and disruption of structures when a subsequent layer of powder is applied (Holland et al., 2019). In **Chapter 3**, non-swelling powder particles, i.e., native starch, were mixed into caseinate powder to minimize swelling. The added starch granules agglomerated and formed a dense packing when binder was added. The reduced volume occupied by inert particles can compensate for the increased volume of rehydrated powders and ensures that the wetted layer surface does not interfere with a subsequent printing layer. The study in **Chapter 3** also shows that by depositing a droplet of binder onto a pile of powder, one can quickly screen swelling behaviour and binder sorption behaviour of a powder formulation.

During powder bed printing usually inkjet nozzles are applied. The binder should be within a range of viscosity and surface tension values to allow accurate ink deposition (Holland et al., 2019). Clogging of these inkjet nozzles may also occur. During our study, we observed the presence of micron-sized crystalline particles in the developed Polysorbate 20 binder. The micron-sized crystalline particles clogged the nozzle and prevented ink deposition. Filtering of the binder prior to filling of the printing head solved this issue.

In **Chapter 3** we have discussed how the amount of deposited binder influenced the texture of printed objects. Printing speed was also found critical for successful printing. In our study, fast printing avoided swelling of powder structures facilitating a smoother printing process, while at slow printing excessive swelling impaired the process.

The selection of a proper binder is equally important as finding a proper powder mixture for powder bed printing. Initially, the work in **Chapter 3** applied unfiltered Polysorbate 20 solutions as binder. However, with time the binder jet flow rate declined which ultimately led blocking of the inkjet printhead. Crystalline particles were detected in the Polysorbate 20 binder solutions after visual inspection (Fig 7.2), which tended to aggregate into fibril-like structures. We hypothesized that these particles were Polysorbate 20 crystals. Polysorbate 20 may self-assemble into micro and nano-sized branched networks and further form crystal-like structures (Cardiel et al., 2015). The problem was solved by filtration of the binder with a 0.2 μm membrane prior to filling the printing cartridge.
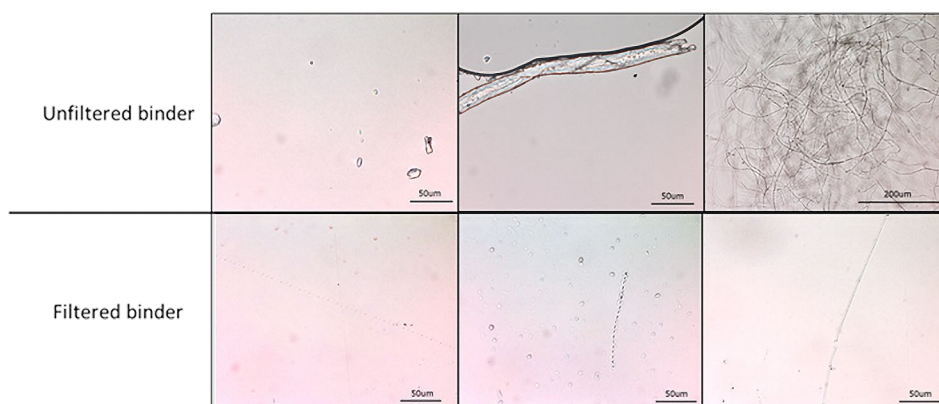
Fig 7.2 Microscopic images of unfiltered binder and binder filtered through 0.2 um membrane. Binder contains 0.0123% Polysorbate 20, and images were taken after storage at room temperature for 4 days.

7.4. How 3D food printing can be effectively used to modulate food structure and thus texture and taste perception of foods

Three major opportunities of 3D food printing are to: 1) create unique anisotropic structures (e.g., fibrils) that are not able to be obtained through other manufacturing technologies; 2) customize printed structures to meet personal demand in taste and texture; and 3) create healthier foods with reduced sugar/salt/fat content by creating structures with inhomogeneous distribution of food components. In this thesis, the first and second opportunity were explored in order to address the second aim of the thesis, i.e., to determine how 3D food printing can be effectively used to modulate food structure and thus texture and

taste perception of foods. We will further discuss how 3D printing can be used to create healthier foods and how competitive it is compared to conventional food production methods.

7.4.1. Creating unique anisotropic structures using 3D printing

Chapter 4 demonstrated that 3D printing can be used to produce fibrous structures at both microscopic and macroscopic length scale. Anisotropic fibrous microstructures were obtained during extrusion in a single filament thanks to protein alignment during flow. Subsequently, we printed the fibrous filaments in a parallel printing design (Fig 7.3A). An alternative approach to obtain a macroscopic fibrous structured is shown in Figure 7.3B, which was achieved by printing alternating strings of a pea protein paste (with added Ca^{2+}) and an alginate solution. The drawback of this approach was that the fibrous structure was only achieved at the macroscopic scale (unpublished results). Recently, Ko et al. (2021) published a study on 3D printing of fibrous structures with a coaxial nozzle using a combination of cross-linked hydrocolloids and soy protein (Fig 7.3C). A study done by (S. M. Kim et al., 2021) also showed the potential of using coaxial extrusion 3D printing to create imitation crab meat.
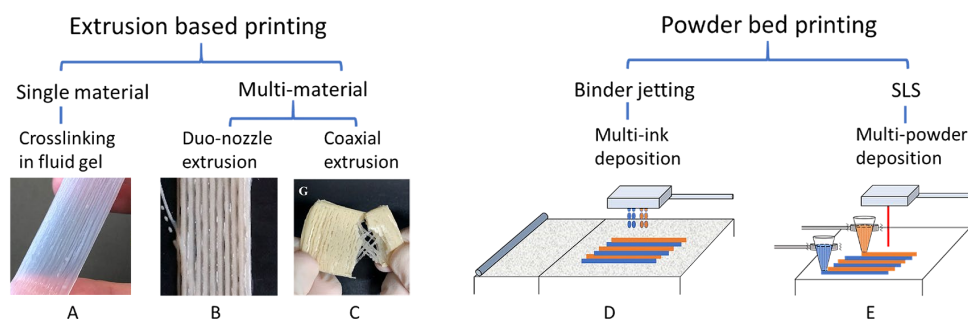
Figure 7.3. Strategies to create anisotropic structures or inhomogeneous tastants distribution using extrusion-based printing (A, B, C) or powder bed printing (D, E). Figure 7.3C is adapted from (Ko et al., 2021).

Other technologies such as extrusion cooking, spinning, and shear cell technology also have been applied for creating anisotropic fibrous meat-like structures (Kyriakopoulou et al., 2018; Manski et al., 2007). So far, extrusion cooking is the commercially most widely applied

131

structuring technology to produce meat analogues. Plant-based blends (e.g., soy-gluten) are used for extrusion cooking (Kyriakopoulou et al., 2018; Grabowska et al., 2016; Jia et al., 2021). During extrusion cooking, proteins are plasticized inside the heated barrel, subjected to extensive mechanical forces and finally aligned during laminar flow inside a cooling die (Dekkers et al., 2018). Shear cell technology was developed to produce fibrous products under well-defined shear flow (Dekkers et al., 2016; Grabowska et al., 2016). The method of using 3D printing to create anisotropic fibrous structure using SC/SA blend described in **Chapter 4** can be considered a new structuring methodology to create a hierarchical fibrous material in one process step. Microscale fibrous structures of individual filaments were created by alignment and fixation of the deformed protein phase while printed filaments were fused together into a bigger piece by additive manufacturing.

The technique of 3D food printing appears a promising way to create unique anisotropic fibril structures that cannot be obtained through other manufacturing technologies. However, no studies investigate sensory perception of these 3D printed anisotropic structures, and it remains a question whether the texture and mouthfeel of these 3D printed anisotropic structures can mimic the texture and mouthfeel of meat products. Moreover, an ideal 3D printed anisotropic structure mimicking meat analogues should not only have a comparable taste and texture, but also have a composition (e.g., protein and fat content) similar to that of real meat. Besides, hydrocolloids or other thickening agents might be necessary to create stable printed products that are appreciated by consumers. Therefore, more research is needed to investigate the sensory properties of printed anisotropic foods.

7.4.2. Customization of printed foods to obtain desired taste and texture

Another added value of 3D food printing is the possibility to change the spatial distribution of tastants or components in foods. This may lead to variation in texture or taste that can be perceived by consumers. We explored the potential of using different 3D printing to customize chocolate-containing food products to modify their taste and texture following a multi-bite and single bite approach. In **Chapter 5** inkjet printing was applied to change the chocolate coating distribution on a rice waffle from one bite to another; In **Chapter 6** extrusion-based printing was used to change the distribution of chocolate in a protein bar.

Both studies demonstrated that by changing the spatial distribution of chocolate in a 3D printed product the sensory properties could be modified.

Customization of printed structures to modify taste perception

In real life, bite-to-bite taste variation can occur. An example of a food with bite-to-bite variation in taste intensity is watermelon. A slice of watermelon tastes sweeter in the first few bites close to the core of the whole fruit (placenta part), while the sweet taste is less for the last bites close to the peel (Kano, 1991). Many consumers appreciate this bite-to-bite contrast and it may even allow design of healthier products (see next section). Several studies have looked into bite-to-bite variation e.g., in sugar/salt for foods like cream cheese filled sandwiches (Dijksterhuis et al., 2014), chocolate ice-creams (Le Berrre et al., 2013) and custards (Mosca et al., 2014). The studies show that an enhancement of sweetness or saltiness perception can be achieved by creating foods with either a high tastant content in the first bite (Dijksterhuis et al., 2014) or in the last bite (Mosca et al., 2014), and the observed results were attributed to cognitive biases (priming or recency effects). In the study presented in **Chapter 5**, we observed differences in sweetness, expected fullness and liking between chocolate coated rice waffles differing in bite-to-bite chocolate content, although the magnitude of the differences was smaller than in the previous studies. Interestingly, it was also concluded that inkjet printing is a very precise and efficient strategy to prepare the spatially distributed foods at a larger scale.

Customization of printed structures to modify texture perception

The study described in **Chapter 6** showed that 3D printed protein bars with different chocolate infill patterns affected sensory hardness. Current protein bars in the market face two challenges, a chewy texture that is not liked by consumers and hardening during storage. In **Chapter 5**, chewiness of protein bars with different chocolate distribution patterns was evaluated. Even though we did not observe statistically significant differences in perceived chewiness among different samples, a tendency of reduced chewiness was noted when chocolate was more evenly distributed inside the protein bar. Therefore, 3D printing is promising to create protein bars with reduced chewiness by locating chocolate in a more scattered way. This can be realized by e.g. keeping the same infill density and infill pattern, while reducing the size of the printing nozzle. Hardening of protein bars is believed to be initiated by phase separation of the lipid and the aqueous phase, followed by moisture-

induced protein aggregation (Mcmahon et al., 2009). It may be that the distributed chocolate pieces in 3D printed protein bars act as physical barriers that retard phase separation and thus hardening of the protein paste, which may be an additional benefit for 3D printed chocolate bars.

7.4.3. Creation of healthier foods with reduced sugar/salt/fat content by creating structures with inhomogeneous distribution of food components

Diets in the WHO European Region are characterized by an overall energy imbalance and excessive intake of sugar, fats and salt, which contributes to an increased risk of non-communicable diseases such as cardiovascular diseases, cancer and diabetes (Lea Nash Castro et al., 2021). Food manufacturers seek thus for solutions to develop healthier foods that are reduced in sugar and fat without compromising sensory properties such as taste and texture. One approach to design healthier foods is to create an inhomogeneous distribution of tastants in foods to enhance sensory perception of single bites of foods. Several studies showed that saltiness, sweetness, and fattiness perception can be enhanced by manipulating the spatial distribution of tastants in foods (Mosca et al., 2010, 2012; Noort et al., 2012). Another approach to design healthier foods is to change food structures to increase expected satiation. An example of this approach is to formulate foods with more aerated structures (Arboleya et al., 2014; Osterholt et al., 2007; Serisier et al., 2014). In these studies, consumption of aerated foods led to less energy intake compared to less aerated foods.

As mentioned in previous sections, 3D printing can be a useful tool to create customized food structures and allows preparation of foods with an inhomogeneous distribution of tastants (Fahmy et al., 2021; Kistler et al., 2021). Kistler et al modified sugar distribution inside confectionary candies using extrusion-based 3D printing. They successfully created confectionary products with enhanced sweetness while maintaining the same sugar content (Kistler et al., 2021). Variation in porosity of 3D printed cookies influenced consumers' chewing time, which might potentially affect satiation (Punpongsanon et al., 2020). These studies demonstrated that 3D printing can be used to create healthier foods by either creating an inhomogeneous distribution of food components or by creating porous structures. Although food products in the above-mentioned studies were made by extrusion-based printing, other printing technologies such as powder bed printing and inkjet printing, are also

promising to be applied to create healthier foods. For instance, modifying tastant distribution can be realized by jetting with multiple cartridges containing binders differing in tastant amount (Fig 7.3D). For SLS, one may consider spreading two or more different food powders by e.g., different piezoelectric activated hoppers (Klomp & Anderson, 2017) (Fig 7.3E).

So, the question remains: Is 3D printing more competitive compared to current manufacturing methods when healthier foods with inhomogeneous distribution of food components are produced? Different traditional manufacturing technologies (e.g., panning, sheeting, filling) allow mass production of foods with coatings, layers, and fillings, and they are less time consuming than 3D printing. Mass produced foods with inhomogeneous distribution of food components are for instance yoghurt with swirled fruit paste fillings, candies with chocolate coatings or filled with nuts, ice creams in various shapes with various layers differing in colour and flavour. However, food structures produced using current manufacturing technologies are relatively limited. While the confectionery products in the study of Kistler et al. (2021) and savoury foods in the study of Fahmy et al. (2021) can easily be achieved through conventional manufacturing (think of candies with liquid fillings or commercial layered cakes), it would be challenging to produce foods with more complex structures such as for example protein bars with rectilinear infill (**Chapter 6)** and cookies with defined porosity (Punpongsanon et al., 2020). Finally, it is expected that 3D printing is more cost effective than conventional manufacturing techniques for local and on-demand production such for example at home or in a local retailer, restaurant, hospital or gym.

7.5. Outlook for future research

The aim of the thesis was to understand the relation between material properties and printing conditions to arrive at a desired printed food, and to determine how 3D food printing can be effectively used to modulate food structure, texture, and taste perception.

In **Chapter 2**, rheological properties of food pastes were correlated with their printing behaviour during extrusion-based 3D printing. Results of the study show that rheological parameters such as flow stress and zero shear viscosity are correlated to extrudability and stability/buildability. However, the established relationship between rheological parameters and printability appeared not valid for fat-based materials due to strain hardening. In addition, the study did not investigate the influence of different printing conditions (e.g., temperature, extrusion speed, nozzle geometry and arbitrary object design). For foods that require elevated

printing temperature and quick solidification post deposition, one needs to consider materials' temperature-dependent flow behaviour. Therefore, more research is needed to better understand the relationship between material rheological property, printing conditions and printability by considering thixotropy and temperature-dependent behaviour of printing materials.

As discussed in section 7.4.3, 3D food printing can be used to modulate food structure, texture, and taste and can even contribute to development of healthier foods. A new development is 4D printing, which in fact is the combination of a 3D printing and subsequent changes of a printed product when contacted with an external stimulus such as temperature, water, etc. (Ahmed, 2018). During the past few years, food researchers started to apply this concept to foods, and several studies (He, Zhang, & Devahastin, 2020; Tao et al., 2019) demonstrated the feasibility of creating 4D printed foods that change in colour or morphology upon stimulation. Because colour and shape are food hints that can affect consumers' eating behaviour (Garber et al., 2000; Labbe et al., 2018; van Ittersum & Wansink, 2012), it is interesting to conceptualize healthier foods made by 4D food printing.

In future studies, multidisciplinary collaboration between mechanical and food engineers is desired to improve 3D printing hardware to facilitate 3D printing of customized complex food structures. For instance, there is a need to develop 3D food printers that allow a wider range of materials to be printed (e.g., by using adaptive control) and that can operate at increased production capacity while retaining printing accuracy.

Recent papers (Jayaprakash et al., 2020; Portanguen et al., 2019) suggested that 3D printing can be a sustainable food manufacturing method. While traditional food manufacturing method applies a "deduction" strategy, the "additive" approach 3D food printing takes, is claimed to reduce food waste. However, so far, no systematic investigations have been done to underpin this claim. Therefore, a thorough life cycle assessment should be carried out to evaluate 3D food printing and compare it to traditional manufacturing methods. In this life cycle assessment, it is also important to consider the scale of production., i.e., at home, at the retailer or in a factory.

7.6. Concluding remarks

3D food printing is an emerging technology well-known for shape customization and personalized nutrition. Three challenges for 3D food printing are 1) how rheological material properties influence successful 3D food printing, 2) how 3D printing can create food structures different from traditional processing methods, and 3) how 3D food printing can be used to alter sensory perception towards foods to achieve healthier products while maintaining sensory properties. The work reported in this thesis provides insights in the relationships between material properties, printing conditions and final physical properties of 3D printed foods. It also demonstrates how 3D food printing can be effectively used to modulate food structure and customize perceived texture and taste. The knowledge gained from this work will facilitate realization of the potential societal impact of 3D food printing, i.e. to create healthier foods products with new structures and textures.

R

References

References

Ahmed, J. (2018). Recent Advances of Novel Materials for 3D/4D Printing in Biomedical Applications. In *3D and 4D Printing in Biomedical Applications* (pp. 239–271). https://doi.org/10.1002/9783527813704.ch10

Arboleya, J. C., García-Quiroga, M., Lasa, D., Oliva, O., & Luis-Aduriz, A. (2014). Effect of highly aerated food on expected satiety. *International Journal of Gastronomy and Food Science*, *2*(1), 14–21. https://doi.org/10.1016/j.ijgfs.2013.12.002

Arnaud Perrot, & Sofiane Amziane. (2017). *3D Printing and Its Impact on the Production of Fully Functional Components* (pp. 1–24). IGI Global. https://doi.org/10.4018/978-1-5225-2289-8

Arrigo, R., Malucelli, G., & Mantia, F. P. la. (2021). Effect of the elongational flow on the morphology and properties of polymer systems: A brief review. In *Polymers* (Vol. 13, Issue 20). MDPI. https://doi.org/10.3390/polym13203529

Augustin, M. A., & Margetts, C. L. (2003). POWDERED MILK | Milk Powders in the Marketplace. In *Encyclopedia of Food Sciences and Nutrition* (pp. 4694–4702). Elsevier. https://doi.org/10.1016/B0-12-227055-X/00955-X

Bayod, E., Månsson, P., & Innings, F. (2007). *Low Shear Rheology of Concentrated Tomato Products. Effect of Particle Size and Time*. 146–157. https://doi.org/10.1007/s11483-007-9039-2

Beakawi Al-Hashemi, H. M., & Baghabra Al-Amoudi, O. S. (2018). A review on the angle of repose of granular materials. *Powder Technology*, *330*, 397–417. https://doi.org/10.1016/j.powtec.2018.02.003

Bireta, T. J., Gabel, A. J., Lamkin, R. M., Neath, I., & Surprenant, A. M. (2018). Distinctiveness and serial position functions in implicit memory. *Journal of Cognitive Psychology*, *30*(2), 222–229. https://doi.org/10.1080/20445911.2017.1415344

Bolhuis, D. P., & Forde, C. G. (2020). Application of food texture to moderate oral processing behaviours and energy intake. In *Trends in Food Science and Technology* (Vol. 106, pp. 445–456). Elsevier Ltd. https://doi.org/10.1016/j.tifs.2020.10.021

Burstein, L. (2014). *Handbook of research on advancements in manufacturing, materials, and mechanical engineering*.

Capron, I., Costeux, S., & Djabourov, M. (2001). Water in water emulsions: Phase separation and rheology of biopolymer solutions. *Rheologica Acta*, *40*(5), 441–456. https://doi.org/10.1007/s003970100161

Cardiel, J. J., Furusho, H., Skoglund, U., & Shen, A. Q. (2015). Formation of crystal-like structures and branched networks from nonionic spherical micelles. *Scientific Reports*, *5*(December), 1–9. https://doi.org/10.1038/srep17941

Caserta, S., Simeone, M., & Guido, S. (2008). Shear banding in biphasic liquid-liquid systems. *Physical Review Letters*, *100*(13), 1–4. https://doi.org/10.1103/PhysRevLett.100.137801

Caulier, S., Doets, E., & Noort, M. (2020). An exploratory consumer study of 3D printed food perception in a real-life military setting. *Food Quality and Preference*, *86*(June), 104001. https://doi.org/10.1016/j.foodqual.2020.104001

Chen, H., Xie, F., Chen, L., & Zheng, B. (2019). Effect of rheological properties of potato, rice and corn starches on their hot-extrusion 3D printing behaviours. *Journal of Food Engineering*, *244*, 150–158. https://doi.org/10.1016/j.jfoodeng.2018.09.011

Choi, S. G., & Kerr, W. L. (2004). Swelling characteristics of native and chemically modified wheat starches as a function of heating temperature and time. *Starch/Staerke*, *56*(5), 181–189. https://doi.org/10.1002/star.200300233

Chow, C. Y., Thybo, C. D., Sager, V. F., Riantiningtyas, R. R., Bredie, W. L. P., & Ahrné, L. (2021). Printability, stability and sensory properties of protein-enriched 3D-printed lemon mousse for personalised in-between meals. *Food Hydrocolloids*, *120*, 1–12. https://doi.org/10.1016/j.foodhyd.2021.106943

Coussot, P. (2014). *Rheophysics - Matter in All Its States*. https://doi.org/10.1007/978-3-319-06148-1

De Grood, J. P. W., & De Grood, P. J. (2013). *Method and device for dispensing a liquid*.

de Vita, F., Rosti, M. E., Caserta, S., & Brandt, L. (2020). Numerical simulations of vorticity banding of emulsions in shear flows. *Soft Matter*, *16*(11), 2854–2863. https://doi.org/10.1039/c9sm01898k

de Wijk, R. A., Engelen, L., Prinz, J. F., & Weenen, H. (2003). The influence of bite size and multiple bites on oral texture sensations. *Journal of Sensory Studies*, *31*(18), 423–435.

Dekkers, B. L., Boom, R. M., & van der Goot, A. J. (2018). Structuring processes for meat analogues. In *Trends in Food Science and Technology* (Vol. 81, pp. 25–36). Elsevier Ltd. https://doi.org/10.1016/j.tifs.2018.08.011

Dekkers, B. L., Nikiforidis, C. v., & van der Goot, A. J. (2016). Shear-induced fibrous structure formation from a pectin/SPI blend. *Innovative Food Science and Emerging Technologies*, *36*, 193–200. https://doi.org/10.1016/j.ifset.2016.07.003

Derossi, A., Caporizzi, R., Paolillo, M., & Severini, C. (2020). Programmable texture properties of cereal-based snack mediated by 3D printing technology. *Journal of Food Engineering*, *289*, 110160. https://doi.org/10.1016/j.jfoodeng.2020.110160

Dhont, J. K. G., & Briels, W. J. (2008). Gradient and vorticity banding. In *Rheologica Acta* (Vol. 47, Issue 3, pp. 257–281). https://doi.org/10.1007/s00397-007-0245-0

Diaz, J. V., Noort, M. W., & Kjeld Jacobus Cornelis, V. B. (2017). *Method for the production of an edible object by powder bed (3D) printing and food products obtainable therewith*.

Dijksterhuis, G., Boucon, C., & Le, E. (2014). Increasing saltiness perception through perceptual constancy created by expectation. *Food Quality and Preference*, *34*, 24–28. https://doi.org/10.1016/j.foodqual.2013.12.003

Division, A. C. S. F. C., Spanier, A. M., Shahidi, F., Parliment, T. H., Mussinan, C., Ho, C. T., & Contis, E. T. (2007). *Food Flavours and Chemistry: Advances of the New Millennium*. Royal Society of Chemistry.

Emorine, M., Septier, C., Andriot, I., Martin, C., Salles, C., & Thomas-Danguin, T. (2015). Combined heterogeneous distribution of salt and aroma in food enhances salt perception. *Food & Function*, *6*(5), 1449–1459. https://doi.org/10.1039/c4fo01067a

Emorine, M., Septier, C., Thomas-Danguin, T., & Salles, C. (2013). Heterogeneous salt distribution in hot snacks enhances saltiness without loss of acceptability. *Food Research International*, *51*(2), 641–647. https://doi.org/10.1016/j.foodres.2013.01.006

Fahmy, A. R., Amann, L. S., Dunkel, A., Frank, O., Dawid, C., Hofmann, T., Becker, T., & Jekle, M. (2021). Sensory design in food 3D printing – Structuring , texture modulation , taste localization , and thermal stabilization. *Innovative Food Science and Emerging Technologies*, *72*, 102743.

FDA. (n.d.). *Electronic Code of Federal Regulations: Title 21 Food and Drugs*. Https://Www.Ecfr.Gov/Cgi-Bin/Text-Idx?SID=d043fdcbe71231c3e1d732ba7f683e72&mc=true&node=se21.2.101_154&rgn=div8.

Felix da Silva, D., Ahrné, L., Ipsen, R., & Hougaard, A. B. (2018). Casein-Based Powders: Characteristics and Rehydration Properties. *Comprehensive Reviews in Food Science and Food Safety*, *17*(1), 240–254. https://doi.org/10.1111/1541-4337.12319

Fi Global. (2020). *Global consumer trends in the protein market*.

Fitzpatrick, J. J., Iqbal, T., Delaney, C., Twomey, T., & Keogh, M. K. (2004). Effect of powder properties and storage conditions on the flowability of milk powders with different fat contents. *Journal of Food Engineering*, *64*(4), 435–444. https://doi.org/10.1016/j.jfoodeng.2003.11.011

Gaiani, C., Scher, J., Schuck, P., Hardy, J., Desobry, S., & Banon, S. (2006). The dissolution behaviour of native phosphocaseinate as a function of concentration and temperature using a rheological approach. *International Dairy Journal*, *16*(12), 1427–1434. https://doi.org/10.1016/j.idairyj.2005.12.004

Gaiani, C., Schuck, P., Scher, J., Desobry, S., & Banon, S. (2007). Dairy powder rehydration: Influence of protein state, incorporation mode, and agglomeration. *Journal of Dairy Science*, *90*(2), 570–581. https://doi.org/10.3168/jds.S0022-0302(07)71540-0

Garber, L. L., Hyatt, E. M., & Starr, R. G. (2000). The Effects of Food Colour on Perceived Flavour. *Journal of Marketing Theory and Practice*, *8*(4), 59–72. https://doi.org/10.1080/10696679.2000.11501880

Ghebremedhin, M., Seiffert, S., & Vilgis, T. A. (2021). Physics of agarose fluid gels: Rheological properties and microstructure. *Current Research in Food Science*, *4*, 436–448. https://doi.org/10.1016/j.crfs.2021.06.003

Gibson, I., Rosen, D., Stucker, B., & Khorasani, M. (2021). Additive Manufacturing Technilogies. In *Yosetsu Gakkai Shi/Journal of the Japan Welding Society*. https://doi.org/10.2207/jjws.89.82

Godoi, F. C., Prakash, S., & Bhandari, B. R. (2016). 3d printing technologies applied for food design: Status and prospects. *Journal of Food Engineering*, *179*, 44–54. https://doi.org/10.1016/j.jfoodeng.2016.01.025

Goh, H. P., Heng, P. W. S., & Liew, C. V. (2018). Comparative evaluation of powder flow parameters with reference to particle size and shape. *International Journal of Pharmaceutics*, *547*(1–2), 133–141. https://doi.org/10.1016/j.ijpharm.2018.05.059

Gonzalez-gutierrez, J., & Scanlon, M. G. (2018). Rheology and Mechanical Properties of Fats. In *Structure-Function Analysis of Edible Fats*. AOCS Press. https://doi.org/10.1016/B978-0-12-814041-3.00005-8

Grabowska, K. J., Zhu, S., Dekkers, B. L., de Ruijter, N. C. A., Gieteling, J., & van der Goot, A. J. (2016). Shear-induced structuring as a tool to make anisotropic materials using soy protein concentrate. *Journal of Food Engineering*, *188*, 77–86. https://doi.org/10.1016/j.jfoodeng.2016.05.010

Guo, Y., Patanwala, H. S., Bognet, B., & Ma, A. W. K. (2017). Inkjet and inkjet-based 3D printing: Connecting fluid properties and printing performance. *Rapid Prototyping Journal*, *23*(3), 562–576. https://doi.org/10.1108/RPJ-05-2016-0076

Hao, L., Mellor, S., Seaman, O., Henderson, J., Sewell, N., & Sloan, M. (2010). Material characterisation and process development for chocolate additive layer manufacturing. In *Virtual and Physical Prototyping* (Vol. 5, Issue 2, pp. 57–64). https://doi.org/10.1080/17452751003753212

Hapgood, K.P., Litster, J.D., Biggs, S.R., Howes, T., 2002. Drop penetration into porous powder beds. Journal of Colloid and Interface Science 253, 353–366. https://doi.org/10.1006/jcis.2002.8527

Hartel, R. W., & Rao, M. A. (1998). *Phase/State Transitions in Foods, Chemical,Structural and Rheological Changes* (R. W. Hartel & M. A. Rao, Eds.; illustrate). CRC Press, 1998.

Hartel, R. W., von Elbe, J. H., & Hofberger, R. (2018). Confectionery Science and Technology. In *Confectionery Science and Technology*. https://doi.org/10.1007/978-3-319-61742-8

He, C., Zhang, M., & Devahastin, S. (2020). Investigation on Spontaneous Shape Change of 4D Printed Starch-Based Purees from Purple Sweet Potatoes As Induced by Microwave Dehydration. *ACS Applied Materials and Interfaces*, *12*(34), 37896–37905. https://doi.org/10.1021/acsami.0c10899

He, C., Zhang, M., & Guo, C. (2020). 4D printing of mashed potato/purple sweet potato puree with spontaneous colour change. *Innovative Food Science and Emerging Technologies*, *59*(July 2019), 102250. https://doi.org/10.1016/j.ifset.2019.102250

Ho, Q. T., Carmeliet, J., Datta, A. K., Defraeye, T., Delele, M. A., Herremans, E., Opara, L., Ramon, H., Tijskens, E., van der Sman, R., van Liedekerke, P., Verboven, P., & Nicolaï, B. M. (2013). Multiscale modeling in food engineering. In *Journal of Food Engineering* (Vol. 114, Issue 3, pp. 279–291). Elsevier Ltd. https://doi.org/10.1016/j.jfoodeng.2012.08.019

Holland, S., Foster, T., MacNaughtan, W., & Tuck, C. (2018). Design and characterisation of food grade powders and inks for microstructure control using 3D printing. *Journal of Food Engineering*, *220*, 12–19. https://doi.org/10.1016/j.jfoodeng.2017.06.008

Holland, S., Foster, T., & Tuck, C. (2019). Creation of Food Structures Through Binder Jetting. In *Fundamentals of 3D Food Printing and Applications* (Vol. 1867, pp. 257–288). Elsevier. https://doi.org/10.1016/B978-0-12-814564-7.00009-2

Holland, S., Tuck, C., & Foster, T. (2018). Selective recrystallization of cellulose composite powders and microstructure creation through 3D binder jetting ☆. *Carbohydrate Polymers*, *200*(July), 229–238. https://doi.org/10.1016/j.carbpol.2018.07.064

Holm, K., Wendin, K., & Hermansson, A.-M. (2009). Sweetness and texture perceptions in structured gelatin gels with embedded sugar rich domains. *Food Hydrocolloids*, *23*(8), 2388–2393. https://doi.org/10.1016/j.foodhyd.2009.06.016

Horvath, J. (2014). A Brief History of 3D Printing. In *Mastering 3D Printing* (pp. 3–10). Apress. https://doi.org/10.1007/978-1-4842-0025-4_1

Hutchings, S. C., O'Sullivan, M., Jacquier, J. C., & O'Riordan, D. (2015). The effect of inhomogeneous quinine and hydrocolloid distributions on the bitterness of model gels. *Food Quality and Preference*, *45*, 132–139. https://doi.org/10.1016/j.foodqual.2015.06.010

Ingaglio, J., Fox, J., Naito, C. J., & Bocchini, P. (2019). Material characteristics of binder jet 3D printed hydrated CSA cement with the addition of fine aggregates. *Construction and Building Materials*, *206*, 494–503. https://doi.org/10.1016/j.conbuildmat.2019.02.065

Irgens, F. (2014). *Rheology and Non-Newtonian Fluids* (1st ed.). Springer International Publishing.

Ismail, I., Hwang, Y. H., & Joo, S. T. (2020). Meat analog as future food: A review. In *Journal of Animal Science and Technology* (Vol. 62, Issue 2, pp. 111–120). Korean Society of Animal Sciences and Technology. https://doi.org/10.5187/jast.2020.62.2.111

Jayaprakash, S., Paasi, J., Pennanen, K., Ituarte, I. F., Lille, M., Partanen, J., & Sozer, N. (2020). Techno-economic prospects and desirability of 3d food printing: Perspectives of industrial experts, researchers and consumers. *Foods*, *9*(12), 1–23. https://doi.org/10.3390/foods9121725

Ji, J., Fitzpatrick, J., Cronin, K., Maguire, P., Zhang, H., & Miao, S. (2016). Rehydration behaviours of high protein dairy powders: The influence of agglomeration on wettability, dispersibility and solubility. *Food Hydrocolloids*, *58*, 194–203. https://doi.org/10.1016/j.foodhyd.2016.02.030

Jia, W., Curubeto, N., Rodríguez-Alonso, E., Keppler, J. K., & van der Goot, A. J. (2021). Rapeseed protein concentrate as a potential ingredient for meat analogues. *Innovative Food Science and Emerging Technologies*, *72*. https://doi.org/10.1016/j.ifset.2021.102758

Jonkers, N., van Dommelen, J. A. W., & Geers, M. G. D. (2020). Experimental characterization and modeling of the mechanical behaviour of brittle 3D printed food. *Journal of Food Engineering*, *278*, 109941. https://doi.org/10.1016/j.jfoodeng.2020.109941

Kano, Y. (1991). Changes of Sugar Kind and Its Content in the Fruit of Watermelon during Its Development and after Harvest. In *Control in Biol* (Vol. 29, Issue 4).

Kelly, A. L., & Fox, P. F. (2016). *Manufacture and Properties of Dairy Powders BT - Advanced Dairy Chemistry: Volume 1B: Proteins: Applied Aspects* (Vol. 1).

Khemacheevakul, K., Wolodko, J., Nguyen, H., & Wismer, W. (2021). Temporal sensory perceptions of sugar-reduced 3D printed chocolates. *Foods*, *10*(9). https://doi.org/10.3390/foods10092082

Kim, H., Bae, H., & Park, H. J. (2017). Classification of the printability of selected food for 3D printing: Development of an assessment method using hydrocolloids as reference material. *Journal of Food Engineering*, *215*, 23–32. https://doi.org/10.1016/j.jfoodeng.2017.07.017

Kim, S. M., Kim, H. W., & Park, H. J. (2021). Preparation and characterization of surimi-based imitation crab meat using coaxial extrusion three-dimensional food printing. *Innovative Food Science and Emerging Technologies*, *71*. https://doi.org/10.1016/j.ifset.2021.102711

Kistler, T., Pridal, A., Bourcet, C., & Denkel, C. (2021). Modulation of sweetness perception in confectionary applications. *Food Quality and Preference*, *88*, 104087. https://doi.org/10.1016/j.foodqual.2020.104087

Klomp, D. J., & Anderson, P. D. (2017). Next generation multi-material 3D food printer concept. *Dutch Polymer Days 2017(DPD2017)*.

Ko, H. J., Wen, Y., Choi, J. H., Park, B. R., Kim, H. W., & Park, H. J. (2021). Meat analog production through artificial muscle fibre insertion using coaxial nozzle-assisted three-dimensional food printing. *Food Hydrocolloids*, *120*. https://doi.org/10.1016/j.foodhyd.2021.106898

Kudrolli, A. (2008). Granular matter: Sticky sand. *Nature Materials*, *7*(3), 174–175. https://doi.org/10.1038/nmat2131

Kyriakopoulou, K., Dekkers, B., & van der Goot, A. J. (2018). Plant-based meat analogues. In *Sustainable Meat Production and Processing* (pp. 103–126). Elsevier. https://doi.org/10.1016/B978-0-12-814874-7.00006-7

Labbe, D., Fries, L. R., Ferrage, A., Lenfant, F., Godinot, N., & Martin, N. (2018). Right sizing: Sensory-based product design is a promising strategy to nudge consumers toward healthier portions. *Nutrients*, *10*(10). https://doi.org/10.3390/nu10101544

Lavoie, F., Cartilier, L., & Thibert, R. (2002). New methods characterizing avalanche behaviour to determine powder flow. *Pharmaceutical Research*, *19*(6), 887–893. https://doi.org/10.1023/A:1016125420577

le Berrre, E., Boucon, C., Knoop, M., & Dijksterhuis, G. (2013). Reducing bitter taste through perceptual constancy created by an expectation. *Food Quality and Preference*, *28*(1), 370–374. https://doi.org/10.1016/j.foodqual.2012.10.010

Le Tohic, C., O'Sullivan, J. J., Drapala, K. P., Chartrin, V., Chan, T., Morrison, A. P., Kerry, J. P., & Kelly, A. L. (2018). Effect of 3D printing on the structure and textural properties of processed cheese. *Journal of Food Engineering*, *220*, 56–64. https://doi.org/10.1016/j.jfoodeng.2017.02.003

Lea Nash Castro, Jo Jewell, Stephen Whiting, Holly Rippin, Clare Farrand, Kremlin Wickramasinghe, & João Breda. (2021). *Nutrition, overweight and obesity Factsheet-Sustainable Development Goals: health targets*. https://www.euro.who.int/en/SDG_factsheets

Li, J., Wu, Y., He, J., & Huang, Y. (2016). A new insight to the effect of calcium concentration on gelation process and physical properties of alginate films. *Journal of Materials Science*, *51*(12), 5791–5801. https://doi.org/10.1007/s10853-016-9880-0

Lille, M., Nurmela, A., Nordlund, E., Metsä-Kortelainen, S., & Sozer, N. (2018). Applicability of protein and fibre-rich food materials in extrusion-based 3D printing. *Journal of Food Engineering*, *220*, 20–27. https://doi.org/10.1016/J.JFOODENG.2017.04.034

Liu, Y., Liu, D., Wei, G., Ma, Y., Bhandari, B., & Zhou, P. (2018). 3D printed milk protein food simulant: Improving the printing performance of milk protein concentration by incorporating whey protein isolate. *Innovative Food Science and Emerging Technologies*, *49*(June), 116–126. https://doi.org/10.1016/j.ifset.2018.07.018

Liu, Z., Bhandari, B., Prakash, S., & Zhang, M. (2018). Creation of internal structure of mashed potato construct by 3D printing and its textural properties. *Food Research International*, *111*, 534–543. https://doi.org/10.1016/j.foodres.2018.05.075

Liu, Z., Dick, A., Prakash, S., Bhandari, B., & Zhang, M. (2020). Texture Modification of 3D Printed Air-Fried Potato Snack by Varying Its Internal Structure with the Potential to Reduce Oil Content. *Food and Bioprocess Technology*, *13*, 564–576. https://doi.org/10.1007/s11947-020-02408-x

Liu, Z., Zhang, M., Bhandari, B., & Wang, Y. (2017). 3D printing: Printing precision and application in food sector. *Trends in Food Science and Technology*, *69*, 83–94. https://doi.org/10.1016/j.tifs.2017.08.018

Liu, Z., Zhang, M., Bhandari, B., & Yang, C. (2018). Impact of rheological properties of mashed potatoes on 3D printing. *Journal of Food Engineering*, *220*, 76–82. https://doi.org/10.1016/j.jfoodeng.2017.04.017

Lundahl, D. (2014). New insights on "liking" and product choice. *Food Techonolgy*, *68*, 40–45.

Lustig, R. H., Schmidt, L. A., & Brindis, C. D. (2012). Public health: The toxic truth about sugar. *Nature*, *482*(7383), 27–29. https://doi.org/10.1038/482027a

Ma, Y., Schutyser, M. A. I., Boom, R. M., & Zhang, L. (2021). Predicting the extrudability of complex food materials during 3D printing based on image analysis and gray-box

data-driven modelling. *Innovative Food Science and Emerging Technologies*, *73*(April), 102764. https://doi.org/10.1016/j.ifset.2021.102764

Mallakpour, S., Azadi, E., & Hussain, C. M. (2021). State-of-the-art of 3D printing technology of alginate-based hydrogels—An emerging technique for industrial applications. In *Advances in Colloid and Interface Science* (Vol. 293). Elsevier B.V. https://doi.org/10.1016/j.cis.2021.102436

Manski, J. M., van der Goot, A. J., & Boom, R. M. (2007). Formation of fibrous materials from dense calcium caseinate dipersions. *Biomacromolecules*, *8*(4), 1271–1279. https://doi.org/10.1021/bm061008p

Mantihal, S., Prakash, S., & Bhandari, B. (2019). Texture-modified 3D printed dark chocolate: Sensory evaluation and consumer perception study. *Journal of Texture Studies*, *50*, 386–399. https://doi.org/10.1111/jtxs.12472

Mantihal, S., Prakash, S., Godoi, F. C., & Bhandari, B. (2017). Optimization of chocolate 3D printing by correlating thermal and flow properties with 3D structure modeling. *Innovative Food Science & Emerging Technologies*, *44*, 21–29. https://doi.org/10.1016/J.IFSET.2017.09.012

Mascia, S., Patel, M. J., Rough, S. L., Martin, P. J., & Wilson, D. I. (2006). Liquid phase migration in the extrusion and squeezing of microcrystalline cellulose pastes. *European Journal of Pharmaceutical Sciences*, *29*(1), 22–34. https://doi.org/10.1016/j.ejps.2006.04.011

McCrickerd, K., Lim, C. M. H., Leong, C., Chia, E. M., & Forde, C. G. (2017). Texture-based differences in eating rate reduce the impact of increased energy density and large portions on meal size in adults. *Journal of Nutrition*, *147*(6), 1208–1217. https://doi.org/10.3945/jn.116.244251

Mcmahon, D. J., Adams, S. L., & Mcmanus, W. R. (2009). Hardening of high-protein nutrition bars and sugar/polyol-protein phase separation. *Journal of Food Science*, *74*(6). https://doi.org/10.1111/j.1750-3841.2009.01225.x

Mezger, T. (2015). *Applied Rheology: With Joe Flow on Rheology Road*. Paar. https://books.google.nl/books?id=Fb9VwAEACAAJ

Mezger, T. G. (2011). *The Rheology Handbook for Users of Rotational and Oscillatory Rheometers* (2nd rev. e). Vincentz Network.

Mirzababaei, S., & Pasebani, S. (2019). A review on binder jet additive manufacturing of 316L stainless steel. *Journal of Manufacturing and Materials Processing*, *3*(3), 8–12. https://doi.org/10.3390/jmmp3030082

Morita, N., Khalate, A. A., Buul, A. M. van, & Wijshoff, H. (2016). Inkjet Printheads. In *Fundamentals of Inkjet Printing: The Science of Inkjet and Droplets* (pp. 57–92). https://doi.org/https://doi.org/10.1002/9783527684724.ch3

Mosca, A. C., Bult, J. H. F., & Stieger, M. (2013). Effect of spatial distribution of tastants on taste intensity, fluctuation of taste intensity and consumer preference of (semi-)solid food products. *Food Quality and Preference*, *28*(1), 182–187. https://doi.org/10.1016/j.foodqual.2012.07.003

Mosca, A. C., Bult, J. H. F., Velde, F. van de, van Boekel, M. A. J. S., & Stieger, M. (2014). Effect of successive stimuli on sweetness intensity of gels and custards. *Food Quality and Preference*, *31*, 10–18. https://doi.org/10.1016/j.foodqual.2013.07.009

Mosca, A. C., Rocha, J. A., Sala, G., van de Velde, F., & Stieger, M. (2012). Inhomogeneous distribution of fat enhances the perception of fat-related sensory attributes in gelled foods. *Food Hydrocolloids*, *27*(2), 448–455. https://doi.org/10.1016/j.foodhyd.2011.11.002

Mosca, A. C., van de Velde, F., Bult, J. H. F., van Boekel, M. A. J. S., & Stieger, M. (2010). Enhancement of sweetness intensity in gels by inhomogeneous distribution of sucrose. *Food Quality and Preference*, *21*(7), 837–842. https://doi.org/10.1016/j.foodqual.2010.04.010

Noort, M., Van Bommel, K., & Renzetti, S. (2017). 3D-printed cereal foods. *Cereal Foods World*, *62*, 272–277. https://doi.org/10.1094/CFW-62-6-0272

Noort, M. W. J., Bult, J. H. F., & Stieger, M. (2012). Saltiness enhancement by taste contrast in bread prepared with encapsulated salt. *Journal of Cereal Science*, *55*(2), 218–225. https://doi.org/10.1016/j.jcs.2011.11.012

Norton, I. T., Jarvis, D. A., & Foster, T. J. (1999). A molecular model for the formation and properties of fluid gels. In *International Journal of Biological Macromolecules* (Vol. 26). www.elsevier.com/locate/ijbiomac

Osterholt, K. M., Roe, L. S., & Rolls, B. J. (2007). Incorporation of air into a snack food reduces energy intake. *Appetite*, *48*(3), 351–358. https://doi.org/10.1016/j.appet.2006.10.007

Oyinloye, T. M., & Yoon, W. B. (2020). Stability of 3D printing using a mixture of pea protein and alginate: Precision and application of additive layer manufacturing simulation approach for stress distribution. *Journal of Food Engineering*, *288*(May 2020), 110127. https://doi.org/10.1016/j.jfoodeng.2020.110127

Pacek, A. W., Ding, P., Nienow, A. W., & Wedd, M. (2000). Phase separation and drop size distributions in "homogeneous" Na-alginate/Na-caseinate mixtures. *Carbohydrate Polymers*, *42*(4), 401–409. https://doi.org/10.1016/S0144-8617(99)00181-2

Paolillo, M., Derossi, A., van Bommel, K., Noort, M., & Severini, C. (2021). Rheological properties, dispensing force and printing fidelity of starchy-gels modulated by concentration, temperature and resting time. *Food Hydrocolloids*, *117*, 106703. https://doi.org/10.1016/j.foodhyd.2021.106703

Phuhongsung, P., Zhang, M., & Devahastin, S. (2020). Investigation on 3D printing ability of soybean protein isolate gels and correlations with their rheological and textural properties via LF-NMR spectroscopic characteristics. *Lwt*, *122*(December 2019), 109019. https://doi.org/10.1016/j.lwt.2020.109019

Pietsch, V. L., Bühler, J. M., Karbstein, H. P., & Emin, M. A. (2019). High moisture extrusion of soy protein concentrate: Influence of thermomechanical treatment on protein-protein interactions and rheological properties. *Journal of Food Engineering*, *251*, 11–18. https://doi.org/10.1016/j.jfoodeng.2019.01.001

Pietsch, W. (2003). An interdisciplinary approach to size enlargement by agglomeration. *Powder Technology*, *130*(1–3), 8–13. https://doi.org/10.1016/S0032-5910(02)00218-8

Písecký, Jan. (2012). *Handbook of milk powder manufacture*. GEA Niro.

Portanguen, S., Tournayre, P., Sicard, J., Astruc, T., & Mirade, P. S. (2019). Toward the design of functional foods and biobased products by 3D printing: A review. *Trends in Food Science and Technology*, *86*(May 2018), 188–198. https://doi.org/10.1016/j.tifs.2019.02.023

Prescott, J. K., & Barnum, R. A. (2000). On powder flowability. *Pharmaceutical Technology*, *24*(10), 60-84+236.

Prinz, J. O. N. F., & Wijk, R. a D. E. (2006). Effect of bite size on the sensory properties of vanilla custard desserts. *Journal of Sensory Studies*, *22*(2007), 273–280.

Punpongsanon, P., Lin, Y. J., Wen, X., Iwai, D., Sato, K., Obrist, M., & Mueller, S. (2020). *Demonstration of FoodFab: Creating Food Perceptual Illusions using Food 3D Printing*. https://doi.org/10.1145/3334480.3383144

Rando, P., & Ramaioli, M. (2021). Food 3D printing: Effect of heat transfer on print stability of chocolate. *Journal of Food Engineering*, *294*. https://doi.org/10.1016/j.jfoodeng.2020.110415

Reina-Romo, E., Mandal, S., Amorim, P., Bloemen, V., Ferraris, E., & Geris, L. (2021). Towards the Experimentally-Informed In Silico Nozzle Design Optimization for Extrusion-Based Bioprinting of Shear-Thinning Hydrogels. *Frontiers in Bioengineering and Biotechnology*, *9*. https://doi.org/10.3389/fbioe.2021.701778

Ross, M. M., Crowley, S. v., Crotty, S., Oliveira, J., Morrison, A. P., & Kelly, A. L. (2021). Parameters affecting the printability of 3D-printed processed cheese. *Innovative Food Science and Emerging Technologies*, *72*(June), 102730. https://doi.org/10.1016/j.ifset.2021.102730

Sanders, T. A. B. (2016). Introduction: The Role of Fats in Human Diet. The Role of Fats in Human Diet. In *Functional Dietary Lipids: Food Formulation, Consumer Issues and Innovation for Health* (pp. 1–20). Elsevier Ltd. https://doi.org/10.1016/B978-1-78242-247-1.00001-6

Schifferstein, H. N. J., & Oudejans, I. M. (1996). Determinants of cumulative successive contrast in saltiness intensity judgments. *Perception & Psychophysics*, *58*(5), 713–724. https://doi.org/10.3758/BF03213103

Schreuders, F. K. G., Sagis, L. M. C., Bodnár, I., Erni, P., Boom, R. M., & van der Goot, A. J. (2021). Small and large oscillatory shear properties of concentrated proteins. *Food Hydrocolloids*, *110*. https://doi.org/10.1016/j.foodhyd.2020.106172

Schutyser, M. A. I., Houlder, S., de Wit, M., Buijsse, C. A. P., & Alting, A. C. (2017). Fused deposition modelling of sodium caseinate dispersions. *Journal of Food Engineering*, *220*, 49–55. https://doi.org/10.1016/j.jfoodeng.2017.02.004

Serisier, S., Pizzagalli, A., Leclerc, L., Feugier, A., Nguyen, P., Biourge, V., & German, A. J. (2014). Increasing volume of food by incorporating air reduces energy intake. *Journal of Nutritional Science*, *3*. https://doi.org/10.1017/jns.2014.43

Severini, C., Azzollini, D., Albenzio, M., & Derossi, A. (2018). On printability, quality and nutritional properties of 3D printed cereal based snacks enriched with edible insects. *Food Research International*, *106*(February), 666–676. https://doi.org/10.1016/j.foodres.2018.01.034

Severini, C., Derossi, A., Ricci, I., Caporizzi, R., & Fiore, A. (2018). Printing a blend of fruit and vegetables. New advances on critical variables and shelf life of 3D edible objects. *Journal of Food Engineering*, *220*, 89–100. https://doi.org/10.1016/j.jfoodeng.2017.08.025

Sivarupan, T., Balasubramani, N., Saxena, P., Nagarajan, D., El Mansori, M., Salonitis, K., Jolly, M., & Dargusch, M. S. (2021). A review on the progress and challenges of binder jet 3D printing of sand moulds for advanced casting. *Additive Manufacturing*, *40*(September 2020), 101889. https://doi.org/10.1016/j.addma.2021.101889

Spierings, A. B., Voegtlin, M., Bauer, T., & Wegener, K. (2016). Powder flowability characterisation methodology for powder-bed-based metal additive manufacturing. *Progress in Additive Manufacturing*, *1*(1–2), 9–20. https://doi.org/10.1007/s40964-015-0001-4

Statovci, D., Aguilera, M., MacSharry, J., & Melgar, S. (2017). The Impact of Western Diet and Nutrients on the Microbiota and Immune Response at Mucosal Interfaces. *Frontiers in Immunology*, *8*(JUL), 838. https://doi.org/10.3389/fimmu.2017.00838

Stribiţcaia, E., Evans, C. E. L., Gibbons, C., Blundell, J., & Sarkar, A. (2020). Food texture influences on satiety: systematic review and meta-analysis. *Scientific Reports*, *10*(1). https://doi.org/10.1038/s41598-020-69504-y

Sun, J., Zhou, W., Huang, D., Fuh, J. Y. H., & Hong, G. S. (2015). An Overview of 3D Printing Technologies for Food Fabrication. *Food and Bioprocess Technology*, *8*(8), 1605–1615. https://doi.org/10.1007/s11947-015-1528-6

Takayama, Y., & Kato, N. (2018). Shear-Induced Structuring for Multiple Parallel Gel Filaments Obtained from Casein-Alginate Hybrids. *Langmuir*, *34*(44), 13352–13360. https://doi.org/10.1021/acs.langmuir.8b03038

Tao, Y., Do, Y., Yang, H., Lee, Y. C., Wang, G., Mondoa, C., Cui, J., Wang, W., & Yao, L. (2019). Morphlour: Personalized flour-based morphing food induced by dehydration or hydration method. *UIST 2019 - Proceedings of the 32nd Annual ACM Symposium on User Interface Software and Technology*, 329–340. https://doi.org/10.1145/3332165.3347949

Thomar, P., Nicolai, T., Benyahia, L., & Durand, D. (2013). Comparative study of the rheology and the structure of sodium and calcium caseinate solutions. *International Dairy Journal*, *31*(2), 100–106. https://doi.org/10.1016/j.idairyj.2013.02.005

Tolstoguzov, V. (2006). Texturising by phase separation. *Biotechnology Advances*, *24*(6), 626–628. https://doi.org/10.1016/j.biotechadv.2006.07.001

Tunick, M. H. (2011). Small-strain dynamic rheology of food protein networks. *Journal of Agricultural and Food Chemistry*, *59*(5), 1481–1486. https://doi.org/10.1021/jf1016237

Tuoc, T., & Glasgow, S. (n.d.). On The Texture Profile Analysis Test. *Chemeca 2012: Quality of Life through Chemical Engineering*.

Udofia, E. N., & Zhou, W. (2019). Microextrusion Based 3D Printing-A Review. *29th Annual International Solid Freeform Fabrication Symposium*, 2033–2060.

Uribe-Wandurraga, Z. N., Zhang, L., Noort, M. W. J., Schutyser, M. A. I., García-Segovia, P., & Martínez-Monzó, J. (2020). Printability and Physicochemical Properties of Microalgae-Enriched 3D-Printed Snacks. *Food and Bioprocess Technology*, *13*(11), 2029–2042. https://doi.org/10.1007/s11947-020-02544-4

van Ittersum, K., & Wansink, B. (2012). Plate size and colour suggestibility: The Delboeuf illusion's bias on serving and eating behaviour. *Journal of Consumer Research*, *39*(2), 215–228. https://doi.org/10.1086/662615

van Vliet, T., van Aken, G. A., de Jongh, H. H. J., & Hamer, R. J. (2009). Colloidal aspects of texture perception. *Advances in Colloid and Interface Science*, *150*, 27–40. https://doi.org/10.1016/j.cis.2009.04.002

Vancauwenberghe, V., Delele, M. A., Vanbiervliet, J., Aregawi, W., Verboven, P., Lammertyn, J., & Nicolaï, B. (2018). Model-based design and validation of food texture of 3D printed pectin-based food simulants. *Journal of Food Engineering*, *231*, 72–82. https://doi.org/10.1016/j.jfoodeng.2018.03.010

Vancauwenberghe, V., Katalagarianakis, L., Wang, Z., Meerts, M., Hertog, M., Verboven, P., Moldenaers, P., Hendrickx, M. E., Lammertyn, J., & Nicolaï, B. (2017). Pectin based food-ink formulations for 3-D printing of customizable porous food simulants. *Innovative Food Science and Emerging Technologies*, *42*(June), 138–150. https://doi.org/10.1016/j.ifset.2017.06.011

Vesco, A., Lipson, H., Cohen, D. L., Lipton, J. I., Cutler, M., & Coulter, D. (2009). Hydrocolloid Printing: A Novel Platform for Customized Food Production. *Twentieth Annual International Solid Freeform Fabrication Symposium*, *January 2009*, 807–818. https://doi.org/10.1017/CBO9781107415324.004

Wang, L., Zhang, M., Bhandari, B., & Yang, C. (2018). Investigation on fish surimi gel as promising food material for 3D printing. *Journal of Food Engineering*, *220*, 101–108. https://doi.org/10.1016/j.jfoodeng.2017.02.029

Wilms, P., Daffner, K., Kern, C., Gras, S. L., Schutyser, M. A. I., & Kohlus, R. (2021). Formulation engineering of food systems for 3D-printing applications – A review. *Food Research International*, *148*(April), 110585. https://doi.org/10.1016/j.foodres.2021.110585

Windhab, E. J. (2006). What makes for smooth, creamy chocolate? *Physics Today*, *59*(6), 82–83. https://doi.org/10.1063/1.2218569

Yang, F., Zhang, M., Bhandari, B., & Liu, Y. (2018). Investigation on lemon juice gel as food material for 3D printing and optimization of printing parameters. *LWT - Food Science and Technology*, *87*, 67–76. https://doi.org/10.1016/j.lwt.2017.08.054

Yu, Z., Zhan, J., Wang, H., Zheng, H., Xie, J., & Wang, X. (2020). Analysis of influencing factors on viscosity of agar solution for capsules. *Journal of Physics: Conference Series*, *1653*(1). https://doi.org/10.1088/1742-6596/1653/1/012059

Zhang, L., Lou, Y., & Schutyser, M. A. I. (2018). 3D printing of cereal-based food structures containing probiotics. *Food Structure*, *18*(October), 14–22. https://doi.org/10.1016/j.foostr.2018.10.002

Zheng, Z., Zhang, M., & Liu, Z. (2021). Investigation on evaluating the printable height and dimensional stability of food extrusion-based 3D printed foods. *Journal of Food Engineering*, *306*. https://doi.org/10.1016/j.jfoodeng.2021.110636

Zhu, S., Ribberink, M., De Wit, M., Schutyser, M., & Stieger, M. (2020). Modifying sensory perception of chocolate coated rice waffles through bite-to-bite contrast: An application case study using 3D inkjet printing. *Food and Function*, *11*, 10580–10587. https://doi.org/10.1039/d0fo01787f

Zhu, S., Vazquez, I., Azua, R. de, Feijen, S., Jan, A., Goot, V. der, Schutyser, M., & Stieger, M. (2021). How macroscopic structure of 3D printed protein bars filled with chocolate influences instrumental and sensory texture. *LWT*, *151*(May), 112155. https://doi.org/10.1016/j.lwt.2021.112155

S

Summary

3D food printing is an emerging technology that allows building of 3D food structures via layer-by-layer deposition following a digital design. Hitherto, most research related to 3D food printing focused on exploration of suitable recipes and optimal printing parameters for making custom-shaped 3D-printed foods, such as chocolates, cookies, cheese and vegetable pastes. Although the previous studies broadened the scope of 3D food printing applications, they did not provide rational guidelines to replace trial-and-error strategies during optimization of new 3D food printing applications. Moreover, most efforts focused on customization of the food design whereas 3D printing also had been suggested to allow preparation of foods with altered perceived texture and taste. The few studies that showed the impact of 3D printed food design on texture properties did primarily employ instrumental analysis while not being complemented with sensory texture and mouthfeel perception. This study therefore aimed at understanding the relationships between material properties, printing conditions and the resulting properties of printed foods (Chapter 2 and 3), and how 3D food printing can be used to affect texture and taste perception of foods through modulating food structure (Chapter 4, 5 and 6).

In **Chapter 2**, tomato puree was applied as a model food material to investigate the correlations between the rheological properties and printability (dispensability and stability) of a material during the extrusion-based printing process. Results showed that the flow point of food material as determined by amplitude sweep oscillatory rheology measurements can be used to predict the printing stability of water-based model foods (tomato pastes) and other commercial food pastes (aqueous- or fat-based). Unfortunately, the flow point could not be used to predict dispensability of fat-based formulations. Based on the findings, a guideline was proposed to develop aqueous food recipes with desired printability based on flow stress measured by shear rheology.

Chapter 3 describes our study on the potential of binder jet 3D printing. It was possible to produce products with food ingredients, but the component mixture strongly determined whether this technique could be applied successfully. Mixtures of CaCas, starch and MCT were taken as model components. The addition of starch to CaCas formulations was found to effectively enable the binder jet printing process by reducing the surface swelling caused by hydration of CaCas powders. Results showed that increasing deposited binder content led to a more cohesive printed foods, while increasing CaCas content in dry powder mixtures contributed to the springiness of the final product.

Chapter 4 investigated how shearing profiles induced by extrusion speed and nozzle geometry, influenced fibrous structure formation of SC/SA blends. Result showed that both printing speed and nozzle geometry could be used to steer the morphology of the smaller micro-scale fibrous filaments. By designing a parallel printing path in the longitudinal direction, a macro-scale fibrous structure consisting of parallel printed filaments was achieved. Both the calcium content in the fluid gel bath and the geometry of printing nozzles were found to influence the fusion of neighbouring printed filaments. The study shows that anisotropic structures can be created by extrusion-based 3D printing of phase-separated sodium caseinate - sodium alginate blends, and the obtained anisotropic structure might become relevant when striving for meat analogues made by 3D-printing.

The findings in Chapters 5 & 6 indicate the feasibility to apply 3D printing to alter sensory perception of food products. In **Chapter 5**, we investigated how sweetness, creaminess, expected fullness and liking of chocolate coated rice waffles were influenced by bite-to-bite variation in chocolate thickness. We first evaluated sensory attributes of rice waffles with a homogeneous chocolate coating. The panel found that increased thickness of chocolate coating led to sweeter and creamier sensation of rice waffles. Based on the study, we designed seven chocolate coated rice waffles containing a constant total chocolate amount but different chocolate thicknesses between three sequential bites. Significant but small effects on sweetness, expected fullness and liking were found when changing the order of chocolate thickness between bites. The observed sweetness and creaminess perception was related to a perceptual contrast mechanism. The study showed that sweetness of chocolate coated rice waffles can be modified without changing the overall amount of chocolate consumed. **Chapter 6** investigated the influence of the macroscopic structure of 3D printed protein bars with chocolate fillings on instrumental texture properties and sensory perception. Protein bars with different printing patterns (layered, rectilinear and concentric) were prepared by extrusion-based 3D printing. Among protein bars with different printing patterns, the ones with concentric chocolate infill pattern were the hardest. The liking and perceived chewiness of printed protein bars were however not influenced by the spatial distribution of the chocolate infill pattern. The study demonstrated that by changing the macroscopic structure (printing pattern) of 3D printed protein bars with chocolate fillings, both instrumental measured hardness and perceived hardness can be modified.

Chapter 7 provided an overall discussion of all results described in this thesis. First the interplay between material properties, printing conditions and physical properties of 3D printed foods was discussed. Then, possibilities and practical solutions to ensure a smooth printing process were described. We further illustrated how 3D food printing can be used to modulate food structure, texture and taste, and how 3D printing can contribute to development of healthier food products.

Appendices

Acknowledgements

About the author

Publications

Overview of completed training activities

Acknowledgements

Recently I have been asked for the same question from my friends and colleagues: What do you think about doing a PhD? Well, to be honest, I kept asking myself the same question over the past four years again and again. Wouldn't it be nicer if I did not choose to go back to academia years ago? If so, maybe I would have earned more by now; maybe I would enjoy a more relaxing time instead of suffering the back-and-forth revision and submission of manuscripts (the last half year is indeed more stressful than I expected). However, looking back the journey I went through, I will never regret doing a PhD. I am really grateful for this experience not only because I can fully dive into projects that I am interested in, but also because I am lucky enough to meet those people who bring me courage and strength. "Dr." is never considered a great achievement by me, but rather a sign of proof that I have been down this road before. It is more a carrier that holds all the memories of every single moment we went through together. Thank you all for stepping into my life in my best time - I would not have gone this far without you.

I would like to acknowledge all people who were involved with the work presented in this thesis. First and foremost, I would like to thank my promoters dr. ir. MAI Schutyser**,** prof. dr. MA. Stieger and prof. dr. ir. AJ. van der Goot. Thank you for your supervision and guidance during the past four and half years. I am truly grateful to you all for their massive support, supervision and inspirational guidance over the years. Thank you *Atze Jan* for recommending me to join the project. It is really nice to be your MSc and PhD student and work together with you. I am truly grateful and enjoy to having so many fruitful discussions with you. Thank you, *Maarten* and *Markus*, for giving me the chance to work in this fantastic project. I faced many miserable and difficult times during the study, and I won't be able to go this far without your daily support. Thank you for the clear explanation on my questions and in-time feedback for my manuscript. You are the first ones visiting my newborns and offered me lots of help and support later. As a mother, there is no word to sufficiently express my gratefulness to you.

I also want to thank all the staff members. I always joke with other PhD fellows that you are sometimes more important than supervisors. Thank you, *Martin*, for all the fun chats we have and the accompany of the great PhD trip in Canada. I cannot remember how many kilometers you drive me to meetings, conferences, and abroad trips. I hope one day I can drive you in

Sweden or any country I live and be your local guide. *Maurice*, thank you for all the supports with SEM analysis, and I really miss all the ironic jokes we have. Thank you for letting me bother you at any moment regardless how busy you are. *Jos*, I already received a lot of help from you when I did my MSc thesis in the group, and I am thankful for all your help during the PhD phase when it comes to problems with rheology and texture analysis. *Wouter*, thank you for always being helpful when I need your help with Smartzoom and Morphology 4, and you are such a good-tempered person that everyone finds it easy to talk to you. *Jarno*, thank you for your help with CLSM and all the nice chats about biological/vegan/vegetarian stuff. *Marjan* and *Ilona*, thank you for the help for arranging all the personal and work-related issues. I would also like to thank technicians in FPH and FHM, *Harry* and *Ingrid*; thank you for your warm greetings and timely help during my stay in Wageningen.

I would like to thank all my FPE colleagues but also FPH friends for creating a cheerful working atmosphere. I would not have enjoyed my PhD without the accompany of you, dear *Isabel*. We started together for our PhD, and I am so glad that we can share the toughness and joyfulness, work related or private life issues. One of the best things I had in my PhD period is knowing you. I wish our friendship can last forever and keep a close relation no matter how far we are. I would also like to thank my officemate *Yu*, *Sirinan*, and *Joanne*. Although I joined you a bit late, you guys treat me like a real family. I can still recall all the conversations about Sirinan's cooking, Joanna's chicken and Yu's funny stories. I miss our happy high tea and hot pot party together with *Polly*, *Wanqing*, and *Ruoxuan*. That was one of the best days I had during my PhD study. Dear *Yu*, *Wanqing* and *Qinhui*, it seems just yesterday that we biked and laughed in Hoge Veluwe, that we cooked and gossiped in student dormitory, that we spent so many great moments together. Thank you for the accompany in the past four years. Although we are now sitting in different parts of the world, I believe we will still encourage and give the best wishes to each other. *Yu*, many thanks for helping me out during my most miserable times, and thanks for all the nice gifts and cuddles that you give to Mushin. *Konstantina*, what a great thing to know you and Rene. I am thankful to all your help not only during my PhD but also after I moved abroad and makes me understand what a true friend in need is a true friend indeed.

I would also like to thank the committee members, prof. E. van der Linden, dr. K. van Bommel, dr. B. Tian and prof. L. Ahrné, for their time and efforts assessing this Ph.D.

Yueting Ke, I would also like to have you in this little book. We have known each other more than twenty years from age thirteen. You are one of the very few friends back in China that I still keep contact with. We witnessed all the most important moments in our life: study, graduation, getting married and being mothers. Thank you for all your caring about my family and work during these years. Life is a journey full of unknown and I will be there with you to face all the difficulties.

My earnest and heartfelt gratitude goes to my families, especially my parents. Your support, encouragement and love are always there no matter where I live. Dear Mom and Dad, thank you for both financial and mental support. When I came abroad eleven years ago, I didn't expect to be away from you that long. Thank you for encouraging me all the time when I face struggles in work and life. It is a pity that you are not able to join my PhD ceremony due to the pandemic. I am grateful to be your child and I hope we can have a reunion soon.

Dear *Xiang*, what a lucky thing to have you by my side. Although you always say that I shouldn't do the PhD, you however fully support me with every single actions. Now that we both have the same PhD experience, we can share our story with our little one when she grows up. Dear little *Mushin*, thank you for the extra challenges you brought to my PhD life which makes me realize how strong I can actually be. You are no doubt the most precious gift from God, and I am looking forward to growing together with you.

About the author

Sicong Zhu was born on December 24th, 1988 in Jiangsu, China. Between 2007 and 2011 she did her BSc study in Biological Science at Sun Yat-Sen University, China. After completing her bachelor study, she moved to the Netherlands and enrolled in the MSc program of Food Science and Technology at Wageningen University. In 2013, she obtained her master degree. Between 2014 and 2016, Sicong lived in Groningen and worked at Royal Avebe U.A. as an application specialist. In 2017, Sicong started her PhD program at Wageningen University under supervision by dr.ir. MAI Schutyser, prof. dr. MA. Stieger and prof. ir. AJ. van der Goot. Her research focused on 3D printing with food materials. In October 2021, Sicong moved to Gothenburg, Sweden and started to work as a food scientist at Mycorena AB. She currently lives in Sweden together with her husband and daughter.

Publications

This dissertation:

Zhu, S., Stieger, M.A., van der Goot, A.J. & Schutyser, M.A.I. (2019) Extrusion-based 3D printing of food pastes: Correlating rheological properties with printing behaviour. *Innovative Food Science and Emerging Technologies, 58, 102214*.

Zhu, S., Vazquez Ramos, P., Heckert, O.R., Stieger, M.A., van der Goot, A.J. & Schutyser, M.A.I. (2022) Creating protein-rich snack foods using binder jet 3D printing. *Journal of Food Engineering, Volume 332, 2022, 111124*.

Zhu, S., Wang, W., Stieger, M.A., van der Goot, A.J. & Schutyser, M.A.I. Shear-induced structuring of phase-separated sodium caseinate - sodium alginate blends using extrusion-based 3D printing: Creation of anisotropic aligned micron-size fibrous structures and macroscale filament bundles. *Submitted*.

Zhu, S., Ribberink, M., de Wit, M., Schutyser, M.A.I. & Stieger, M.A. (2020) Modifying sensory perception of chocolate coated rice waffles through bite-to-bite contrast: an application case study using 3D inkjet printing. *Food & Function, 11(12), 10580-10587*.

Zhu, S., Vazquez Ruiz de Azua, I., Feijen, S., van der Goot , A.J., Schutyser, M.A.I. & Stieger, M.A. (2021). How macroscopic structure of 3D printed protein bars filled with chocolate influences instrumental and sensory texture. *LWT*, 151*, 112155*.

Other scientific publications:

Grabowska, K. J., **Zhu, S.**, Dekkers, B. L., de Ruijter, N. C. A., Gieteling, J., & van der Goot, A. J. (2016). Shear-induced structuring as a tool to make anisotropic materials using soy protein concentrate. *Journal of Food Engineering*, 188, 77–86.

Overview of completed training activities

Discipline specific activities

Courses

Rheology: the do's and don'ts, Wageningen, the Netherlands, (2018)

Food proteins: functionality, modification and analysis, Wageningen, the Netherlands, (2018)

Advanced food analysis, Wageningen, the Netherlands, (2019)

Microscopy and Spectroscopy in food and plant science, Wageningen, the Netherlands, (2019)

Conferences and symposium

Thermodynamics and Phase Transitions in Food Processing, Wageningen, the Netherlands (2018)

Science and Technology for Meat Analogues, Wageningen, the Netherlands, (2018)

Effost conference, Rotterdam, the Netherlands, (2019*)

3D Food printing conference, Venlo, the Netherlands, (2018, 2019*, 2020, 2021*)

Food structure and functionality symposium, online, (2021*)

General courses

VLAG PhD week, Baarlo, the Netherlands, (2018)

introduction to R, Wageningen, the Netherlands, (2018)

Interpersonal communication for PhD students, Wageningen, the Netherlands, (2017)

Competence Assessment, Wageningen, the Netherlands, (2017)

Scientific writing, Wageningen, the Netherlands, (2018)

Advanced statistics course Design of Experiments, Wageningen, the Netherlands, (2018)

supervising BSc and MSc thesis students, Wageningen, the Netherlands, (2019)

Effective behaviour in your professional surroundings, Wageningen, the Netherlands, (2019)

Optional activities

Preparation of research proposal

PhD study tour to Canada

Weekly group meetings at Food Process Engineering

Joint meetings with Tue/TNO on 3D food printing